POLITECNICO DI MILANO

M.Sc. Thesis of Civil Engineering for Environmental Risk Mitigation

Experimental Analysis of Scour Countermeasures at Abutments

MASTER OF SCIENCE IN CIVIL ENGINEERING

CERM

SUPERVISOR : Dr. ALESSIO RADICE

VAHID DAVARI 749435

APRIL 2013

CONTENTS:

Abstract

Sediment transport processes in rivers have been studied for many decades. Estimation of the depth of scour at bridge foundations is a problem that has troubled designers for many years, thus local scour at bridge piers and abutments has attracted considerable research interest. Local scour around bridge piers and abutments is widely recognized as one of the major causes of the failure of bridges during floods. Scour at a bridge structure can cause damage or failure of bridges and result in excessive repairs, loss of accessibility or sometimes even cause death to humanity. On the basis of experimental findings, most researchers have proposed a general description of the scouring flow field where the main erosive agent is a vertical structure that develops in front of the obstacles: this is called the horseshoe vortex, which is one of the main cause of scour under a steady current in the case of pier scour, and the principal vortex in the case of abutment scour. The average intensity of the vortex decreases as the scour depth increases.

Potential scour levels can be reduced using a variety of countermeasures. One way is to alter the flow to transfer the scour potential away from bridge abutments. This includes guide banks, spur dikes, bend-way weirs, and Iowa vanes, sacrificial piles in front of piers/abutments, circular collars around piers/abutments or a slot through piers/abutments. However most of the existing scour-control measures are expensive. Another way is bed armoring countermeasures, including riprap, cable-tied blocks, geo-bags, grout-filled bags, etc. Generally their objective is to form a layer at the area where the scour takes place and have the capability to withstand high shear stresses during high flow events so the bed materials underneath the armoring layer are protected from being scoured away.

The experimental campaign related this work started in July 2012, in the Hydraulics laboratory of Politecnico di Milano. In particular, following preliminary indications of a previous work, we carried out several experiments using roughening elements on vertical wall of the abutment as scour countermeasures. The first experiment was with an abutment without any protection under certain experimental condition to observe the scour process on this abutment to be discussed and compared with protected abutments, which will be fully described in this report.

In total we carried out 10 scour runs with the abutment, 2 out of 10 begin with unprotected abutment and the others with different protected abutments. The measurements were made with rulers attached to 3 points of the abutment to obtain the scour depth. The tests were performed in two different series of abutments in terms of protrusion of the roughening elements. In one series we have used protrusion equal to 1cm for all the abutments and in each test we changed the space between the elements. In the other series a protrusion of 0.5 mm and the same spaces were used. During the scour measurement tests after certain times I made surveys to obtain data of the shape of the scour hole using particular Laser, subsequently this information was used in creating cross section.

In this Thesis, Chapter 1 is an introductory part where the basics about sediment motion, flow field, local scour and local scour countermeasures are reviewed. Chapter 2 presents the experimental setup, with details about the experimental channel, the sediments, the measuring devices and the experimental procedure can be found. In Chapter 3 the experiments with abutments are studied and analyzed, so the results and some primary plots are reported and

discussion and comments are made in this chapter.

At the end of this report my conclusion about the experiments will be stated. All the plots and tables related to the data obtained during the experiments are reported in Annex.

The diary of our experiments on which an overview of the works that we have done during this several months is also provided at the end.

Introduction

Waters flowing in natural streams and rivers have the ability to scour channel beds, to carry particles (heavier than water) and to deposit materials, hence changing the bed topography. This phenomenon (i.e. *sediment transport*) is of great economical importance, numerous failures resulted from the inability of engineers to predict sediment motion: e.g. bridge collapse due to local scour at piers or abutments.

As a matter of fact, scour is the result of the erosive action of flowing water, excavating and carrying away material from the bed and banks of streams. A factor in scour at highway crossings and encroachments is whether the scour is clear-water or live-bed scour. Clear-water scour occurs where there is no transport of bed material upstream of the crossing or encroachment and live-bed scour occurs where there is transport of bed material from the upstream reach into the crossing or encroachment.

Local scour involves removal of material from around piers, abutments, spurs, and embankments. It is caused by an acceleration of flow and resulting vortices induced by the flow obstructions (the horseshoe vortex for piers and the principal vortex for abutments). Local scour can also be either clear-water or live-bed scour.

The problem of local scour of sediment around bridge piers and abutments has been studied extensively for several decades. In places where the river bed is easily vulnerable by flow field, which gets created around a bridge pier or abutment, it is required that the pier/abutment is embedded deeply into the river bed, however it is not profitable to anyone to do so. Consequently, there is an interest in finding reliable ways to reduce scour depth and thereby, requisite pier/abutment embedment depth. Scour mitigation at bridges has received much attention in the past. In recent years, extensive research has been aimed at finding methods to efficiently reduce the expected scour levels at both piers and abutments, the latter being within the scope of this work.

Basically, scour countermeasures are typically divided into (a) bed-armoring devices and (b) flow-altering devices. The former increase the resistance of the riverbed and have been studied by many researchers.

Throughout this experimental campaign we have performed some tests regarding local scour depth at abutments using flow-altering countermeasures, which was the scope of our work whereas some preliminary tests have been conducted before performing the scour test such as, velocity measurements, and preliminary test for characterization of the critical discharge in the flume used. The former is done in order to see how flow is distributed along the channel; the latter is done to find the critical discharge. It should be mentioned that before performing these tests, we have calibrated the channel and the instruments, which we have utilized in this campaign.

In particular we have used roughening element in order to protect our abutments and the effect of these protection has been studied and compared to the abutment without protections. These kind of structures have been proposed (in terms of threading cables) for bridge piers, showing

interesting scour reductions even though for not fully feasible dimensions of the cables. To date, roughening elements have never been tried for abutments, except in some preliminary tests recently carried on at the Politecnico within a previous Thesis. In this work an attempt has been made to realize a well-structured experimental campaign.

In this thesis, in chapter 1, I have described some explanation of sediments transport, scour, local scour and etc. Furthermore, chapter 1 contains some theories related to our experimental work and the researches that have been done by other researchers are mentioned as well.

In chapter 2, the procedures in order to set up the experiments has been fully described, plus the fact that, in this chapter the results of our preliminary test is also reported.

In chapter3, the results regarding the main tests namely scour countermeasures tests are discussed; these results have been compared to the abutment without any countermeasures. A synoptic discussion is proposed.

At the final section of this report, I have stated my conclusion from this experimental campaign and my recommendation in terms of which would be the best abutments (among the abutments that we have used) is also given in this section.

Supplementary material is provided in terms of a diary of all the operations performed (Annex 1) and a summary of all the plots and tables related to the experimental campaign (Annex 2).

Introduction

1. Sediment transport in open channel:

Waters flowing in natural streams and rivers have the ability to scour channel beds, to carry particles (heavier than water) and to deposit materials, hence changing the bed topography. This phenomenon (i.e. *sediment transport*) is of great economical importance: e.g. to predict the risks of scouring of bridges, weirs and channel banks; to estimate the siltation of a reservoir upstream of a dam wall; to predict the possible bed form changes of rivers and estuaries. Numerous failures resulted from the inability of engineers to predict sediment motion: e.g. bridge collapse (pier foundation erosion), formation of sand bars in estuaries and navigable rivers, destruction of banks and levees.

The transport of sediment is often more visible in mountain streams, torrents and creeks. However, larger rivers are also famous for their capacity to carry sediment load: e.g. the Nile River, the Mississippi River and the Yellow River.

The transported material is called the *sediment load*. Distinction is made between the *bed load* and the *suspended load*. The bed load characterizes grains rolling along the bed while suspended load refers to grains maintained in suspension by turbulence. The distinction is, however, sometimes arbitrary when both loads are of the same material.

1.1. Bed formation:

In most practical situations, the sediments behave as a non-cohesive material (e.g. sand and gravel) and the fluid flow can distort the bed into various shapes. The bed form results from the drag force exerted by the bed on the fluid flow as well as the sediment motion induced by the flow onto the sediment grains.

In a simple approach, the predominant parameters which affect the bed form are the bed slope, the flow depth and velocity, the sediment size and particle fall velocity. At low velocities, the bed does not move. With increasing flow velocities, the inception of bed movement is reached and the sediment bed begins to move. The basic bed forms, which may be encountered, are the ripples (usually of heights less than 0.1 m), dunes, flat bed, standing waves and anti-dunes. At high flow velocities (e.g. mountain streams and torrents), chutes and step-pools may form. They consist of succession of chutes and free-falling napes (i.e. supercritical flow) connected by pools where the flow is usually subcritical.

The typical bed forms are summarized in Fig. 1.1 and Table. 1.1 Ripples and dunes move in the downstream direction. Anti-dunes and step-pools are observed with supercritical flows and they migrate in the upstream flow direction.

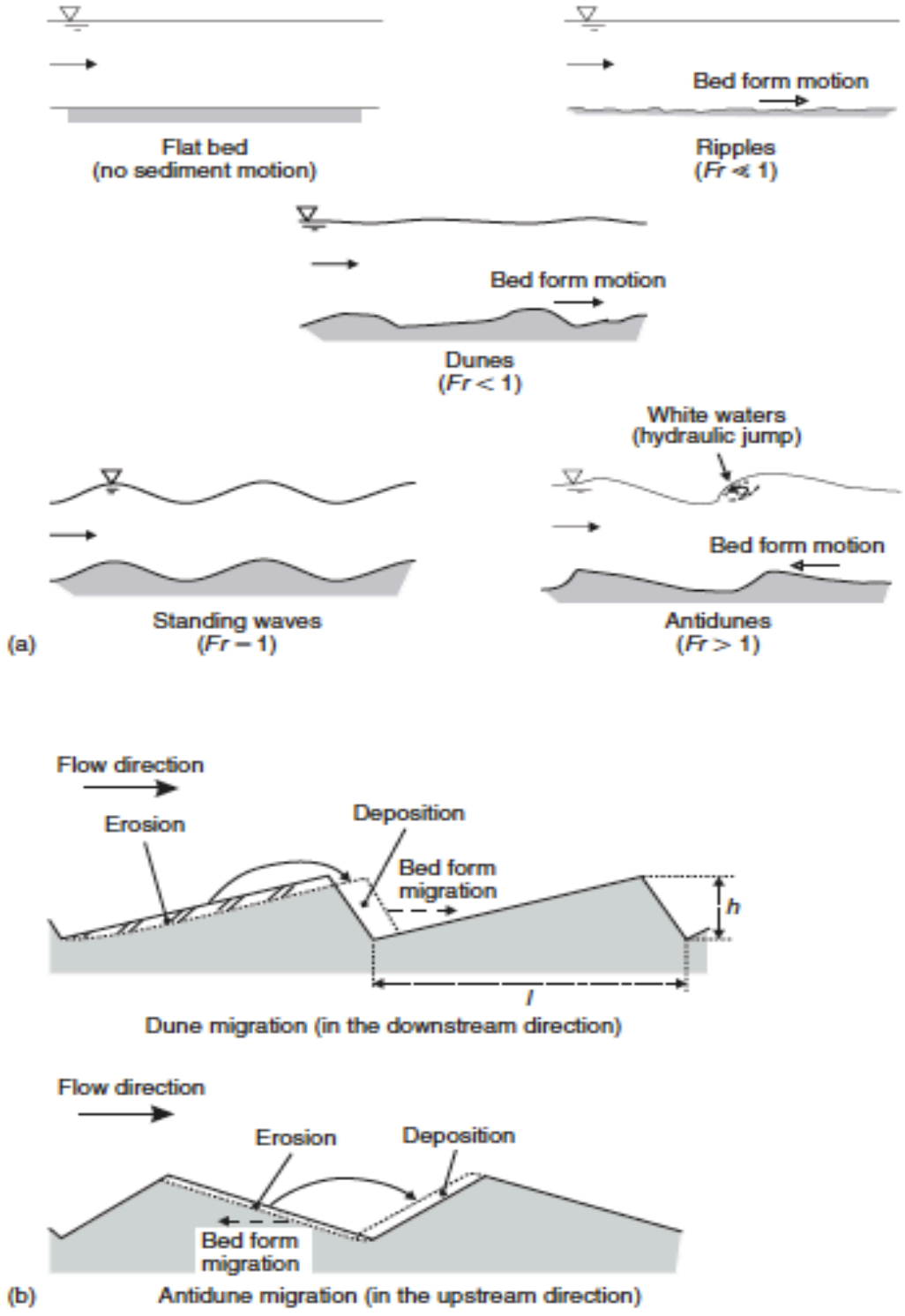

Fig. 1.1. Bed forms in movable boundary hydraulics: (a) typical bed forms and (b) bed form motion.

Bed form (1)	Flow (2)	Bed form motion (3)	Comments (4)
Flat bed	No Flow (or $Fr \ll 1$)	NO	No sediment motion
Ripples	$Fr \ll 1$	D/S	Three-dimensional forms; observed also with air flows (e.g. sand ripples in a beach caused by wind)
Dunes	$Fr < 1$	D/S	Three-dimensional forms; sand dunes can also be caused by wind
Flat bed	$Fr \leq 1$	NO	Observed also with wind flow
Standing waves	$Fr = 1$	NO	Critical flow conditions; bed standing waves in phase with free-surface standing waves
Antidunes	$Fr > 1$	U/S	Supercritical flow with tumbling flow and hydraulic jump upstream of antidune crests
Chute-pools	$Fr > 1$	U/S	Very active antidunes
Step-pools	$Fr > 1$	–	Cascade of steps and pools; steps are often caused by rock bed

References: Henderson (1966) and Graf (1971).
Notes: D/S = in downstream flow direction; Fr = Froude number; U/S = in upstream flow direction.

Table. 1.1. Basic bed forms in alluvial channels (classification by increasing flow velocities)

1.2 Sediment properties:

A typical sediment size classification is shown in Table. 1.2

Class name (1)	Size range (mm) (2)	Phi-scale (ϕ) (3)	Remarks (4)
Clay	$d_s < 0.002$ to 0.004 mm	$+8$ to $+9 < \phi$	
Silt	0.002 to $0.004 < d_s < 0.06$ mm	$+4 < \phi < +8$ to $+9$	
Sand	$0.06 < d_s < 2.0$ mm	$-1 < \phi < +4$	Silica
Gravel	$2.0 < d_s < 64$ mm	$-6 < \phi < -1$	Rock fragments
Cobble	$64 < d_s < 256$ mm	$-8 < \phi < -6$	Original rocks
Boulder	$256 < d_s$	$\phi < -8$	Original rocks

Table. 1.2. Sediment size classification

The most important property of a sediment particle is its characteristic size. It is termed the diameter or sediment size, and denoted ds. In practice, natural sediment particles are not spherical but exhibit irregular shapes.

1.2.1 Particle size distribution:

Natural sediments are mixtures of many different particle sizes and shapes. The particle size distribution is usually represented by a plot of the weight percentage of total sample, which is smaller than a given size plotted as a function of the particle size. A cumulative curve fitted to data points is shown in Fig. 1.2. The characteristic sediment size d_{50} is defined as the size for which

50% by weight of the material is finer. Similarly the characteristic sizes d_{10}, d_{75} and d_{90} are values of grain sizes for which 10%, 75% and 90% of the material weight is finer, respectively. d_{50} is commonly used as the characteristic grain size and the range of particle size is often expressed in terms of a sorting coefficient *S*:

$$S = \sqrt{\frac{d_{90}}{d_{10}}} \tag{1-1}$$

Another descriptor is the *geometric standard deviation* based upon a log-normal distribution of grain sizes σ_g:

$$\sigma_g = \sqrt{\frac{d_{84}}{d_{16}}} \tag{1-2}$$

Small values of *S* and σ_g imply a nearly uniform sediment size distribution. A large value of *S* means a broad sediment size distribution.

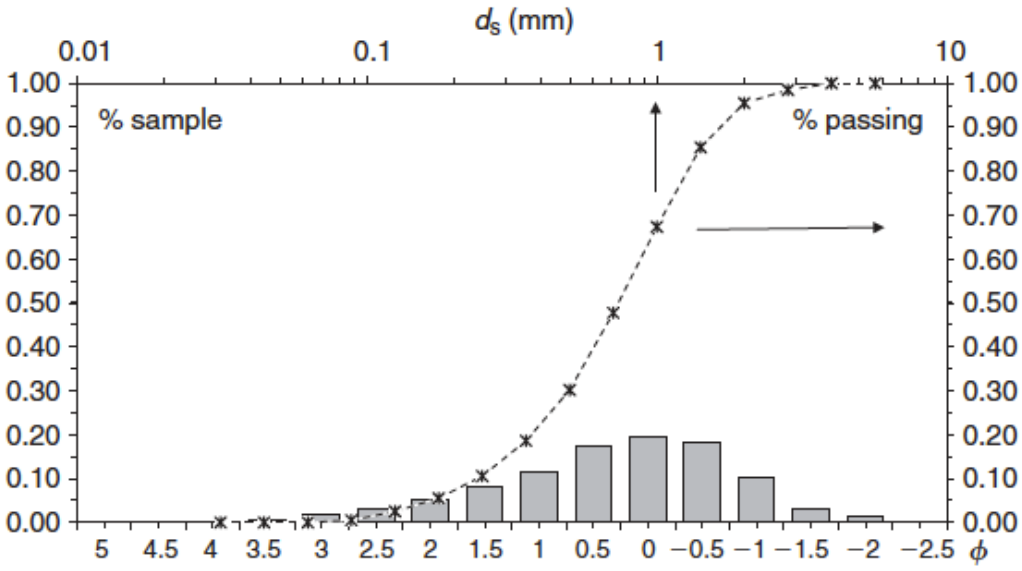

Fig. 1.2. Typical particle size distribution curve: (a) percentage sampling as a function of sediment logical size parameter _ (linear scale) and (b) cumulative percentage passing as a function of the particle size d_s in mm (semi-logarithmic scale).

1.2.2 Angle of Repose:

Considering the stability of a single particle in a horizontal plane, the threshold condition

(formation) is achieved when the center of gravity of the particle is vertically above the point of contact. The critical angle at which motion occurs is called the *angle of repose* Φ_s.

The angle of repose is a function of the particle shape and, on a flat surface, it increases with angularity. Typical examples are shown in Fig. 1.3. For sediment particles, the angle of repose ranges usually from 26° to 42°. For sands, Φ_s is typically between 26° and 34°.

For a two-dimensional polygon, the angle of repose equals 180° divided by the number of sides of the polygon. For example: Φ_s = 60° for an equilateral triangle and Φ_s = 0° for a circle.

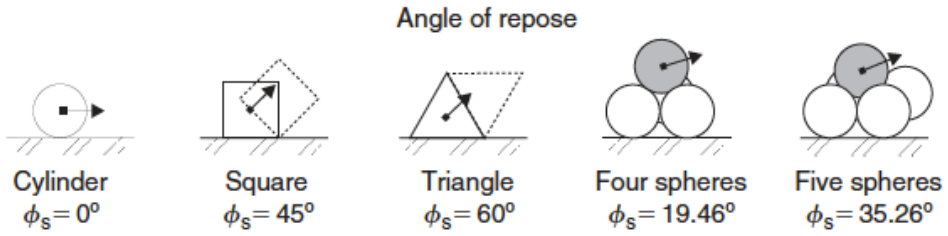

Fig. 1.3. Examples of angle of repose.

1.3 Forces acting on a Sediment particle

For an open channel flow with a movable bed, the forces acting on each sediment particle are (Fig. 1.4.):

- The gravity force $\rho_s\, g v_s$
- The buoyancy force $F_b = \rho g v_s$
- The drag force $C_d \rho A_s V^2/2$
- The lift force $C_L \rho A_s V^2/2$
- The reaction forces of the surrounding grains

Where v_s is the volume of the particle, A_s is a characteristic particle cross-sectional area, C_d and C_d are the drag and lift coefficients, respectively, and V is a characteristic velocity next to the channel bed.

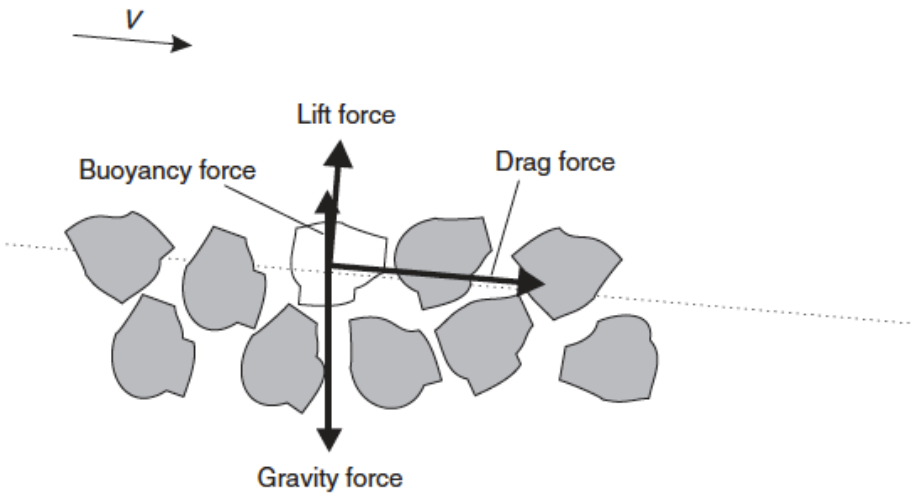

Fig. 1.4. Forces acting on a sediment particle (inter-granular forces not shown for the sake of clarity).

The gravity force and the buoyancy force act both in the vertical direction while the drag force acts in the flow direction and the lift force in the direction perpendicular to the flow direction (Fig. 1.4). The inter-granular forces are related to the grain disposition and packing.

1.4 Sediment transport mechanisms:

There are two types of sediment transport mechanisms. Transported sediment material that is maintained in *suspension* and sediment material transported by *rolling*, *sliding* and *saltation motion* along the bed.

1.4.1 Bed-Load Transport:

When the bed shear stress exceeds a critical value, sediments are transported in the form of bed load and suspended load. For bed-load transport, the basic modes of particle motion are rolling motion, sliding motion and saltation motion (Fig. 1.5).

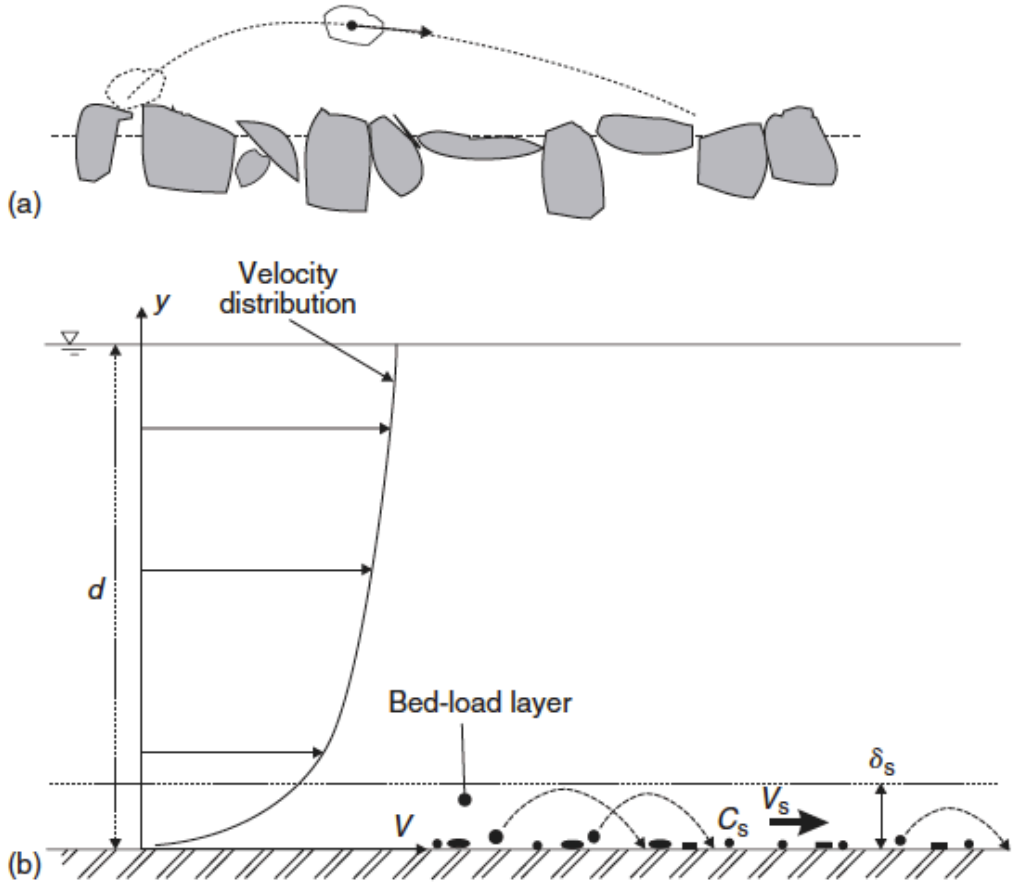

Fig. 1.5. Bed-load motion: (a) sketch of saltation motion and (b) definition sketch of the bed-load layer.

The sediment transport rate may be measured by weight (units: N/s), by mass (units: kg/s) or by volume (units: m^3/s). In practice the sediment transport rate is often expressed by meter width and is measured either by mass or by volume. These are related by:

$$\dot{m}_s = \rho_s q_s \tag{1-3}$$

Where $\dot{m}_s$ is the mass sediment flow rate per unit width, q_s is the volumetric sediment discharge per unit width and ρ_s is the specific mass of sediment.

1.4.1.1 Threshold of sediment bed motion:

The term *threshold of sediment motion* describes the flow conditions and boundary conditions for which the transport of sediment starts to occur. The threshold of sediment motion cannot be defined with an exact (absolute) precision but most experimental observations have provided reasonably accurate and consistent results.

The relevant parameters for the analysis of sediment transport threshold are: the bed shear stress τ_0, the sediment density ρ_s, the fluid density ρ the grain diameter d_s, the gravity acceleration g and the fluid viscosity μ:

$$f_1(\tau_o,\ \rho,\ \rho_s,\ \mu,\ g,\ d_s) = 0 \tag{1-4}$$

In dimensionless terms, it yields:

$$f_2\left(\frac{\tau_o}{\rho g d_s};\ \frac{\rho_s}{\rho};\ \frac{d_s\sqrt{\rho\tau_o}}{\mu}\right) = 0 \tag{1-5}$$

The ratio of the bed shear stress to fluid density is homogeneous (in units) with a velocity squared. Introducing the shear velocity $V*$ defined as:

$$V_* = \sqrt{\frac{\tau_o}{\rho}} \tag{1-6}$$

Note: For alluvial streams, the characteristic velocity near the sediment bed is the shear velocity $V*$.

Equation (1-5) can be transformed as:

$$f_3\left(\frac{V_*}{\sqrt{g d_s}};\ \frac{\rho_s}{\rho};\ \rho\frac{d_s V_*}{\mu}\right) = 0 \tag{1-7}$$

The first term is a form of *Froude number*. The second is the *relative density* (also called specific gravity). The last term is a *Reynolds number* defined in terms of the grain size and shear velocity. It is often denoted as *Re** and called the *shear Reynolds number* or *particle Reynolds number*.

Particle movement occurs when the moments of the destabilizing forces (i.e. drag, lift and buoyancy), with respect to the point of contact, become larger than the stabilizing moment of the weight force. The resulting condition is a function of the angle of repose.

A critical value of the stability parameter may be defined at the inception of bed motion: i.e. $\tau^* = (\tau^*)_C$. Shields (1936) showed that $(\tau^*)c$ is primarily a function of the shear Reynolds number $V * d_s/\nu$ (Fig. 1.6). Bed load motion occurs for:

$$\tau_* > (\tau_*)_c \qquad \text{Bed load motion} \tag{1-8}$$

In summary: the initiation of bed load transport occurs when the bed shear stress τ_0 is larger than a critical value:

$$(\tau_o)_c = \rho(s-1)gd_s(\tau_*)_c \tag{1-9}$$

The stability parameter τ^* is called commonly the *Shields parameter.*

$(\tau^*)_c$ is commonly called the *critical Shields parameter.*

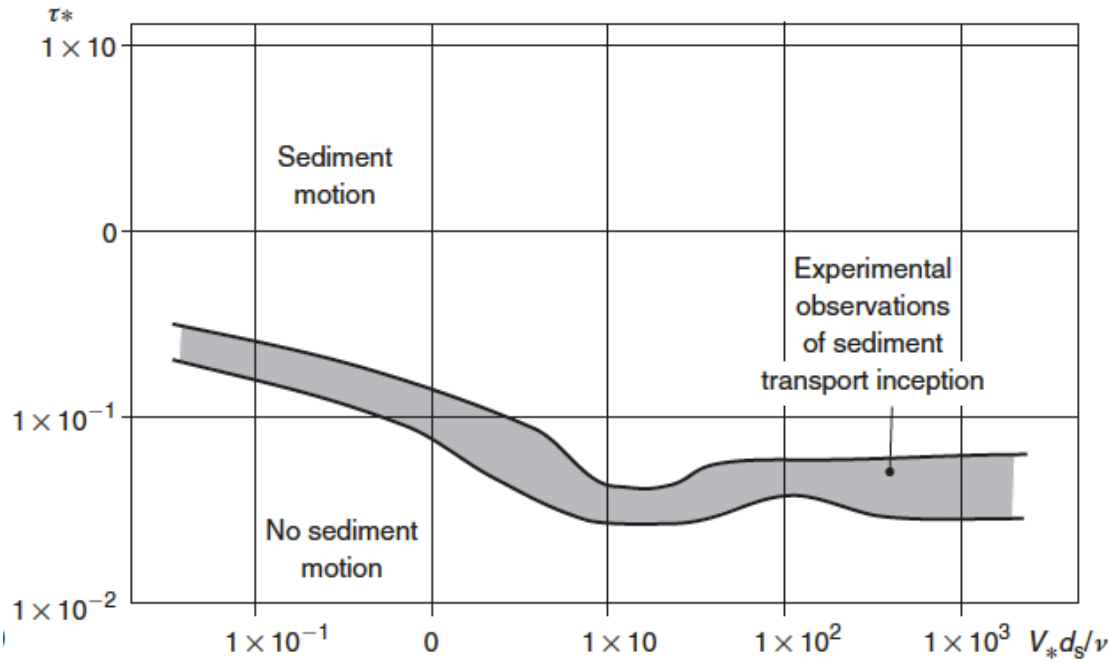

Fig. 1.6. Threshold of bed load motion (Shields diagram) Shields parameter as a function of the particle Reynolds number for sediment in water (experimental data reviewed by Yalin and Karahan (1979))

1.4.1.2 Bed-load transport rate:

The bed-load transport rate per unit width may be defined as:

$$q_s = C_s \delta_s V_s \tag{1-10}$$

Where Vs is the average sediment velocity in the bed-load layer (Fig.1.7). Physically the transport rate is related to the characteristics of the bed-load layer: its mean sediment concentration Cs, its thickness s which is equivalent to the average saltation height measured normal to the bed, and the average speed Vs of sediment moving along the plane bed.

1.4.2 Suspended-load transport:

Sediment suspension can be described as the motion of sediment particles during which the particles are surrounded by fluid. The grains are maintained within the mass of fluid by turbulent agitation without (frequent) bed contact. Sediment suspension takes place when the flow turbulence is strong enough to balance the particle weight.

The amount of particles transported by suspension is called the *suspended load*.

The transport of suspended matter occurs by a combination of *advective* turbulent diffusion and convection. Advective diffusion characterizes the random motion and mixing of particles through the water depth superimposed to the longitudinal flow motion. In a stream with particles heavier than water, the sediment concentration is larger next to the bottom and turbulent diffusion induces an upward migration of the grains to region of lower concentrations. A time-averaged balance between settling and diffusive flux derives from the continuity equation for sediment matter:

$$D_s \frac{dc_s}{dy} = -w_o c_s \tag{1-11}$$

Where $c_s$is the local sediment concentration at a distance y measured normal to the channel bed, D_s is the sediment diffusivity and w_0 is the particle settling velocity. Sediment motion by convection occurs when the turbulent mixing length is large compared to the sediment distribution length scale. Convective transport may be described as the entrainment of sediments by very-large scale vortices: e.g. at bed drops, in stilling basins and hydraulic jumps .(Fig. 1.7).

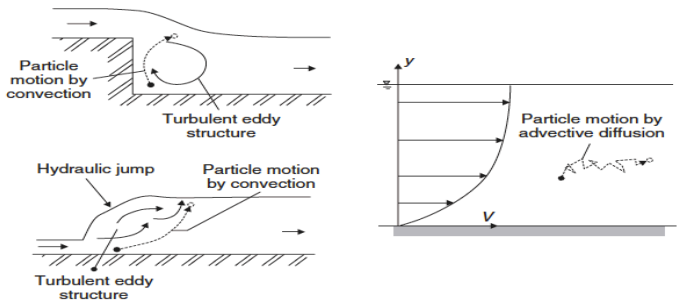

Fig. 1.7. Suspended-sediment motion by convection and diffusion processes

1.4.2.1 Inception of suspended load motion:

With increasing shear velocities, the number of particles bouncing and rebounding increases until the cloud of particles becomes a suspension. The onset of sediment suspension is not a *clearly* defined condition. Considering a particle in suspension, the particle motion in the direction normal to the bed is related to the balance between the particle fall velocity component ($w\,cos\theta$) and the turbulent velocity fluctuation in the direction normal to the bed. Turbulence studies *(e.g. Hinze, 1975;Schlichting, 1979)* suggested that the turbulent velocity fluctuation is of the same order of magnitude as the shear velocity.

With this reasoning, a simple criterion for the initiation of suspension (which does not take into account the effect of bed slope) is:

$$\frac{V_*}{w_o} > \text{Critical value} \tag{1-12}$$

Several researchers proposed criterion for the onset of suspension (Table.1.3). In a first approximation, suspended sediment load occurs for:

$$\frac{V_*}{w_o} > 0.2 \text{ to } 2 \tag{1-13}$$

Reference (1)	Criterion for suspension (2)	Remarks (2)
Bagnold (1966)	$\frac{V_*}{w_o} > 1$	As given by van Rijn (1993)
van Rijn (1984b)		Deduced from experimental investigations
	$\frac{V_*}{w_o} > \frac{4}{\sqrt[3]{\frac{(s-1)g}{\nu^2}}d_s}$	For $1 < \sqrt[3]{\frac{(s-1)g}{\nu^2}}d_s \le 10$ where $d_s = d_{50}$
	$\frac{V_*}{w_o} > 0.4$	For $\sqrt[3]{\frac{(s-1)g}{\nu^2}}d_s > 10$ where $d_s = d_{50}$
Raudkivi (1990)		Note: *rule of thumb* (Raudkivi, 1990: p. 142)!
	$\frac{V_*}{w_o} > 0.5$	Inception of suspension (i.e. saltation)
	$\frac{V_*}{w_o} > 1.2$	Dominant suspended load (i.e. suspension)
Julien (1995)		Turbulent water flow over rough boundaries.
	$\frac{V_*}{w_o} > 0.2$	Inception of suspension
	$\frac{V_*}{w_o} > 2.5$	Dominant suspended load
Sumer *et al*. (1996)		Experimental observations in sheet flow.
	$\frac{V_*^2}{(s-1)gd_s} > 2$	Sediment size: $0.13 < d_s < 3$ mm

Notes: $s = \rho_s/\rho$; V_* = shear velocity; w_o = terminal settling velocity.

Table. 1.3. Criterion for suspended-load motion

1.4.2.2 Suspended sediment transport rate:

Considering sediment motion in an open channel (Fig. 1.8), the suspended-load transport rate equals:

$$q_s = \int_{\delta_s}^{d} c_s V \, dy \tag{1-14}$$

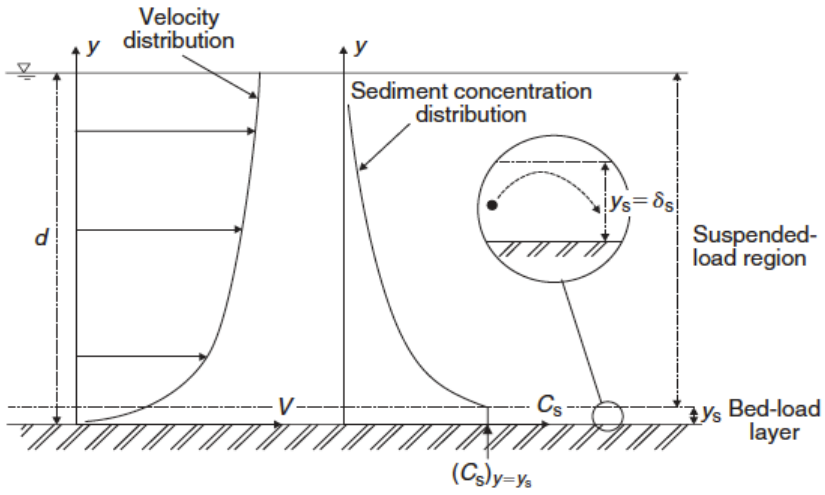

Fig. 1.8. Sketch of sediment-laden flows.

Where q_s is the volumetric suspended-load transport rate per unit width, c_s is the sediment concentration (equation (1-13)), V is the local velocity at a distance y measured normal to the channel bed, d is the flow depth and δs is the bed-load layer thickness.

1.5 Scour:

Scour is the result of the erosive action of flowing water, excavating and carrying away material from the bed and banks of streams. Different materials scour at different rates. Loose granular soils are rapidly eroded by flowing water, while cohesive or cemented soils are more scour resistant. However, ultimate scour in cohesive or cemented soils can be as deep as scour in sand-bed streams. Under constant flow conditions, scour will reach maximum depth in sand and gravel bed materials in hours; cohesive bed materials in days; glacial tills, sand stones and shale in

months; limestone's in years and dense granites in centuries. Under flow conditions more typical of actual bridge crossings, several floods will be needed to attain maximum scour.

A factor in scour at highway crossings and encroachments is whether the scour is clear-water or live-bed scour. Clear-water scour occurs where there is no transport of bed material upstream of the crossing or encroachment and live-bed scour occurs where there is transport of bed material from the upstream reach into the crossing or encroachment.

1.6 Local Scour

Local scour involves removal of material from around piers, abutments, spurs, and embankments. It is caused by an acceleration of flow and resulting vortices induced by the flow obstructions, and is usually cyclic in nature. Local scour can also be either clear-water or live-bed scour.

The basic mechanism causing local scour at piers or abutments is the formation of vortices (*known as the horseshoe vortex*) at their base (Figure. 1.9). The horseshoe vortex results from the pileup of water on the upstream surface of the obstruction and subsequent acceleration of the flow around the nose of the pier or embankment. The action of the vortex removes bed material from around the base of the obstruction. The transport rate of sediment away from the base region is greater than the transport rate into the region, and, consequently, a scour hole develops. As the depth of scour increases, the strength of the horseshoe vortex is reduced, thereby reducing the transport rate from the base region. Eventually, for live-bed local scour, equilibrium is reestablished and scouring ceases. For clear-water scour, scouring ceases when the shear stress caused by the horseshoe vortex equals the critical shear stress of the sediment particles at the bottom of the scour hole.

In addition to the horseshoe vortex around the base of a pier, there are vertical vortices downstream of the pier called the *wake vortex* (Figure. 1.9). Both the horseshoe and wake vortices remove material from the pier base region. However, the intensity of wake vortices diminishes rapidly as the distance downstream of the pier increases. Therefore, immediately downstream of a long pier there is often *deposition* of material.

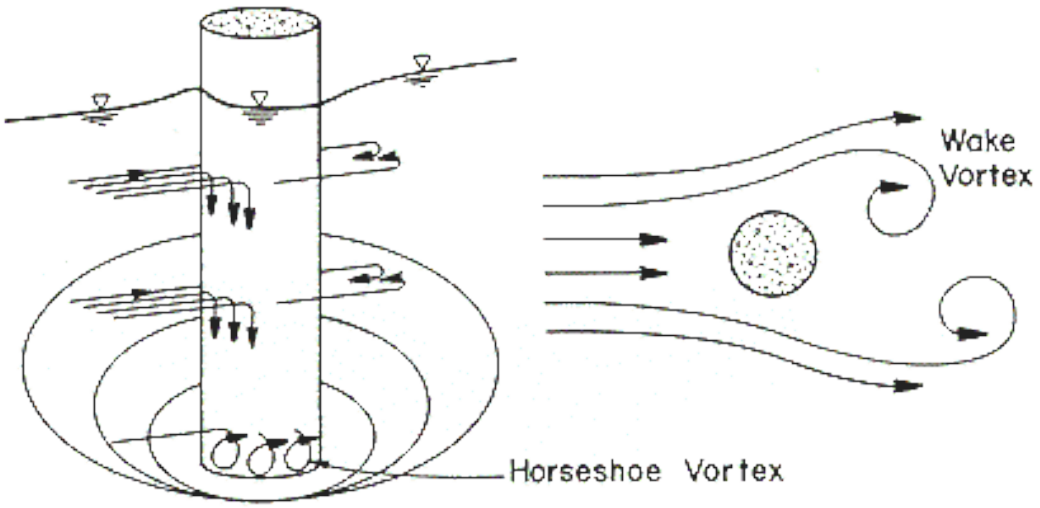

Fig. 1.9. Schematic Representation of Scour at a Cylindrical Pier

Factors which affect the magnitude of local scour at piers and abutments are (1) width of the pier/abutment, (2) discharge intercepted by the abutment and returned to the main channel at the abutment (in laboratory flumes this discharge is a function of projected length of an abutment into the flow), (3) length of the pier/abutment if skewed to flow, (4) depth of flow, (5) velocity of the approach flow, (6) size and gradation of bed material, (7) angle of attack of the approach flow to a pier or abutment, (8) shape of a pier or abutment, (9) bed configuration, (10) ice formation or jams, and (11) debris.

1.6.1 Flow Field:

In nature a stream has its natural flow, but if it is influenced by any obstacles, the flow changes, hence various consequences occur. In case of hydraulic buildings like bridges (abutments, piers) the flow creates a flow field around them. The major scour forces are considered to be the horseshoe vortex and downflow, though the average intensity of the vortex decreases with an increase of scour hole. Also the flow field decreases as the scour hole increases. Since river bed has a relative roughness on the bed, the flow velocities decrease getting closer to the river bed, therefore the velocity profile in longitude cross section forms a curve similar to a parabola. So the velocities are higher at the surface of the flow thereby creating a high pressure in the top layer when the flow runs into a pier or abutment. When that happens the flow divides in two separate sub-flows. One of them is downflow, which has a vertical direction downwards at the obstacle (shown in Fig. 1.10). The other one is the horseshoe vortex (in case of pier scour) or the principal vortex (in case of abutment scour). An illustration of flow pattern in a vertical plane is shown in Fig. 1.11. Horseshoe and wake vortices around a cylindrical pier and an abutment are shown in Figs. 1.12 and 1.13, respectively.

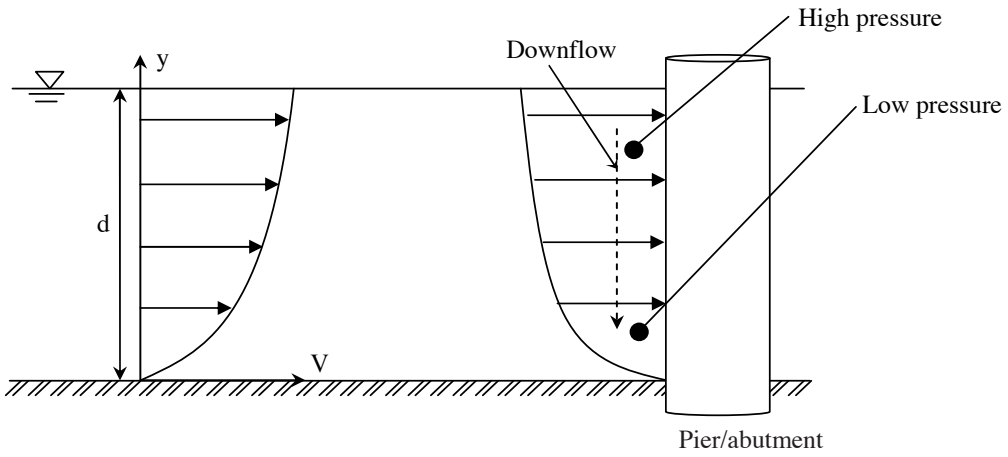

Figure. 1.10. Two-dimensional flow field at pier or abutment.

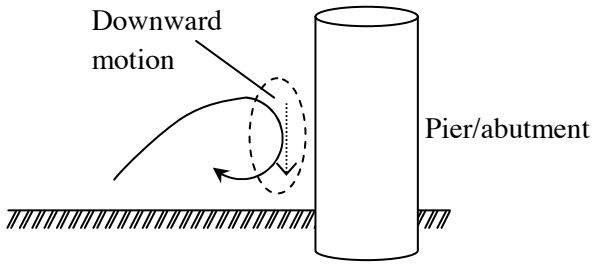

Figure. 1.11. Illustration of the flow pattern in a vertical plane.

Structures constructed in a river become submerged when the flow depth is higher than the height of the structure. For instance, a well foundation of a bridge pier gets submerged when it receives a high flood during its construction. Also, the bridge piers act as submerged piers when an overdesign flood discharge that flows over the bridge deck passes the bridge site. Sometimes a structure along the riverbanks for the bank protection behaves as if it were a submerged structure during high floods. The main component features of the flow field at a cylindrical obstacle resting vertically on a rigid flat bed and that within a scour hole are shown in Figs. 1.14(a-d). For un-submerged obstacles (such as bridge piers), the flow is characterized by the downflow, horseshoe vortex, wake vortex and bow wave (Figs. 1.14(a and b)). On the other hand, for submerged obstacles the additional component of flow is the trailing vortex developed at the top of the cylinder. However, the size and the strength of the horseshoe vortex diminish and those of the downflow become feeble for submerged obstacles (Figs. 1.14(c and d)).

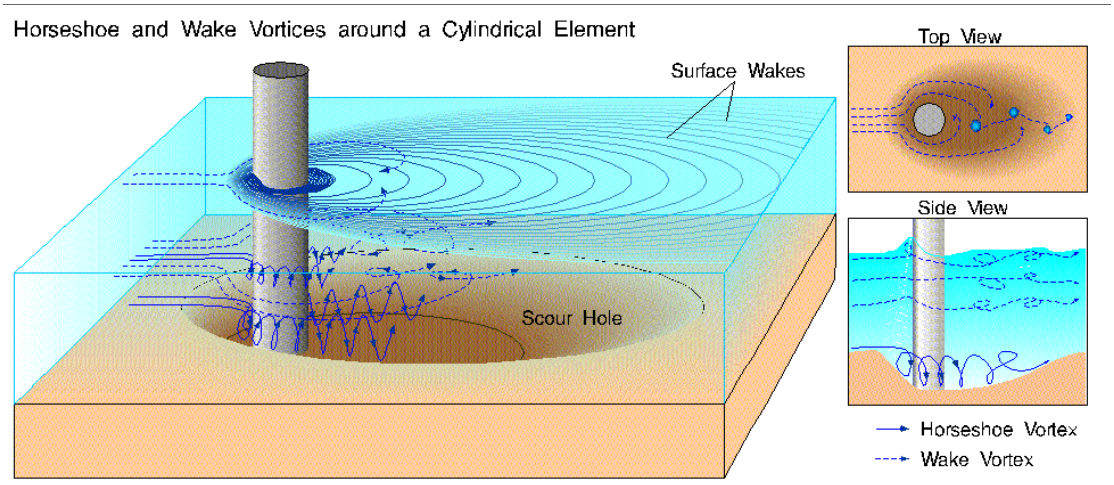

Figure 1.12. Three-dimensional flow field around a cylindrical pier.

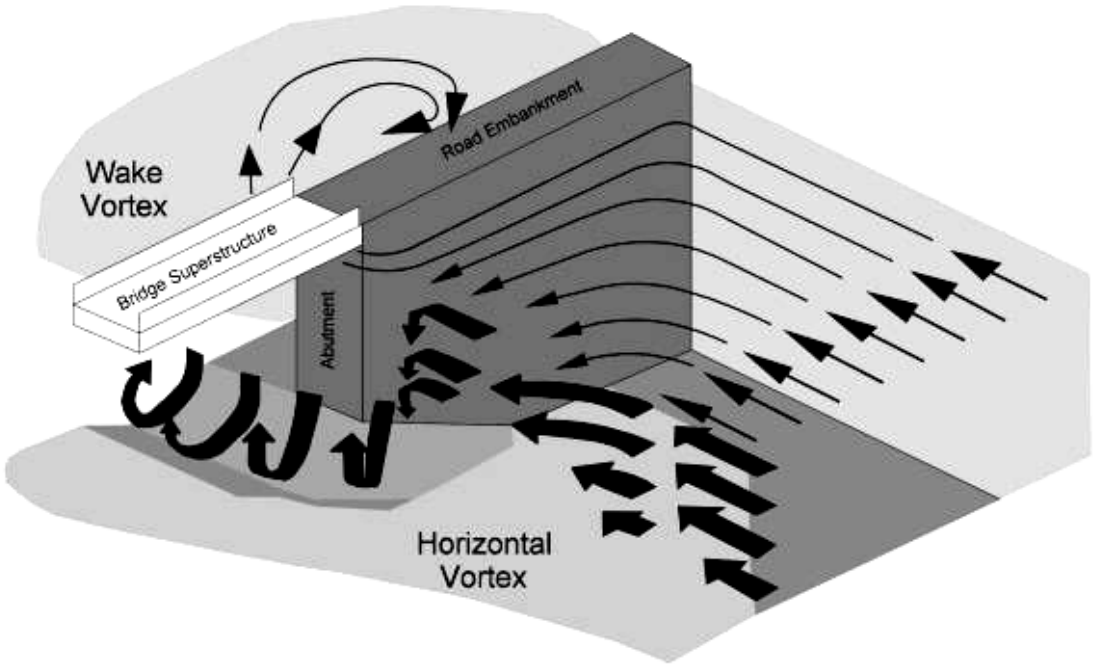

Figure 1.13 Three-dimensional flow field around an abutment.

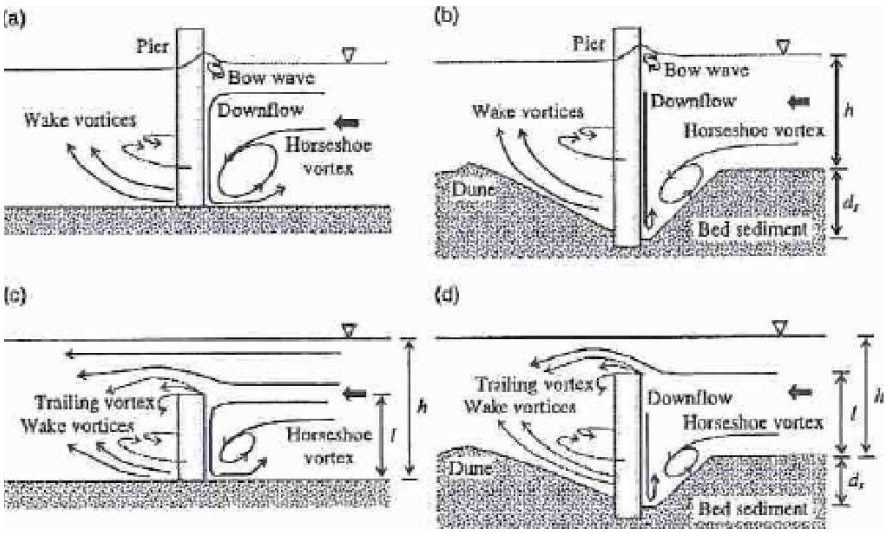

Figure 1.14. Flow features at circular cylinders: (a) un-submerged cylinder on rigid flat bed; (b) un-submerged cylinder in scour hole; (c) submerged cylinder on rigid flat bed; and (d) submerged cylinder in scour hole.

1.6.2 Clear-water and Live-Bed scour:

There are two conditions for contraction and local scour. These are *clear-water* and *live-bed s*cour. Clear-water scour occurs when there is no movement of the bed material in the flow upstream of the crossing, but the acceleration of the flow and vortices created by the piers or abutments causes the material in the crossing to move. Live-bed scour occurs when the bed material upstream of the crossing is moving.

Typical clear-water scour situations include (1) coarse bed material streams, (2) flat gradient streams during low flow, (3) local deposits of larger bed materials that are larger than the biggest fraction being transported by the flow (rock riprap is a special case of this situation), (4) armored streambeds where the only locations that tractive forces are adequate to penetrate the armor layer are at piers and/or abutments, and (5) vegetated channels where, again, the only locations that the cover is penetrated is at piers and/or abutments.

During a flood event, bridges over streams with coarse bed material are often subjected to clear-water scour at low discharges, live-bed scour at the higher discharges and then clear-water scour on the falling stages. Clear-water scour reaches its maximum over a longer period of time than live-bed scour (See Figure. 1.15). This is because clear-water scour occurs mainly in coarse bed material streams. In fact, local clear-water scour may not reach a maximum until after several floods.

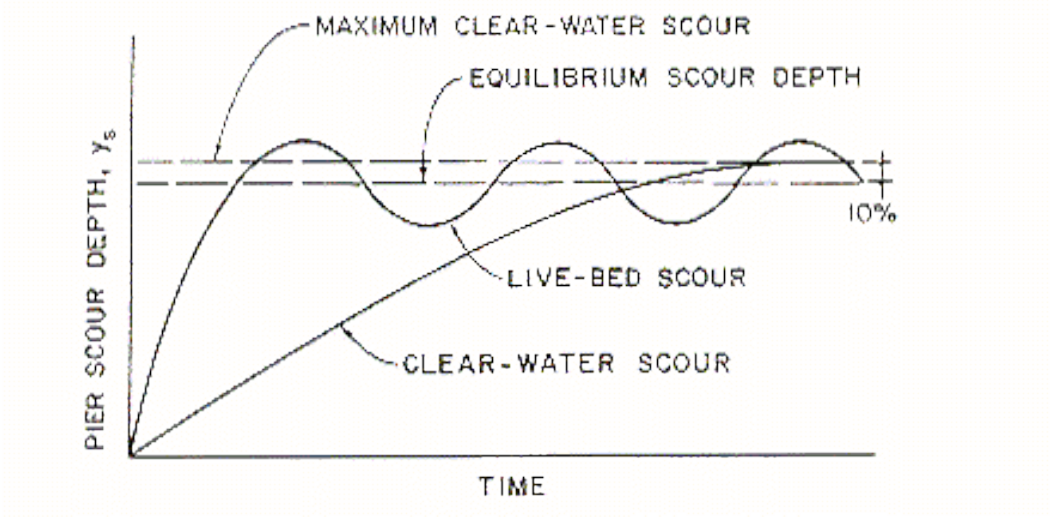

Fig. 1.15. Illustrative Pier Scour Depth in a Sand-Bed Stream as a Function of Time (not to scale)

Live-bed pier scour in sand-bed streams with a dune bed configuration fluctuates about the equilibrium scour depth (Figure. 1.15). This is due to the variability of the bed material sediment transport in the approach flow when the bed configuration of the stream is dunes. However, with the exception of crossings over large rivers (i.e., the Mississippi, Columbia, etc.), the bed configuration will plane out during flood flows due to the increase in velocity and shear stress. For general practices, the maximum depth of pier scour is approximately *10 percent greater* than equilibrium scour. This is not illustrated in Figure. 1.15.

1.6.3 Estimation of Local scour depth:

Equilibrium depth of local scour, d_s at an abutment can be written as follows.

$$d_s = f(\rho, v, U, y, \rho_s, d_{50}, \sigma_g, L, Sh, Al, G, g) \tag{1-15}$$

Where ρ and v – fluid density and kinematic viscosity, respectively; U – mean flow velocity; ρ_s – sediment density; d_{50} and σ_g – median size and geometric standard deviation of the sediment particle size distribution; Sh and Al – parameters describing the shape and alignment of the abutment, G – parameter describing the effects of lateral distribution of flow and cross-sectional shape of the approach channel; g – acceleration of gravity; L – the length of a pier or abutment; y – flow depth; and f denotes a function of.

Assuming constant relative density of sediment and the absence of viscous effects (1) can be written as:

$$\frac{d_s}{L} = f\left(\frac{U^2}{g d_{50}}, \frac{y}{L}, \frac{d_{50}}{L}, \sigma_g, Sh, Al, G\right)$$

Or

$$\frac{d_s}{y} = f\left(\frac{U^2}{g d_{50}}, \frac{L}{y}, \frac{d_{50}}{y}, \sigma_g, Sh, Al, G\right) \tag{1-16}$$

(1-17)

Where the scour depth is normalized with abutment or pier length and flow depth in (1-15) and (1-16), respectively. It is shown below that (1-15) is more applicable to short piers or abutments (L/y < 25) while (1-16) is better for long piers or abutments (L/y > 25).

Kwan (1988) measured the velocity field around a relatively short (i.e. small L/y) wing-wall abutment. He found that the primary vortex, which is analogous to the well-known horseshoe vortex at bridge piers, is primarily responsible for scour hole development. Kwan concluded it was the down-flow associated with the primary vortex that was the main scour agent – a similar conclusion to that for piers. Kwan also showed that the flow pattern was relatively unaffected by changes in approach flow depth – again, a similar conclusion to that for piers. In particular, he found that the primary vortex and down-flow are confined predominantly within the scour hole beneath the original bed level, and that the maximum down-flow was of the same magnitude regardless of the flow depth. Kwan, thus concluded that, as for piers, scour depth scales with abutment length. Thus for short abutments, (2) is appropriate. At the other extreme (i.e. large L/y), it is postulated and confirmed by the data that local scour depth at long abutments scales with flow depth. Equations (2) and (3) can be evaluated using laboratory data by writing them in the form

$$\frac{d_s}{L} = K_I K_y K_d K_\sigma K_s K_\theta K_G \tag{1-18}$$

$$\frac{d_s}{y} = K_I K_L K_d K_\sigma K_s K_\theta K_G \tag{1-19}$$

Where the K-factors are expressions describing the influence of each parameter in (1-15) and (1-16); K_I - flow intensity; K_y - flow depth; K_d - sediment size; K_σ - sediment gradation; K_L - abutment length; K_s and K_θ - abutment shape and alignment, respectively; and K_G - approach channel geometry. This approach is based on that adapted by Melville and Sutherland (1988) for their design method for local scour at bridge piers. The parameters in 1.18 and 1.19 are now considered individually.

1.6.4 Obstacle size and flow depth

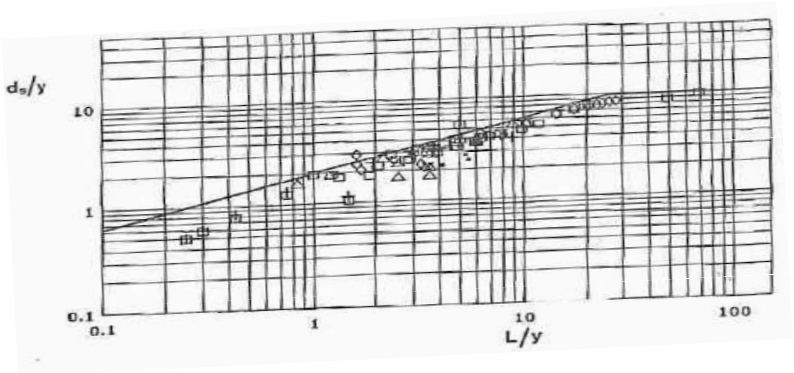

Fig. 1.16. Influence of Abutment Length on Scour Depth.

As shown in Fig. 1.16 scour depth increases with increasing abutment length toward the following limiting scour depth: $d_s = 10y \quad \frac{L}{y} \geq 25.$

Symbol (1)	Abutment Type (2)	Authors (3)
◊	Vertical wall with semicircular end	Kwan (1984), Tey (1984)
□	Wing wall	Kandasamy (1989), Kwan (1988), Dongol (unpublished abutment scour data, 1990)
+	Vertical wall	Gill (1972), Dongol (unpublished abutment scour data, 1990)
×	Spill-through (H:V = 0.5:1)	Dongol (unpublished abutment scour data)
■	Spill-through (H:V = 1:1)	Wong (1982), Tey (1984)
Δ	Spill-through (H:V = 1.5:1)	Wong (1982)

Table.1.4. Key for Symbols in Figures 1.16 and 1.17.

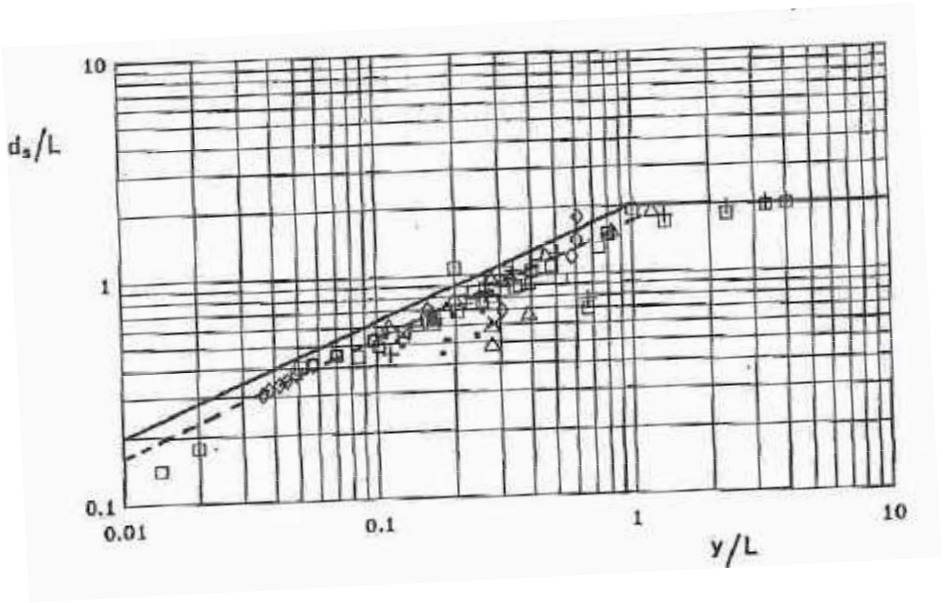

Figure. 1.17. Influence of Flow Depth on Scour Depth

In Fig. 1.17 the scour depth increases with increasing flow depth toward the following limiting scour depth $d_s = 2L \quad \frac{y}{L} \geq 1.$

1.6.5 Pier and Abutment Alignment and Shape:

Bridge abutments and piers are designed in a large variety of sizes and shapes. Generally, the geometry of bridge abutments can be described in terms of the size of the obstruction (i.e. the length L) together with a shape factor to account for differences in shape and the angle between the approach flow and the abutment (i.e. the alignment).

It is well established that local shape is important in abutment scour. Different shapes divert flows

in a different manner and as expected, streamlined shapes create fewer disturbances and hence produce less scour than blunt shapes. The effect of shape is expressed using the shape factor Ks. Values of the shape factor are given in Table 4 and the shapes are shown in Fig. 1.19.

Foundation type (1)	Shape (2)	K_s (3)
Pier	Circular cylinder	1.0
	Round nosed	1.0
	Square nosed	1.10
	Sharp nosed	0.90
Abutment	Vertical wall	1.0
	Vertical wall (with semicircular end)	0.75
	Wing wall	0.75
	Spill through 0.5:1 (H:V)	0.60
	Spill through 1:1	0.50
	Spill through 1.5:2	0.45

Table. 1. 4. Shape factors for Piers and Abutments

The Ks. Values for piers in Table 4 apply only for piers aligned with the flow.

The abutment alignment is defined by the angle θ, as shown in Fig. 1.18. It has generally been found that the scour depth increases with an increase in θ, as shown in Fig. 1.18. Using the perpendicularly aligned abutment (θ = 90°) as a reference, abutments pointed upstream are seen to produce larger scour depths (as much as 10% increase for angles between 150-180°). By contrast, the scour depth is reduced as θ is decreased, and for the range of values investigated, the maximum decrease is 17% when the abutment is pointed downstream at 30°.

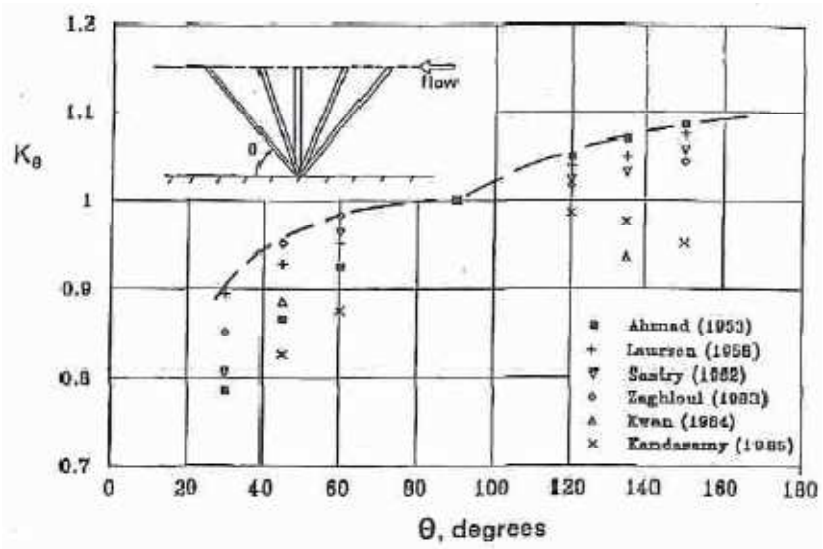

Figure. 1.18. Influence of Abutment Alignment on Scour Depth.

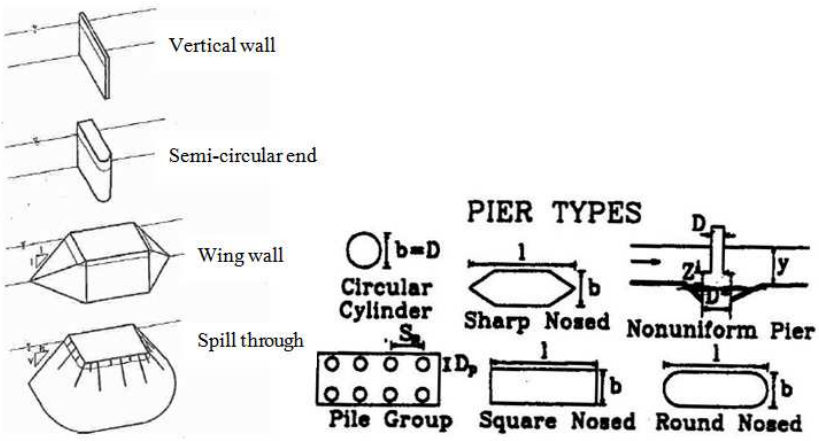

Figure. 1.19. Geometric classification of piers and Abutments for scour purposes.

1.6.6 Sediment Size:

Ettema (1980) for clear-water flows and *Chiew (1984)* for live-bed scour, defined the influence of sediment size on scour depth at circular piers for uniform sediments. Their data show that d_s increases with the relative sediment size $\left(\frac{b}{d_{50}}\right)$ up to $\frac{b}{d_{50}}$ =50.

For $\frac{b}{d_{50}} > 50$, d_s is independent of the sediment size. *Ettema* explained that the reductions in scour depth for relatively large sediments were due to large particles impeding the erosion process at the base of the scour hole and dissipating some of the flow energy in the erosion zone.

The pier data by *Ettema* and *Chiew* are plotted in Fig. 1.20. in terms of the sediment size multiplying factor K_d , which is defined generally as the ratio of scout depth for a particular $\frac{W}{d_{50}}$ to that for $\frac{W}{d_{50}} \geq 50$. The pier data are augmented with abutment scour data by *Dongol (1994)*, plotted in term of $\frac{L}{d_{50}}$ rather than $\frac{b}{d_{50}}$. The latter were obtained at the threshold condition for sediment movement using a vertical-wall abutment model and uniform sediments. All the data shown in Fig. 1.20.(a) were obtained for relatively deep flows and thus have no influence of flow depth. The plot shows that the influence of relative sediment size on scour depth is the same for both and abutments, although more data are needed to confirm this finding for abutments.

Because the condition $\frac{W}{d_{50}} < 50$ is unlikely in practice, it is considered that the few abutment data shown in Fig. 1.20. are adequate for preliminary definition of K_d for design purpose.

The envelope curves in Fig. 1.19(a) define the sediment size factor for design purposes and have the following equations:

$$K_d = 0.57 \log\left(2.24 \frac{W}{d_{50}}\right), \frac{W}{d_{50}} \leq 25;\ K_d = 1.0, \frac{W}{d_{50}} > 25 \qquad (1\text{-}20)$$

Where $W = b$ for piers; and W = L for abutments. These equations are identical to those given in *Melville and Sutherland (1988)*.

The data used to determine (1-18) apply to uniform sediments. Consideration is now directed to sediment size effects for non-uniform sediments, which are characterized by channel bed armoring. In Fig. 1.19(b), data for non-uniform sediments are plotted for different values of the velocity parameter $[V - (V_a - V_c)]/V_c$.

The data are plotted in terms of $\frac{\mathrm{b}}{\mathrm{d_{50a}}}$ or $\frac{\mathrm{L}}{\mathrm{d_{50a}}}$ because the median size of the armor layer is considered to be the characteristic sediment size. Thus for non-uniform sediments, (1-18) is expressed in terms of $\frac{W}{d_{50a}}$ Fig. 1.20(b) includes data by *Ettema (1980), Chiew (1984),* and *Baker (1986)* for piers and *Dongol (1994)* for abutments. The former were obtained at the value $[V - (V_a - V_c)]/V_c = 1.0$, while those from the other authors were obtained for a range of flow velocities, including $[V - (V_a - V_c)]/V_c$ = 1.0, 2.0, 3.0, and 4.0, as shown. With two minor exceptions, the data lie within the envelope curves for uniform sediments. The agreement between the data and the envelope curves improves with increasing velocity.

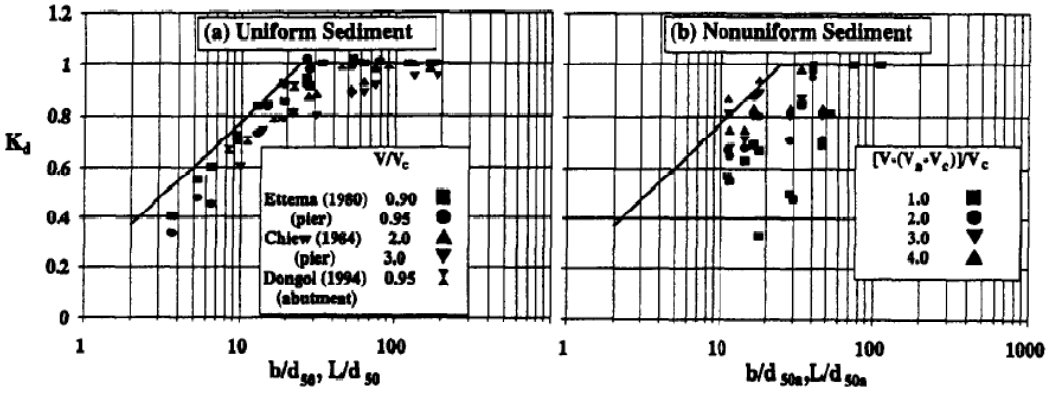

Figure. 1.20. Sediment Size Factor for Piers and Abutments: (a) Uniform Sediment Data; (b) Non-uniform Sediment Data.

1.6.7 Sediment Gradation:

The materials that form the boundaries of river channels may range from boulders to silts and clays and are usually inhomogeneous. The deposits may also have complex grain size distributions and be stratified.

It is normal to divide the deposits into cohesive and non-cohesive (or alluvial) sediments.

The simplest means of describing alluvial river sediment is the median particle size, d_{50}. For uniform materials d_{50} is adequate, but it is quite inadequate for non-uniform materials. The different size fractions have entirely different resistance to scour and their interactions are complex. Sediment non-uniformity is described by the *geometric standard deviation*, σ_g of the particle size distribution. Sediments with $\sigma_g \leq 1.3$ can be assumed to be uniform.

A streambed may also be composed of a series of strata of different resistance to scour. Where a relatively resistant material overlies a more readily erodible material, large scour depths may result if the scour breaks through the resistant material. Conversely, if a highly resistant material is known to exist at a particular level, it may be unnecessary to extend bridge foundations below that level. Variation in material type is not restricted to vertical stratification. Variation of sediment over the cross section can influence the scouring process.

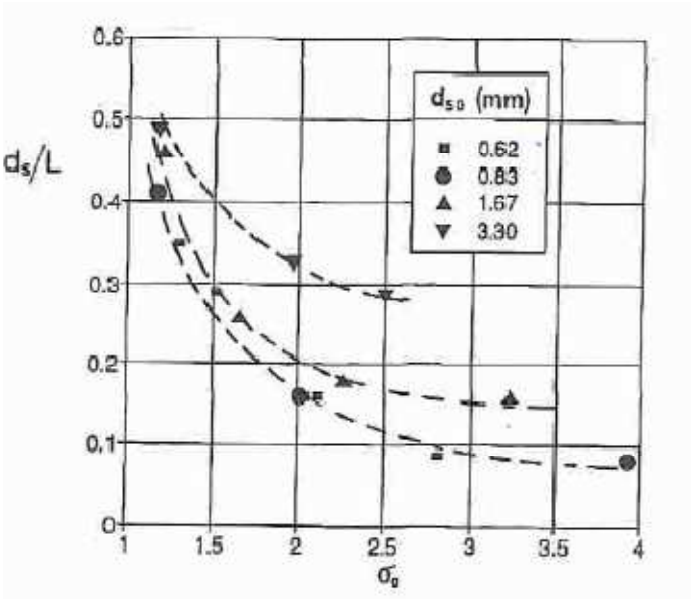

Figure. 1.20. Influence on Sediment Gradation on Scour Depth.

The variation of particle size distribution has a pronounced influence on local scour depth. Non-uniform sediment mixtures (σ_g > 1.5-2.0) have been reported to consistently produce lower scour depths than uniform sediments. Data by *Wong (1982)* for a wing-wall abutment are plotted in Fig. 1.20. The plot demonstrates the dramatic decrease in scour depth that occurs for widely graded sediments. Wong obtained similar results for spill-through abutments. However, Wong's data were measured under clear-water scour conditions. Data by *Baker (1986)* for pier scour graded sediments under live-bed conditions show that sediment gradation effects are considerably reduced at higher flow intensities. This is because bed armoring, which limits scour at lower flows, diminishes with increasing flow velocity until all for non-uniform sediments, K_σ is assumed herein to be unity. This means that scour depths given apply to uniform sediments.

1.6.8 Flow Intensity:

The Shield diagram defines the critical shear velocity for a given d_{50}.A corresponding critical mean

velocity, U_c can be found for the given flow depth, and thus the parameter $U^2/g\mathrm{d}_{50}$ can be written using given data as U/U_c . This ratio is thus a measure of flow intensity and determines whether grain motion occurs. If U/U_c . < 1, clear-water scour conditions pertain, whereas for U/U_c > 1, live-bed scour occurs.

There is ample evidence that the maximum scour depth at bridge piers occurs at the threshold condition for sediment movement, i.e., at the boundary between clear-water and live-bed conditions. There is additional evidence that the same may hold true for scour at abutments. Under clear-water conditions, scour depths increase with increasing flow velocity and the maximum clear-water scour depth occurs at the threshold of sediment movement. There are many data that substantiate this finding, and for this reason most experiments have been conducted at the threshold condition.

1.6.9 Approach Channel Geometry:

The approach channel geometry can have very significant influence on local scour depth, particularly for longer abutments. Bridge abutments can be set back from the natural stream bank or can project out into the flow, and there can be varying amounts of overbank flow that are intercepted by the approaches to the bridge and returned to the stream at the abutment. Scour at an abutment can be caused by the abutment projecting into the flow, it can be caused by the bridge approaches intercepting overland flow and forcing it back into the channel at the abutments, or it can be a combination of conditions, as discussed by Richardson et al. (1988).

Approach channel geometrical effects are included in the factor K_G. In general, K_G will depend on the relative size, shape and roughness of the main channel and flood plain channel, and on the abutment length in relation to the flood plain width.

1.7 Local Scour Countermeasures:

The problem of local scour of sediment around bridge piers has been studied extensively for several decades. In places where the river bed is easily vulnerable by flow field, which gets created around a bridge pier or abutment, it is required that the pier/abutment is embedded deeply into the river bed, however it is not profitable to anyone to do so. Consequently, there is an interest in finding reliable ways to reduce scour depth and thereby, requisite pier embedment depth. Scour mitigation at bridges has received much attention in the past. In recent years, extensive research has been aimed at finding methods to efficiently reduce the expected scour levels at both piers and abutments, the latter being within the scope of this work.

Scour countermeasures are typically divided into (a) bed-armoring devices and (b) flow- altering devices. The former increase the resistance of the riverbed and include riprap blocks or similar tools *(recent examples for abutments include Melville et al., 2006a and 2006b; Korkut et al., 2007; Cardoso and Fael, 2009; Sui et al., 2010)*. The latter (examples for pier protection are given when they are not available for abutments) reduce the strength of the turbulent flow field and include collars and/or slots *(e.g., Dargahi, 1990; Chiew, 1992; Kumar et al., 1999; Zarrati et al., 2004; Heidarpour et al., 2010),* vanes *(e.g., Johnson et al., 2001; Li et al., 2006)*, sacrificial piles *(Melville*

and Hadfield, 1999; Haque et al., 2007), structure threading *(Dey et al., 2006)*, and sills *(e.g., Chiew and Lim, 2003; Grimaldi et al., 2009), roughened abutment (e.g., Radice and Lauva, 2013)*. In some cases, combinations of bed-armoring and flow-altering devices has been proposed *(e.g., Mashahir et al., 2010; Zarrati et al., 2010)*

The former considerations in choosing the appropriate method of mitigation, other than design constraints, include maintenance and inspection requirements, enhancement of the physical environment, and constructability. Design specifications for many of these scour mitigation techniques can be found in Hydraulic Engineering Circular No. 23 (Lagasse et al. 2001).

1.7.1 Armoring Countermeasures:

Armoring countermeasures for bridge piers/abutments include *riprap, cable-tied blocks*, *geo-bags*, *grout- filled bags*, etc. Generally they form a layer at the area where scour takes place and have the capability to withstand high shear stresses during high flow events. As a consequence, the bed materials underneath the armoring layer are protected from being scoured away. *Riprap* is by far the most commonly used of the armoring methods (Fig. 1.21).

1.7.1.1 Riprap:

The riprap matting around piers/abutments creates a physical barrier intended to resist the eroding capacity of the flow and it is the most widespread countermeasure. Some guidance for the use of riprap at piers/abutments is included, for example in Ministry of *Works and Development (1979), Austroads (1994)*, or *Richardson* and *Davis (1995*). According to *Melville et al. (2007)*, the theoretical and empirical basis of the existing equations for the sizing of riprap blocks is limited.

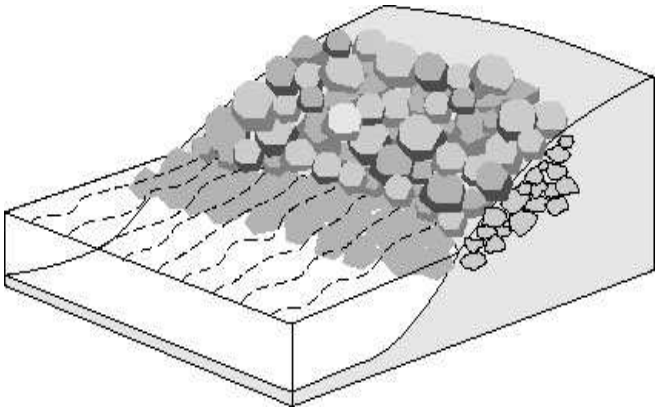

Fig . 1.21. Riverbed armoring method-Riprap

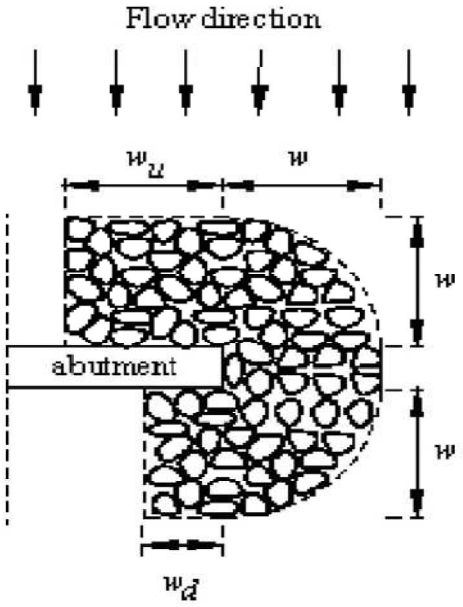

Fig. 1.22. Layout of Riprap mattress for vertical wall abutments

Recently, there has been a significant research effort focused on the design of riprap aprons to protect piers/abutments. Most of these studies are described in *Melville et al. (2006 a, b; 2007)*. They cover spill- through as well as wing-wall abutments for both clear water and live bed flow conditions. In spite of these recent efforts, studies concerning countermeasures for vertical-wall abutments are not abundant, and engineering practice is still based on limited evidence. Ignoring that protection itself is a factor influencing scour, engineers frequently assume, for instance, that mattresses should cover the predicted scour area of the riverbed around bridge piers or abutments. One way how to lay out the riprap around a vertical-wall abutment is shown in Fig. 1.22.

Problems encountered with armoring at abutments include winnowing of sands through the armor and an inability to keep the armor in place. In addition, armor can constrict the channel, causing additional contraction scour *(Chiew and Lim 2000; Lauchlain and Melville 2001; Lim and Chiew 2001, Chiew 2004).*

The correct characterization of design variables such as the stone size, layer thickness, and mattress plan dimensions requires an understanding of mattress failure mechanisms. According to *Eve and Melville (2000),* the failure mechanisms of riprap are essentially the same for bridge abutments as for piers. For clear-water conditions, *Parola (1993), Chiew (1995), and Lauchlan (1999)* identified three failure mechanisms: *shear failure, winnowing failure, and edge failure*. Shear failure is clearly linked with the riprap size; winnowing depends on the thickness of mats and on the gradation coefficient of the riprap stones; and edge failure and plan dimensions are strongly interrelated.

1.7.2 Flow-altering countermeasures:

Flow-altering countermeasures for bridge abutments include *guide banks, spur dikes, bend way weirs and Iowa vanes, slot, collar, splitter plate and threaded pile, sacrificial piles*. They basically work to alter the flow alignment to transfer the scour potential away from the vicinity of bridge

abutments.

1.7.2.1 Spur Dikes:

Spur dikes (Fig. 1.23) have been used extensively in all parts of the world as river training structures to enhance navigation, improve flood control and protect erodible banks (Copeland (1983). An example of spur dike design for realignment of a channel at a bridge crossing was shown in Lagasse et al. (2001).

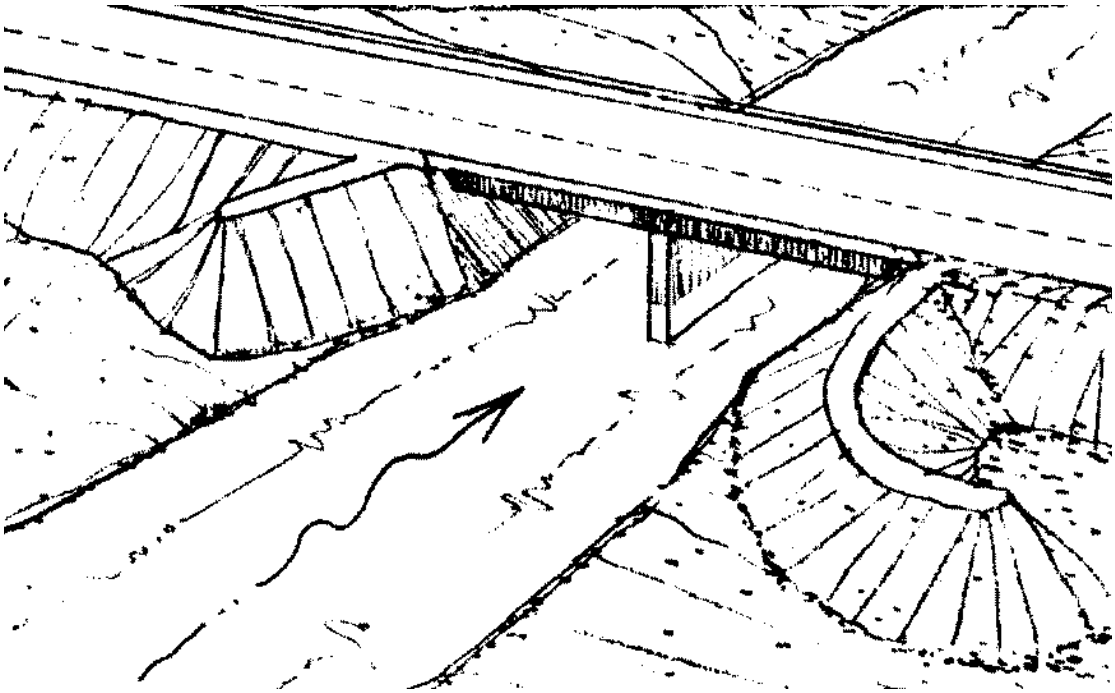

Figure 1.23. Spur dike at bridge construction.

1.7.2.2 Bendway weirs:

Bendway weirs (Fig. 1.24), also referred to as stream barbs, bank barbs and reverse sills are low-level, upstream-angled stone sills attached (and keyed into) the outer bank of the bend. They are generally used to improve lateral stream stability and to reduce erosion on the outer banks of the bends by reducing near bank velocities, reducing the concentration currents on the outer bank of the bend, producing a better current alignment through the bends and crossings, and aligning flow to correctly pass through the highway bridge opening. *Derrick (1994)* reported use of bendway weirs to redirect river flow to protect highway bridge abutments.

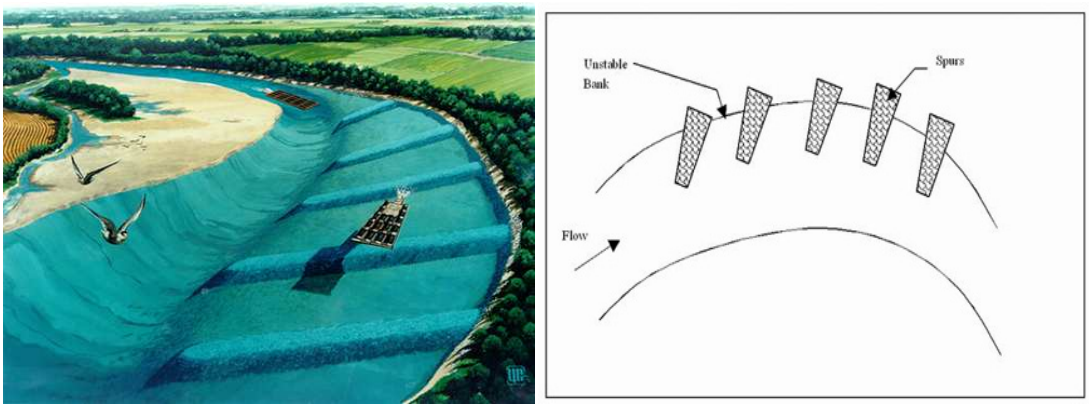

Figure 1.24. Models of Bendway Weirs in rivers.

1.7.2.3 Submerged Vanes:

Submerged vanes (Fig. 1.25) are small river training structures used for protection of streambanks against erosion and for amelioration of shoaling problems in navigation channels, at water intakes, in bridge crossings and at diversions. A field installation at a highway crossing of the West Fork Cedar River in Butler County, Iowa *(Odgaard and Wang 1991)* demonstrated the effectiveness of submerged vanes in ameliorating prototype-shoaling problems and protecting the abutment. *Johnson et al. (2001)* studied the effectiveness of vanes for preventing scour at single-span bridges with vertical wall abutments based on laboratory experiments.

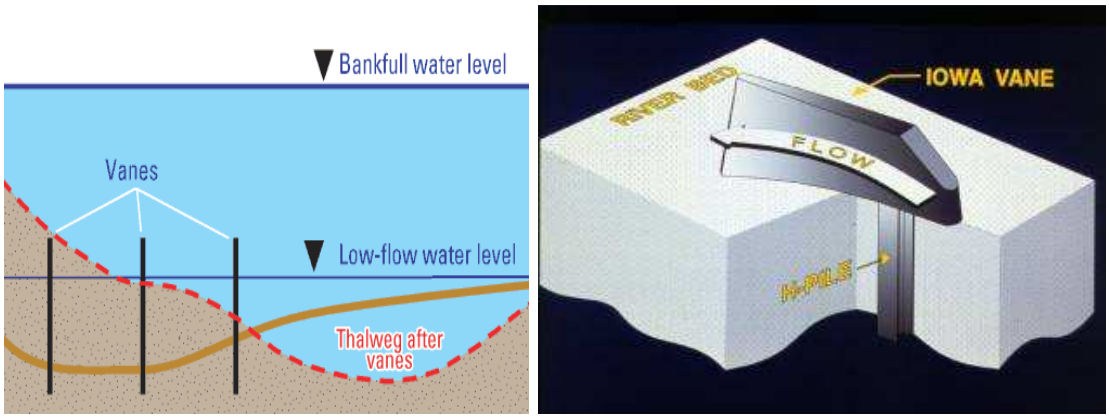

Figure. 1.25. (a) Example of Submerged vanes in river, (b) Iowa vane.

1.7.2.4 Guide Banks:

Guide banks are earth and rock embankments placed at abutments to improve the flow alignment and move the local scour away from the embankment and bridge abutment. The guide bank provides a smooth transition for flow on the flood plain to the main channel. The major use of

guide banks in the United States has been to prevent erosion by eddy action at bridge abutments or piers where concentrated flood flow traveling along the upstream side of an approach embankment enters the main flow at the bridge *(Langasse et al. 2001).* Guide banks have been specifically designed for spill-through abutments on rivers with wide floodplains where the guide bank can be designed such that the slope of the guide bank is tangent to the slope of the abutment and there is no protrusion of the abutment into the flow beyond the slope of the guide bank. However, in a wing-wall case, this point may not be achieved readily because of the vertical front faces of the abutments. In this situation either the slope of the guide bank protrudes out beyond the abutment face or the abutment face protrudes out beyond the guide bank slope.

1.7.2.5 Rectangular Slot:

Local scour around a solid pier results from the downflow at the upstream face of the pier and the horseshoe vortex at the base of the pier. Hence, one way of reducing scour is to weaken and possibly prevent the formation of the downflow and horseshoe vortex. Depending on its location, a slot may deflect the downflow away from the bed by accelerating the bottom boundary layer flow through itself as a horizontal jet, and by breaking up the horseshoe vortex when the slot is placed near the bed. When placed near the water surface, a slot effectively reduces the downflow and horseshoe vortex. A slot is shown to be effective in reducing scour, particularly if the slot extends into the bed. Nevertheless, the slot is practically ineffective if the approach flow has a high obliquity with respect to the slot.

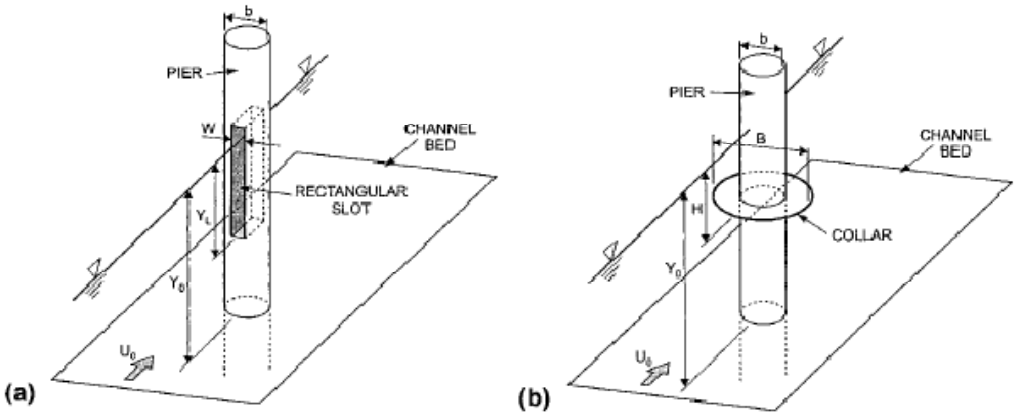

Figure. 1.26. (a) Slot through Pier; (b) Collar on Pier.

1.7.2.6 A Collar around a pier:

A collar at any level above the bed divides the flow into two regions above and below the collar (Fig. 1.27). For the region above the collar, it acts as an obstacle against the down flow and the down flow loses its strength on impingement at the collar. For the region below the collar, the strength of down flow and therefore the horseshoe vortex is reduced. The efficiency of a collar depends on its size and location on the pier with respect to the bed.

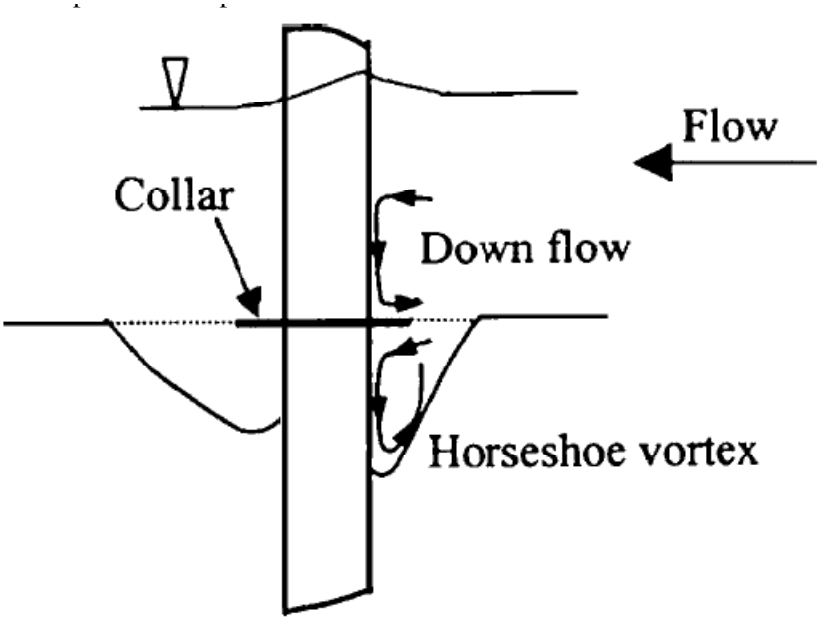

Figure 1.27. Scouring and flow pattern around a pier protected by a collar.

In general, the deepest scour occurs at the upstream face of the pier for smaller-sized collars placed at higher elevations, and in the wake for larger-sized collars placed at lower elevations. If there is a *2.5b* sized collar at bed level (*b* is pier diameter shown in Fig.128) there is considerably less scour in the front of the pier than on the sides and in the rear of the plate. A 4.0b sized collar produces no scour at all in the front and on the sides, but deep scour in the piers rear. The absence of scour in the front and sides precludes deposition of material in the wake and at higher scour in the wake is thus understandable.

Figure below is shown using a group of two arranged in line. For each arrangement the spacing *S/b* of the piers was varied, where *S* – the distance between center of the piers sections; and *b* – pier diameter. In the group of two piers (i.e., in line) two types of collars were employed: circular collars with a diameter of three times the pier diameter were used as independent collars [Fig. 1.28(a)]. Also, a continuous collar was attached around a group of two piers as shown in Fig. 1.28(b). The width of continuous collar was equal to the diameter of the independent collar. Two series of tests were also carried out with a continuous collar on two piers in line, where the space between the piers [Fig. 1.28(b)] was covered with riprap.

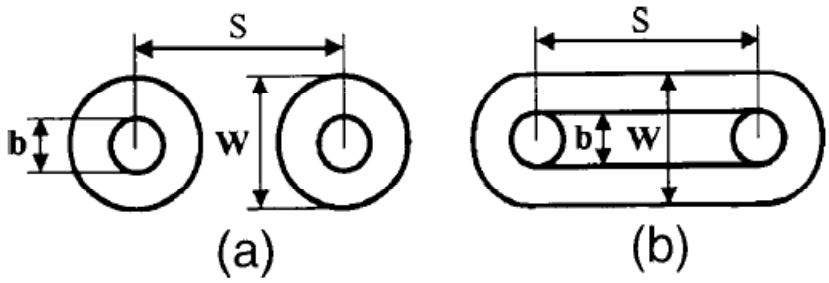

Figure 1.28. Type of collars: (a) independent and (b) continuous.

Collars were installed at the initial bed level for all experiments. The collar width and elevation were chosen based on previous studies. Wider collars are more effective, but construction of collars wider than 3 times the pier diameter is considered impracticable. Also, the efficiency of a collar increases at lower elevations since less flow can penetrate below it *(Tanaka and Yano 1967)*. When a collar is installed below the bed level, penetration of flow below the collar is reduced however the depth above the collar becomes a part of the scour hole.

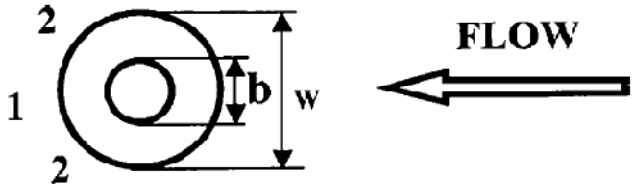

Figure 1.29. Single circular pier with a collar (b – the diameter of the pier; w – the width of the collar).

1.7.2.6 .1 One pier with a collar:

The problem of using the collar at the bed level is that strong wake vortices develop at the rear of the pier, resulting in scouring in region 1 (see Fig. 1.29). These vortices are so strong that form a deep scour hole downstream of the collar. A depression is also developed at both sides of the collar (Region 2, Fig. 1.29). With time grooves at Region 2 move around the rim of the collar at both sides of the pier until they join each other at the front edge of the collar. At this moment, the flow is intensified through the groove, reducing the side slope of the groove and with sediment removal from the grooves the scour hole extends upstream of the pier and below the collar. By penetration of flow beneath the front edge of the collar the rate of sediment removal increases, that gives the opportunity for the horseshoe vortex to appear under the collar.

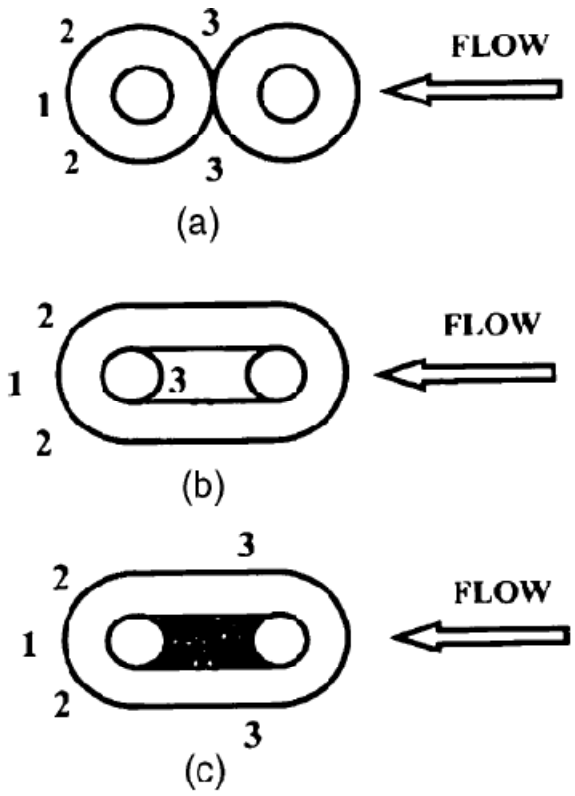

Figure. 1.30. Two piers in line with S/b=3: (a) Independent collars; (b) continuous collar; and (c) continuous collar and riprap.

		Pier scour reduction (%)	
S/b	Type of the collar	Front	Rear
3	Independent	30	75
4	Independent	25	70
2	Continuous	25	-
3	Continuous	25	35
3	Continuous and riprap	50	60

Table 5. Scour Depth Reduction for Piers in Line in Comparison with Hannah (1978)

1.7.2.6 .2 Two piers in line with continuous collars:

It is observed that the space between two piers, which is not covered by the collar [Region 3, Fig. 1.30(b)], is subjected to down flow as well as wake vortices, causing sediment removal from that area and depositing them downstream of the rear pier. Sediment deposition causes some delay in scouring at downstream of the rear pier, which is usually subjected to wake vortices. Also, a couple of grooves form in Region 2, Fig. 1.30(b) and develop in the upstream direction. In further development, the scour hole extends below the collar and all around the rear pier. Scouring then develops around the front pier moving from downstream toward upstream until it causes the

removal of sediment from below the collar at the upstream edge of the front pier. Development of scouring around the front pier is much faster than the case with independent collars. For *S/b* = 2 and 3 reduction of scour depth is about 25% for the front pier (Table 5).

1.7.2.6 .3. Two piers in line with continuous collars and riprap

Experience with continuous collars shows that the space between the piers, which is not covered with collar [Region 3, Fig. 1.30(b)], scours very fast and the depression in this region extends upstream. It was also observed that when the scour hole extends below the collar at the upstream face of the front pier, thereby allowing flow to penetrate below the collar. With penetration of flow below the collar the action of Horseshoe vortex (HSV) is started, accelerating the excavation of the scour hole. It is therefore decided to cover this space inside the continuous collars and between the piers with riprap leveled with the streambed. Two layers of riprap are used with a median diameter equal to 5 mm, which is large enough not to be washed away by the flow. Spacing *S/b* = 3 is tested in this case. At the beginning scouring starts at the back rim of rear collar due to wake vortices [Region 1, Fig. 1.30(c)]. Similar to previous cases two grooves also develop at two sides of this collar [Region 2, Fig. 1.30(c)] extending slowly and with almost constant scour depth in the upstream direction. Two depressions in the same time develop at both sides of the upstream edges of collar in Region 3 and extend upstream. These depressions later reach below the front pier collar creating the down flow. After this, down flow causes scouring around the upstream face of the front pier letting the riprap slide into the scour hole and armor it. At the same time the remaining riprap between the piers is enough for armoring the space between the two piers. Development of scouring around the pier is much slower here comparing with the previous case, which shows the effectiveness of riprap in reducing the rate of scouring. Efficiency of collar at the upstream face of the front pier is about 50% and at the sides of the rear pier's collar is about 60% (Table 5).

1.7.2.7 Splitter Plate and Threaded Pile:

Splitter plate and threaded pile (helical wires or cables wrapped spirally on the pile to form thread) (Fig. 1.31.) are used to control the local flow and vortex shedding so that the development of the scour depth at piles under waves is restricted. The splitter plate that is placed vertically along the streamwise direction helps to divide the flow by the two sides of the pile. Thus, the process of alternate vortex shedding is disrupted, as they are disconnected by the splitter plate. On the other hand, in the case of threaded piles, the projection of the helical wires that formed the threads disturbed the vortex shedding *(Sumer and Fredsoe 1997).* However, the use of larger thread angles (α=60 and 65°), which can encounter well with the wave motion as the line of flow separation on the pile surface is almost vertical, were found to be effective in disrupting vortex shedding.

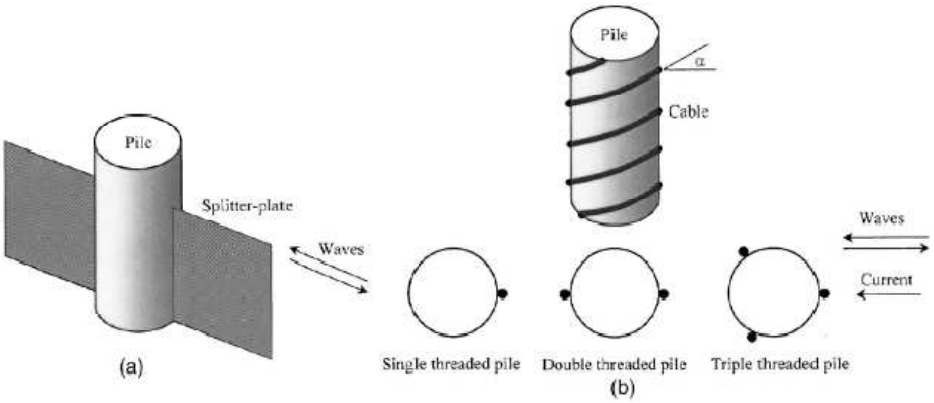

Figure 1.31. (a) Splitter plate attached to the pile along the vertical plane of symmetry; and (b) threaded pile (helical wires or cables wrapped spirally on the pile to form thread).

The scour depth consistently decreases with increasing cable diameter and number of threads. The reduction of scour depth by a triple threaded pile is very effective. Moreover, the thread angle of a cable wrapped on the pile has a significant role toward reduction of scour depth. A relatively less thread angle is found to be more efficient than a greater thread angle, as the cable can encounter well with the downflow and horseshoe vortex to weaken them at a relatively less thread angle (Fig. 1.32). However, further reduction of the thread angle or an increase of the cable diameter with respect to the pile diameter is not a practical proposition.

The average reduction of scour depth by the splitter plate was measured as 61.6%. For threaded piles the most efficient cable–pile diameter ratio was found to be 0.75, which reduced scour depth by an average of 51.1%. The average reductions of scour depths for other cable–pile diameter ratios of 0.33 and 0.5 are 43.2 and 48.1%, respectively. The splitter plate divides the flow by the two sides of the pile and disrupts the vortex shedding from its usual frequency, whereas for threaded piles, the helical wires that form the threads disturbs the vortex shedding. On the other hand, in a steady current, the threaded pile is found to be a useful means to reduce scour depth at piles to a considerable extent. Cables wrapped spirally on the pile help to diminish the strengths of the downflow and horseshoe vortex, which are the main cause of scour under a steady current. The methods recommended to control scour depth are easy to implement and inexpensive.

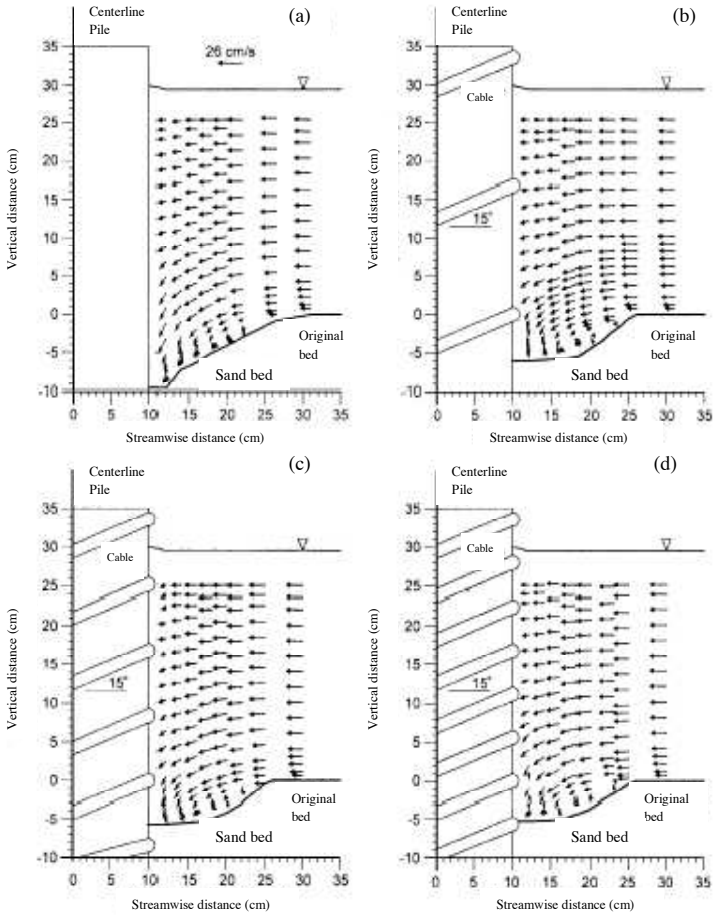

Figure 1.32. Vortex flow fields at the upstream plane of symmetry of the piles: (a) unprotected pile; (b) single threaded pile; (c) double threaded pile; and (d) triple threaded pile.

1.7.2.8 Sacrificial Piles:

Sacrificial piles are piles placed upstream of a bridge pier for the purpose of protecting it from local scour. The piles, which themselves may be subject to substantial scour, protect the pier from scour by deflecting the high-velocity flow and creating a wake region behind them. The effectiveness of this method as a pier scour countermeasure is dependent on the number of piles, the size of the piles relative to the pier, the protrusion of the piles (partly or fully submerged), and the geometric arrangement of the piles in relation to one another and the bridge pier. The piles can be arranged in a variety of configurations. A triangular array, with the apex of the triangle pointing upstream, has been shown to be one of the better configurations among those tested. Laboratory studies of sacrificial piles for pier scour protection are reported by *Chabert and Engeldinger (1956), Levi and Luna (1961), Shen et al. (1966), Chang and Karim (1972), Herbertson and Ibrahim (1992), Paice and Hey (1993), Wang (1994), and Singh et al. (1995).* These studies showed up to 50% scour reduction due to the presence of the sacrificial piles; however, the laboratory data were all measured in experiments of limited duration and under clear-water scour conditions. *Chang and Karim (1972)* and *Paice and Hey (1993)* also report some field experience of the technique. The data by Chang and Karim (1972) indicate the importance of placing the piles to generate an

overall wake region that encompasses the bridge pier.

The field studies by *Chang and Karim (1972)* were undertaken on a bridge over the Big Sioux River, South Dakota. The bridge is supported on three pairs of circular piers. Three piles were driven upstream of one of these in a triangular pattern with a pile spacing of about three pile diameters. As much as 44% scour reduction was realized.

When deviations in the direction of flow occur, the effectiveness of sacrificial piles has been shown *[e.g., Chabert and Engeldinger 1956; Chang and Karim 1972]* to reduce or entirely diminish. There are a number of reasons why flow can be skewed to the pier (and, therefore, to the sacrificial pile arrangement), including long-term changes in the river direction due to meander migration and variations in flow direction with changes in river stage. *Chang and Karim (1972)* investigated the effect of a long-term change in the direction of flow such that the pier was no longer aligned with the flow. Sacrificial piles were placed (Fig. 1.30) so as to best protect the pier once the flow deviation had occurred. The sacrificial pile arrangements studied by *Chabert and Engeldinger (1956),* however, were designed to best protect the pier when it was aligned with the flow. The same pile arrangement was then tested for various angles of skewed flow (Fig. 1.33).

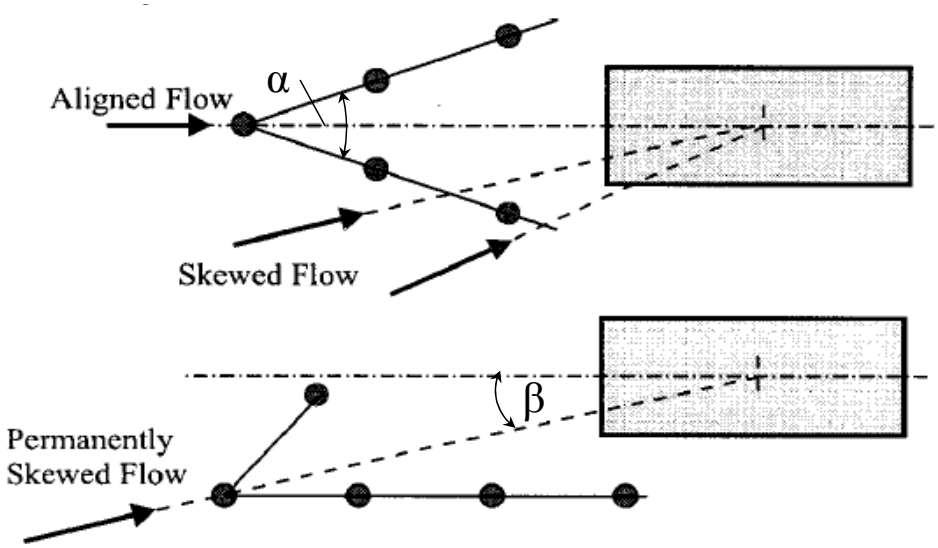

Figure 1.30. Sacrificial Pile arrangements.

Number of piles (3 and 5 piles), indicates an advantage in using the larger number of piles for both skewed and aligned piers. When the number of piles is increased, the span of the outside piles, and therefore the wake region and corresponding protective capacity of the piles, improves. For piles aligned with the flow, the effect of increasing the wedge angle (α) from 30° to 53.67° has a decrease in the protection afforded by the pile group. Piles should be placed such that each rear pile lies on the edge of the wake region of an upstream pile, thereby extending the width of the wake of the entire group. Otherwise, high velocity flow can occur between adjacent piles, the flow impacting on the pier and inducing deeper scour. A benefit of increasing the wedge angle is that the piles remain effective for a wider range of flow skew angles.

Variations in the direction of flow are the most important factor in the use of sacrificial piles as a bridge scour countermeasure. The reason for the scour depth increase with the increase of flow

angle is that this arrangement of piles, when skewed, gives no protection to the pier. Instead, the piles appear to divert the oncoming flow directly onto the centerline of the pier. If the piles are arranged so as to provide protection to the pier for a range of skew angles then a scour reduction of 20% or more can be achieved when the flow is skewed by 30°.

Under live-bed conditions, scour depth reductions based on maximum instantaneous scour depths are significantly less than those based on average scour depths. The effect of the passage of bed forms is, therefore, significant. Generally, the effect of increasing either the flow intensity or the flow skew angle has an impact of increase in the depth of scour.

Submerged sacrificial piles are found to be at least as effective as full-length piles when aligned with the flow and at the lower flow intensity. At the higher flow intensity, when the flow is skewed at 20°, the scour is deeper than that for the full-length piles. In total the effectiveness of sacrificial piles as a scour countermeasure is dependent on the approach flow angle β and flow intensity V/V_c. The reduced effectiveness under live-bed conditions is due to the passage of bed forms. Increasing flow skewness reduces the sheltering effect of the pile group. For $\beta > 20°$, sacrificial piles are ineffective as scour countermeasures under live-bed conditions. For $\beta < 20°$, sacrificial piles give moderate reductions in scour depth. In general, sacrificial piles are not recommended unless the flow remains aligned and the flow intensity is relatively small. Under such conditions, submerged and full-depth piles give similar reductions in scour depth.

2. Experimental set up and preliminary tests

2.1. Sketch of experimental facility

The experiments stated here were run at the Hydraulic Engineering Laboratory of the Politecnico di Milano, Italy. The experimental facility where we run scour tests is shown in figure below.

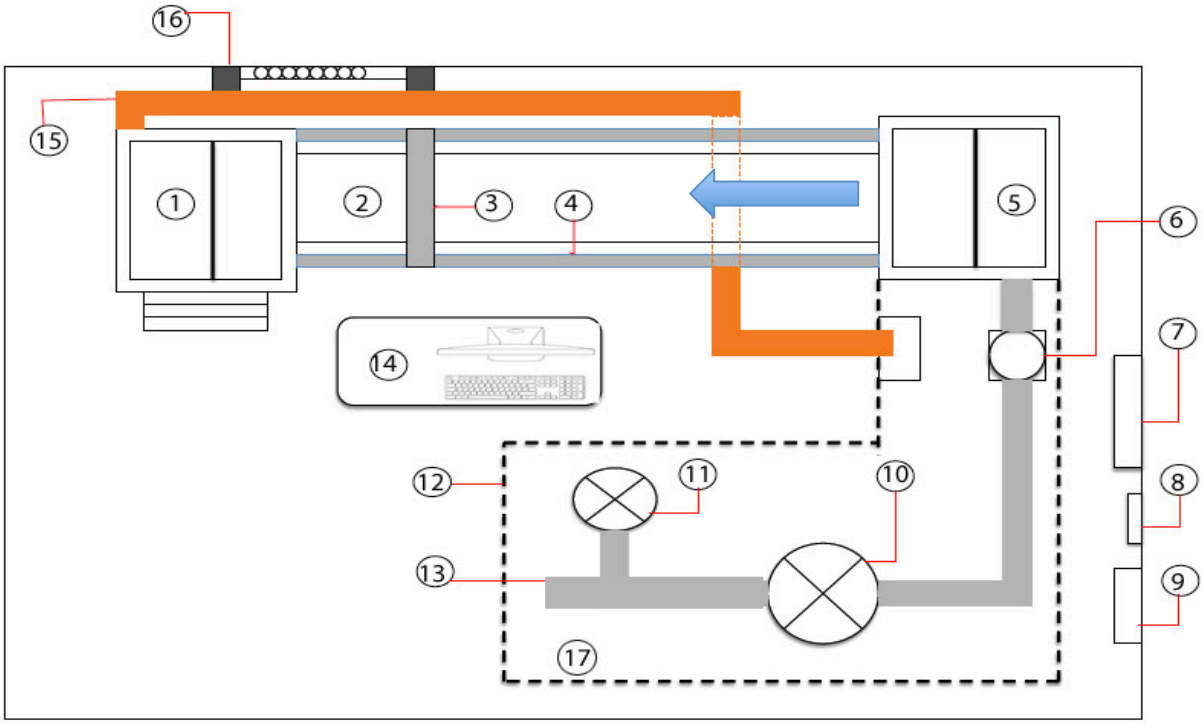

Fig. 2.1. Experimental campaign Design

The flow comes from a pipe, mounted on the left side of the tank (No.13), which is Ø120, but right before the tank it spreads to Ø220. The discharge is regulated with the help of a water pump and a magnetic flow meter (No.6), which is installed on the pipe. Nevertheless in the following section all these parts will be fully described.

1. The outlet Tank
2. A rectangular channel
3. Transverse positioning system
4. Longitudinal positioning system
5. The inlet Tank
6. Magnetic flow meter
7. Control of sediment feeder (not used in our experiment)
8. Magnetic flow meter
9. Electric power
10. Valve
11. Pump
12. Pipe
13. PC
14. Plastic pipe to recirculate water
15. Gauges and piezometers

2.2. Set up the channel and sediments

In order to calibrate the channel, piezometers and perform a preliminary test, generally for the first part of our experiments, the rectangular channel with constant section was installed.

2.2.1. Channel lay out and parameters

From Figure 2.2:

Fig.2.2. The channel layout

- *Section 1 – The Inlet tank:*

This tank is approximately 1x1 m long and wide and 1.80 m deep (Fig.2.3).

Fig.2.3. The inlet Tank, top view

In the middle cross section of the tank a grid is inserted to help even out the flow going out from the tank into the channel. The inlet tank has a discharge valve Ø40, which is connected to the sewers so that the tank can be fully emptied when no experiments are performed. Right before water flows into the channel, a flow straightener is installed (Fig.2.4).

Fig.2.4. Flow Configurator

This configurator is a network of PVC pipes; by putting wood stick into these pipes we can configure the flow. For our experiments we filled out the perimeters of this network by putting some sticks to concentrate the flow into the center of channel to help development of the velocity profile.

- *Section 2 – Channel:*

  A rectangular channel 6m long with cross section 0.4m wide and 0.16m deep was used. The channel consists of several rectangular transparent Plexiglas sections, which are connected with bolts. As it is shown in the figure this channel is supported by stands which is installed roughly every 30cm

- *Section 3 – The sediment trap tank and the outflow tank:*

  The tank is actually divided in two parts by a metal wall.

Fig.2.5. Outflow Tank

Just before this tank there is a wooden gate consisting of rectangular sticks in order to configure boundary condition of the channel (Fig.2.6).

Fig.2.6. Down stream boundary

In the first part of the tank the sediment particles get captured in a specially designed rectangular metal basket, which can be elevated with the help of chains in order to be able to take the sediment particles out and refill the sediment tank (Fig.2.5). The water flows below the metal wall and falls freely in the second part of the tank, from where the water is recirculated through a plastic pipe Ø 200 (in Fig. 2.2 the orange pipe on the floor) to a rectangular concrete basin from where the water is pumped back in to the channel through the inlet tank. The outflow tank has also a discharge valve Ø40 so the tank can be fully emptied when not in use.

The channel also is equipped with instruments, this measuring instruments will be described in the following.

2.2.2. Sediments

In this experimental campaign we have used natural sand from Ticino river with granulometric composition shown in figure below.

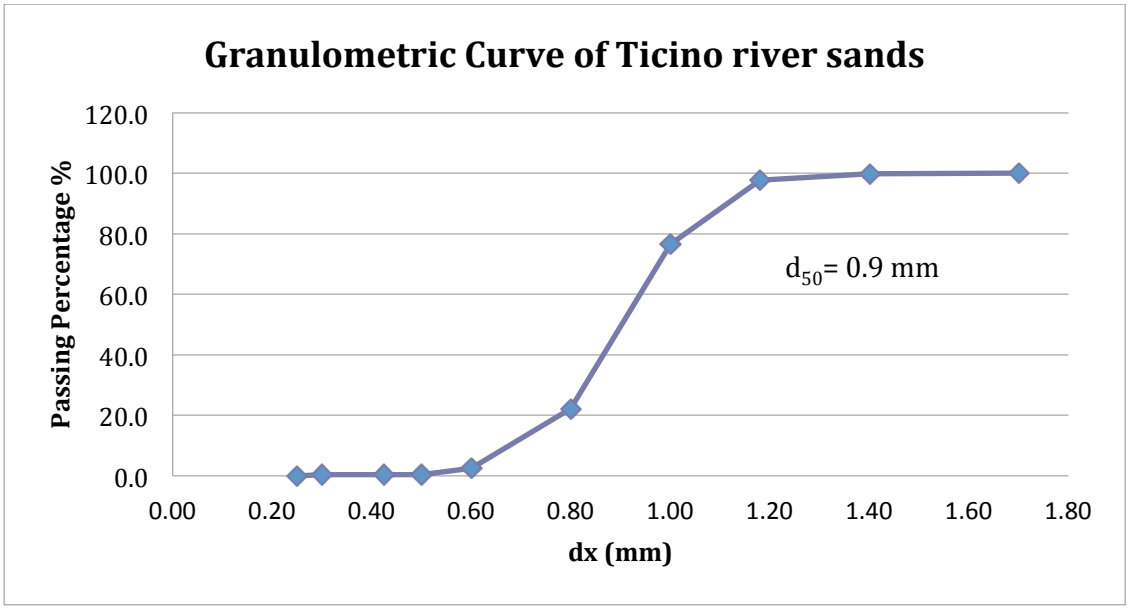

Fig.2.7. Granulometric curve of sands used in the experiments

Hence, in order to prepare a fixed bed these sands have been glued to the metal plates. (Fig.2.8).

Fig.2.8. Preparation of fixed bed

2.3. Calibration of the channel

By calibration of the channel we mean:

- Measurement of channel bed elevation
- Calibration of the piezometers

2.3.1. Measurement of channel bed elevation

The purpose this work is to obtain the bed elevation in the reference of piezometers.

The procedure is as follows: We pure some water in the special glass which is shown in figure above, this glass is connected to the gauge fixed on the wall by a pipe (Fig.2.10.), we measure water elevation in the gauge, water elevation in the glass and the elevation of channel bed using the particular gauge (Fig.2.11), by applying the following formula we can obtain the real bed elevation in different points of the channel, we scoped 8 points along the channel where there were piezometers.

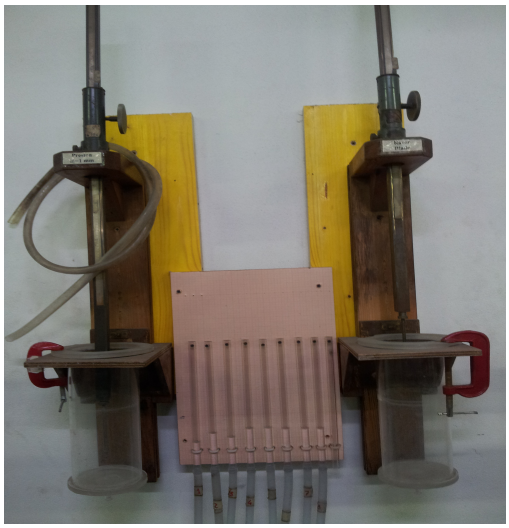

$$Z_{bed,Real} = Z_{gauge} - (Z_w - Z_{bed})$$

Noted that, in order to rebate errors, each measurement has been repeated for 3 times. The results is reported in table.2.1 and figure.2.11

Piezometer	1	2	3	4	5	6	7	8
x (m) from DS upwards	0.73	1.34	1.94	2.53	3.13	3.54	4.14	4.74
Left gauge 1	24.87	24.98	25.03	25.03	25.04	25.04	24.99	24.91
Left gauge 2	24.87	24.99	25.03	25.03	25.04	25.04	24.99	24.91
Left gauge 3	24.85	24.99	25.04	25.03	25.03	25.04	24.99	24.91
Left gauge mean (cm)	24.86	24.99	25.03	25.03	25.04	25.04	24.99	24.91
Glass 1	50.75	50.69	50.55	50.42	50.40	50.42	50.46	50.51
Glass 2	50.76	50.69	50.55	50.42	50.40	50.42	50.46	50.50
Glass 3	50.76	50.69	50.55	50.41	50.40	50.41	50.45	50.51
Glass mean (cm)	50.76	50.69	50.55	50.42	50.40	50.42	50.46	50.51
Bed 1	44.74	44.76	44.76	44.54	44.56	44.66	44.61	44.57
Bed 2	44.71	44.72	44.67	44.54	44.56	44.66	44.62	44.58
Bed 3	44.71	44.78	44.67	44.55	44.59	44.62	44.61	44.59
Bed mean (cm)	44.72	44.75	44.70	44.54	44.57	44.65	44.61	44.58
z_bed (cm)	18.83	19.05	19.18	19.16	19.21	19.27	19.15	18.98
z_bed interp (cm)	19.02	19.04	19.07	19.09	19.12	19.13	19.16	19.18

Table.2.1 Bed calibration

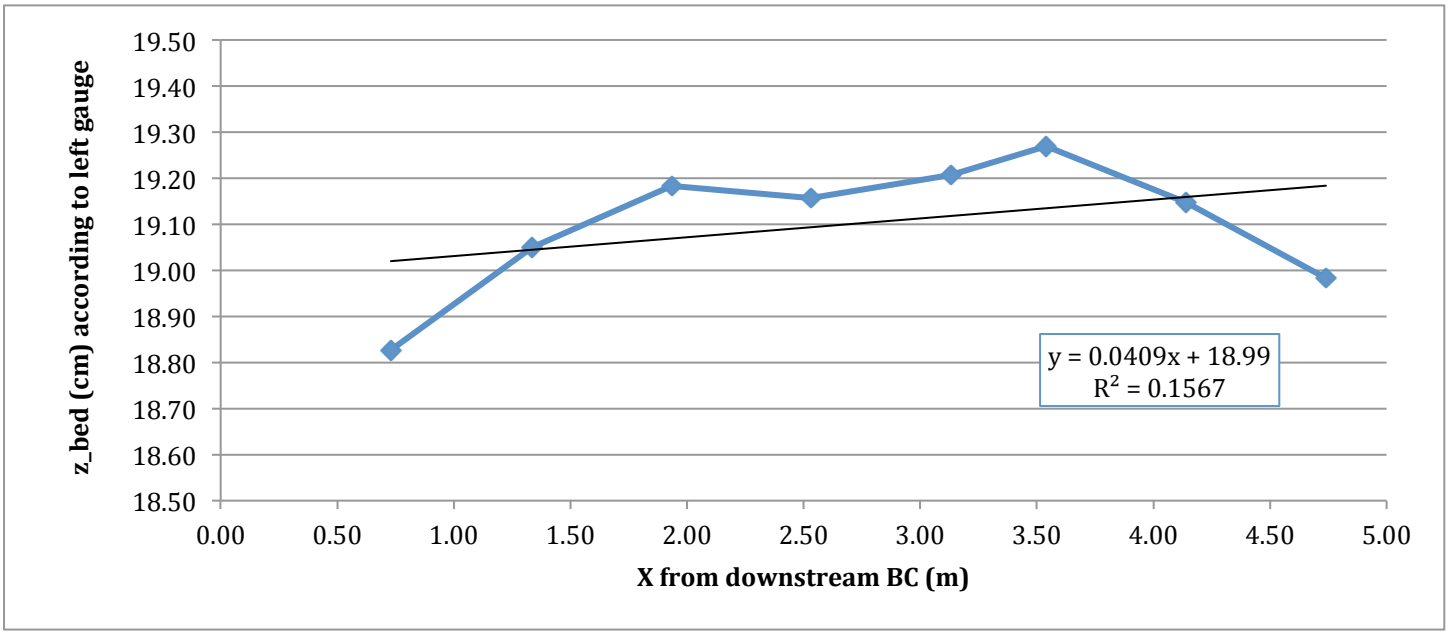

Fig.2.12. Bed Calibration

2.3.2. Calibration of the piezometers

For this calibration we have referred to the left gauge, this gauge is connected with each piezometers same as previous calibration using following formula:

$$Z_{p,bed} = Z_p - (Z_{left\ gauge} - Z_{bed,real})$$

$$depth = Z_p - Z_{p,bed}$$

The results are reported in table.2.2 and figure.2.12

Piezometer	1	2	3	4	5	6	7	8
x (m)	0.73	1.34	1.94	2.53	3.13	3.54	4.14	4.74
Left gauge 1	26.94	22.58	21.85	21.50	20.96	20.00	19.48	19.04
Left gauge 2	26.93	22.58	21.85	21.50	20.96	20.00	19.48	19.04
Left gauge 3	26.94	22.58	21.85	21.50	20.96	20.00	19.47	19.04
Left gauge mean (cm)	26.94	22.58	21.85	21.50	20.96	20.00	19.48	19.04
Piezometer (cm)	104.10	99.80	99.00	98.60	98.10	97.10	96.50	96.00
Piezometer actual bed (cm)	95.99	96.27	96.33	96.26	96.35	96.37	96.17	95.94
Piezometer interp bed (cm)	96.18	96.26	96.22	96.19	96.26	96.23	96.18	96.14

Table.2.2 Piezometers Calibration

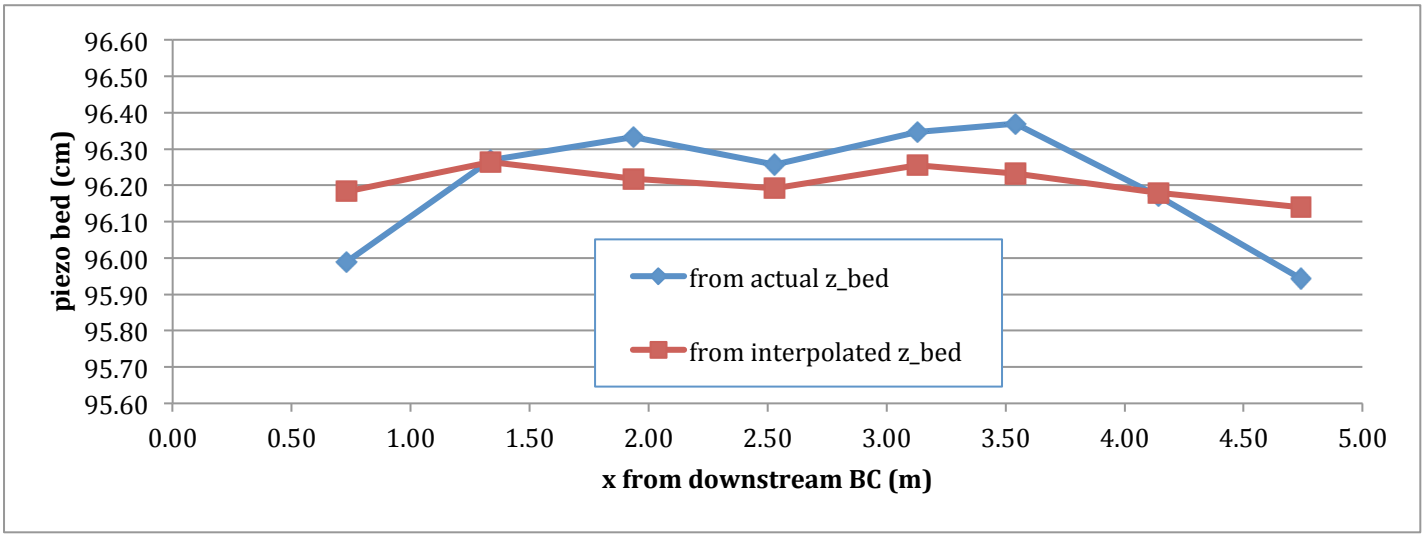

2.4. Preliminary Tests

Before running the scour tests, some preliminary tests have been done, such as velocity measurements of 3 sections namely x=1.63m, x=2.69m and x=3.77m from downstream, of the channel. Moreover some tests have been performed in order to obtain critical discharge, which will be fully described in this section.

2.4.1. Velocity measurements

In this part of our experimental campaign, we measured velocity profiles of some sections along the channel (Fig.2.13) using specific instrument called "DOP" to be compared to see how the flow is distributed in our channel, finally from profiles of velocity obtained, we will compute shear velocity v^*.

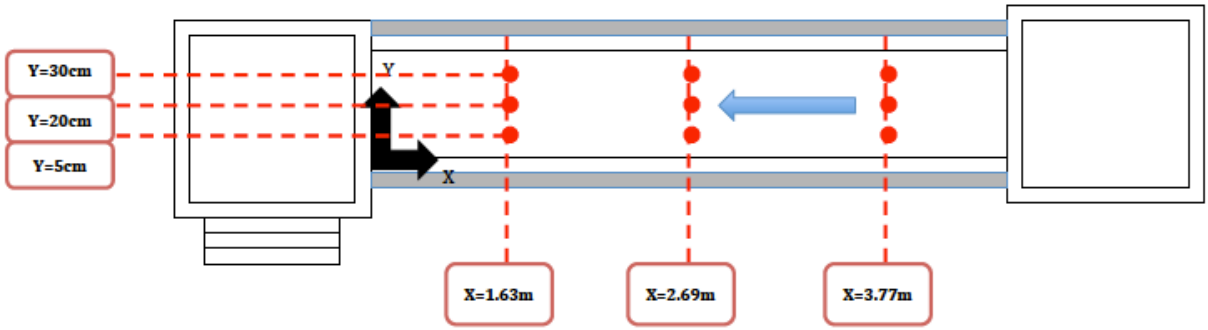

Fig.2.14. Velocity profiles sections

It is noted that, we have been repeated all the procedures for different discharges 8, 10, 12, 14, 16 lit/sec, therefore in total, 45 profiles of velocity have been measured. However the measurement for all points have been conducted, but due to the fact that DOP was not working properly we had some errors in our data, therefore we aborted to process and analysis of the data.

2.4.1.1. Measuring tools

As it is said above, in order to perform this test a particular instrument called DOP is used (Fig.2.14). *Doppler ultrasound velocimetry* was originally applied in medical field and dates back more than 30 years. The use of pulsed emissions has extended this technique to the other fields and has opened the way to new measuring techniques in fluid dynamics. The term " Doppler ultrasound velocimetry" implies that the velocity is measured by finding the Doppler frequency in the received signal, as it is the case in Laser Doppler velocimetry. In fact, in ultrasonic pulsed Doppler velocimetry, this is never the case. Velocities are derived from shifts in positions between pulses, and the Doppler effect plays a minor role.

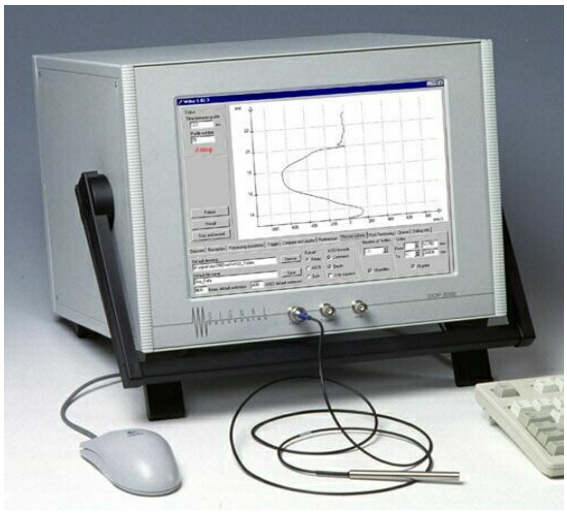

Fig.2.15 and Fig.2.16. DOP

The Doppler effect is the change in frequency of an acoustic or electromagnetic wave resulting from the movement of either the emitter or receptor.

This device is connected to the specific monitor (Fig.2.15) on which we can see the process of collecting data by DOP. In the next paragraph, briefly, it is expressed how this device works:

2.4.1.2. Test procedure:

As a matter of fact, we repeated the test for different discharge from 8 lit/sec to 16 lit/sec to see how the flow is distributed along the channel, as it is mentioned above we located DOP on 9 point of the channel (Fig.2.13). So for each discharge we should measure 9 points.

Initially, we start with 8-lit/sec discharges; it has been decided to start from downstream going to upstream, therefore the starting point was at x= 1.63m y= 20 cm from downstream of the channel. Afterwards we located the DOP at y= 5 cm and y= 35 cm at the same section x=1.63m, next we moved t DOP to other sections x=2.69 and x=3.77m.

Using two probes installed on the device, namely downstream and upstream, we will measure inclined velocity, which has 75 degree with respect to the vertical line (Fig.2.17).

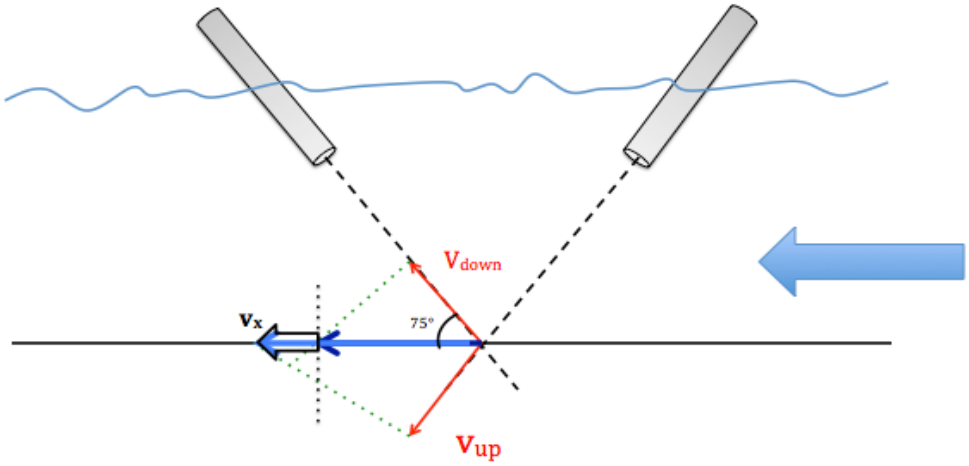

Fig.2.17.Position of the probes with respect to the channel direction

However we need velocity along horizontal direction Vx, therefore by applying trigonometric composition we transfer these velocities to the horizontal one.

$$v_x = \frac{1}{2}\left(v_{up} + v_{down}\right)\frac{1}{Cos\ 75}$$

$$z = \left(z_{bed,echo} - z_{each\ point,echo}\right)Sin\ 75$$

Subsequently, I give an example expressing the process that we measured and plotted the velocity profiles. Table.2.3. shows conversion of velocities measured by DOP to velocity along horizontal direction.

UP		
OP (mm/s)	echo	P (mm)
0.00	316.60	0.75
0.00	74.68	3.38
0.00	040.00	6.00
0.00	040.00	8.63
0.00	040.00	11.25
44.55	981.25	13.88
68.74	036.80	16.50
96.18	028.94	19.13
68.18	719.77	21.75
85.43	848.42	24.38
139.93	438.46	27.00
140.11	035.17	29.63
136.55	912.13	32.25
133.14	823.94	34.88
129.80	811.93	37.50
126.91	845.59	40.13
123.97	704.58	42.75
121.84	693.16	45.38
118.93	653.48	48.00
116.74	624.54	50.63
114.11	609.03	53.25
111.62	589.80	55.88
109.35	563.95	58.50
106.64	528.81	61.13
104.27	505.64	63.75
101.79	497.47	66.38
98.02	558.71	69.00
94.66	519.21	71.63
91.25	457.09	74.25
86.74	483.25	76.88
80.96	538.23	79.50
65.40	585.12	82.13
53.84	779.56	84.75
48.20	707.41	87.38
42.77	770.64	90.00
35.22	891.45	92.63
17.25	940.51	95.25
0.00	980.49	97.88
17.38	008.32	00.50
0.00	040.00	03.13
21.88	868.52	05.75
22.49	836.41	08.38

DOWN		
DOP (mm/s)	echo	zDOP (mm)
0.00	280.03	0.75
0.00	42.58	3.38
-29.50	1686.50	6.00
-59.30	2030.69	8.63
-81.95	1928.84	11.25
-104.72	1647.44	13.88
-106.40	1613.99	16.50
-106.61	1499.43	19.13
-106.11	1460.21	21.75
-105.95	1440.60	24.38
-105.82	1422.88	27.00
-105.26	1408.61	29.63
-104.73	1415.27	32.25
-103.90	1389.70	34.88
-103.15	1373.14	37.50
-102.47	1369.67	40.13
-102.19	1354.45	42.75
-101.31	1323.92	45.38
-100.98	1315.81	48.00
-99.85	1292.62	50.63
-99.83	1278.19	53.25
-98.60	1257.57	55.88
-97.22	1247.74	58.50
-96.04	1213.86	61.13
-94.34	1203.92	63.75
-92.35	1185.89	66.38
-87.04	1341.72	69.00
-82.44	1696.10	71.63
-81.53	1373.02	74.25
-72.05	1675.41	76.88
-59.67	1480.72	79.50
-47.68	1438.03	82.13
-39.76	1611.86	84.75
-39.31	1487.73	87.38
-29.52	1589.80	90.00
0.00	2040.00	92.63
0.00	2040.00	95.25
-17.74	2026.90	97.88
-20.89	1991.44	100.50
-11.20	2039.96	103.13
-20.14	1951.14	105.75
-19.64	1475.90	108.38

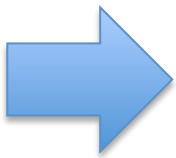

Vx (mm/s)	z (mm)
0.00	91.28
0.00	88.74
56.98	86.21
114.55	83.67
158.31	81.14
288.36	78.60
338.35	76.07
391.77	73.53
336.72	71.00
369.71	68.46
474.76	65.92
474.01	63.39
466.11	60.85
457.93	58.32
450.03	55.78
443.14	53.25
436.92	50.71
431.10	48.18
424.83	45.64
418.42	43.10
413.30	40.57
406.10	38.03
399.08	35.50
391.53	32.96
383.69	30.43
375.05	27.89
357.51	25.36
342.12	22.82
333.80	20.28
306.76	17.75
271.67	15.21
218.46	12.68
180.81	10.14
169.05	7.61
139.64	5.07
68.04	2.54
33.32	0.00
34.27	-2.54
73.94	-5.07
21.64	-7.61
81.17	-10.14

The filled cells by yellow color is showing the channel bed, this can be recognized by observing the jumping in echo value, for instance there is a sudden increase from 891.45 to 1940.51.

Afterwards, we plot Vx vs Z:

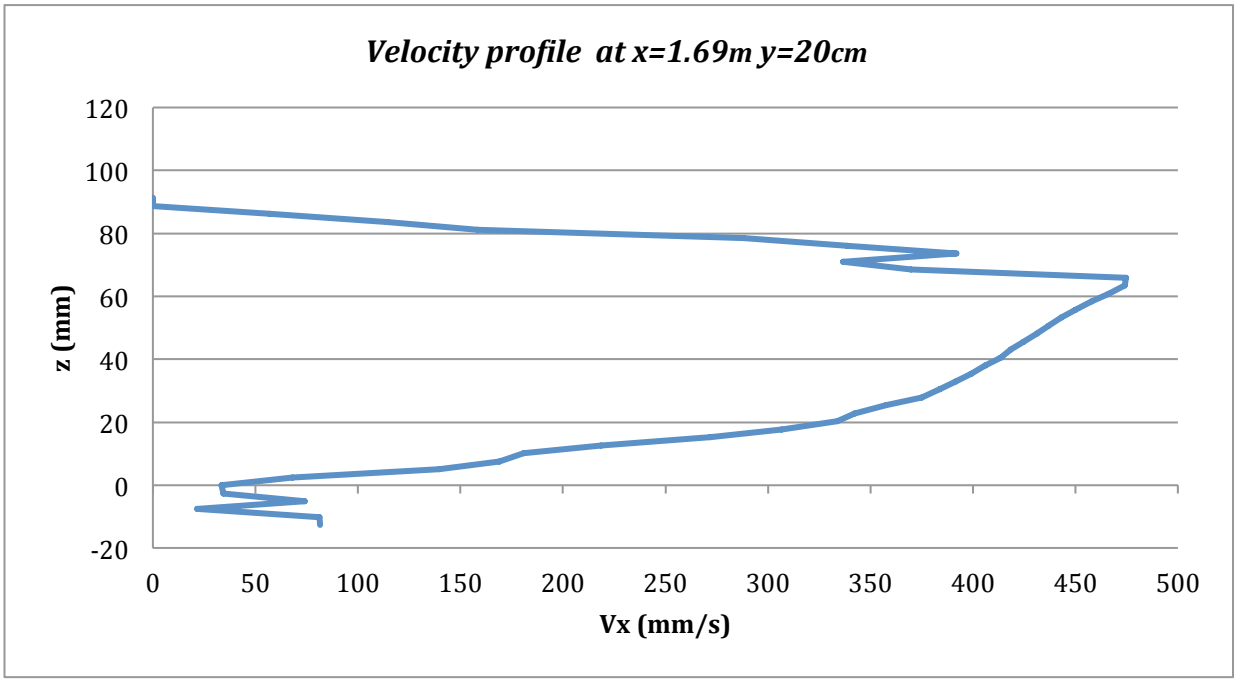

Fig.2.18. Velocity profile at x=1.63m y=20cm

The condition for this test is:

Q= 16 lit/sec
Water Depth= 10 cm
Clear-water and fixed bed condition

As it can be seen in the graph, despite the fact that we expect to see 10 cm of water velocity profile, we see 8 cm, this reduction is due to the fact that, the probes deep into the water about 1 cm so we will have perturbation of the flow by these probes.

After that, the point is estimation of shear velocity v^*. We have now our points in the plot $Vx - z$. There are different formulas by different investigators to estimate the shear velocity but the most used equations are *logarithmic equations* that are:

$$a) v_z = \frac{v^*}{k_0} Ln\left(\frac{z}{z_0}\right)$$

$$b)\ v_z = \frac{v^*}{k_0} Ln\left(\frac{z}{d}\right) + B$$

$z_0 = virtual\ origin\ v(z_0) = 0$

k_0=$Karman\ constant\ (0.4 - 0.41)$

B= $Constant$

Generally speaking, with respect to the above equations, the logarithmic plot is more used due to the fact that if we have logarithmic profiles then we will see straight line (Fig.2.18)

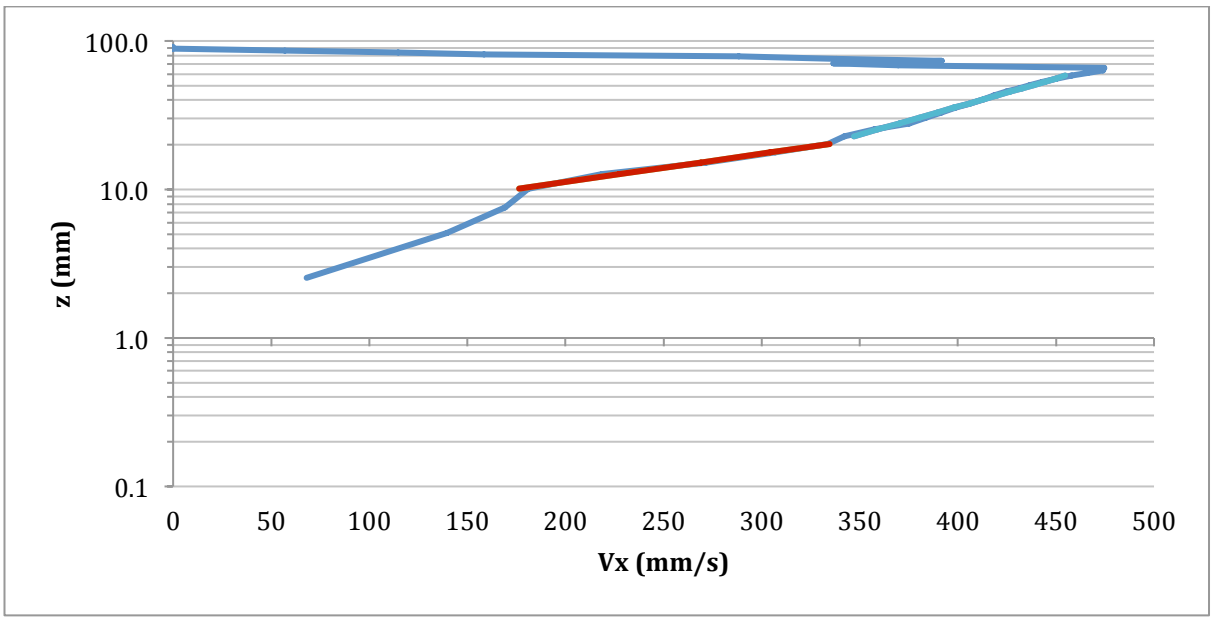

Fig.2.19. Logarithmic velocity profile

Actually, if we fit the straight line to our points we will measure the parameters of above equations. The red line in above plot is points computed by equations, now the point is changing these values (that are parameters of the equations) until the red line is well super imposed in our points. We used fitting by least square error.

FIRST APPROACH (a)		*SECOND APPROACH (b)*	
u* (mm/s)	**93.59**	**u* (mm/s)**	**93.59**
k	**0.41**	**k**	**0.41**
z0 (mm)	**4.68**	**B**	**-4.02**
τ*	**0.620**	**τ***	**0.620**

What is interesting in our computation, is the fact that the value of shear velocity that we obtained is the same in both approach, but what is not acceptable is that value of shields number t* is too high (10 times of critical value which is 0.05)

The question is on which straight line we must super impose our equations because there are two straight lines in the plot (light blue line) which is from 20mm from 60 mm, therefore in the following we will repeat all the steps for this line, to see the differences because we were not satisfied with results obtained before, this time the shields number that we computed is 3 times above critical value:

FIRST APPROACH (a)		*SECOND APPROACH (b)*	
u* (mm/s)	**47.08**	**u* (mm/s)**	**47.07**
k	**0.41**	**k**	**0.41**
z0 (mm)	**1.11**	**B**	**-0.51**
τ*	**0.157**	**τ***	**0.157**

Therefore, when we find the critical discharge we should find shields number related to it.

2.4.2. Profiles of free surface

It is of a great importance, control test condition in terms of discharge, water depth while performing test, this is due to the fact that we should keep constant the condition as much as possible and we must not have change in their value dramatically. Not only for this part of our experiments but also for each test that we have carried out we controlled this conditions, for instance every couple of minutes, typically every half an hour we read the water level on piezometers and value of discharges to observe it is remaining constant. In the annex … all the tables and graph related to this part are given out.

As an example, for discharge of 16.5 lit/sec, table.2.4.and figure.2.20 illustrate reasonably, how we controlled the situation:

Time 11:30 am										
Profile 1										
Q (l/s)		Piezometers	1	2	3	4	5	6	7	8
1	16.209	x (m)	0.73	1.34	1.94	2.53	3.13	3.54	4.14	4.74
2	16.469	Reading (cm)	106.1	106.0	106.1	106.1	106.1	106.1	106.1	106.2
3	16.216	Bed, actual (cm)	96.0	96.3	96.3	96.3	96.3	96.4	96.2	95.9
4	16.231	Depth, actual (cm)	10.1	9.7	9.8	9.8	9.8	9.7	9.9	10.3
5	16.311	Bed, interp (cm)	96.2	96.3	96.2	96.2	96.3	96.2	96.2	96.1
6	16.419	Depth, interp (cm)	9.9	9.7	9.9	9.9	9.8	9.9	9.9	10.1
7	16.488									
8	16.477									
9	16.446									
10	16.272									
Average	**16.35**									

Table.2.4.

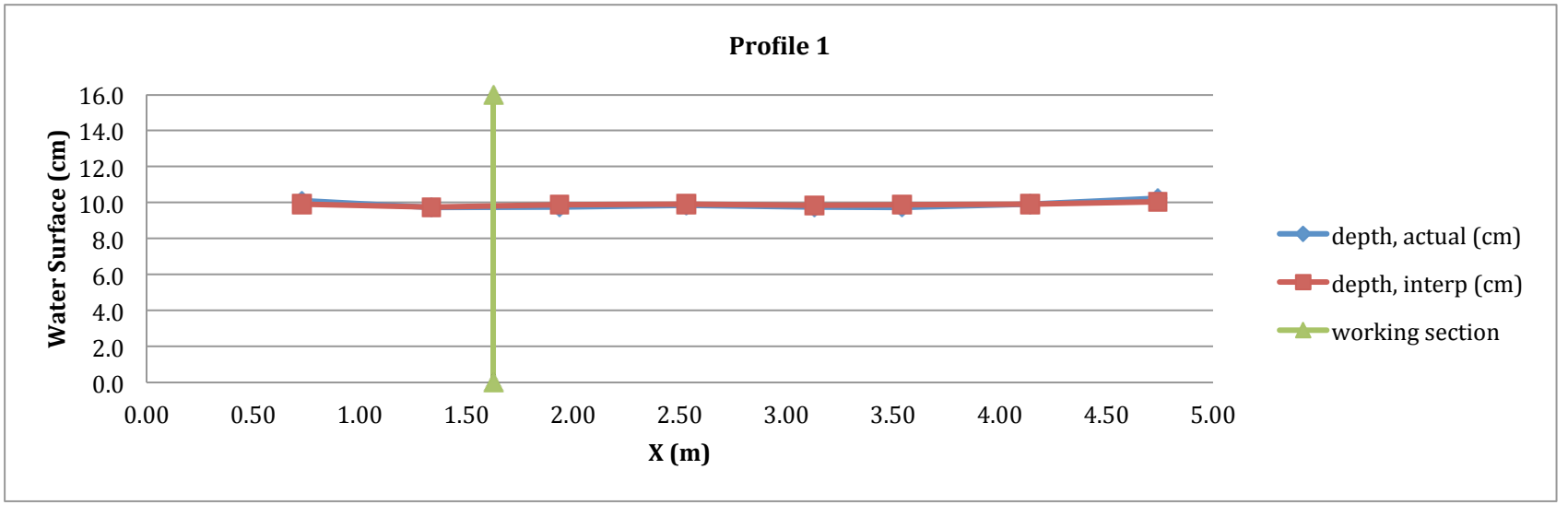

Figure.2.20

This process has been repeated every couple of minutes, afterwards we collect 5 profiles of free surfaces for this test (Q=16.5 lit/sec), in figure below the comparison between all profiles that we obtained is shown:

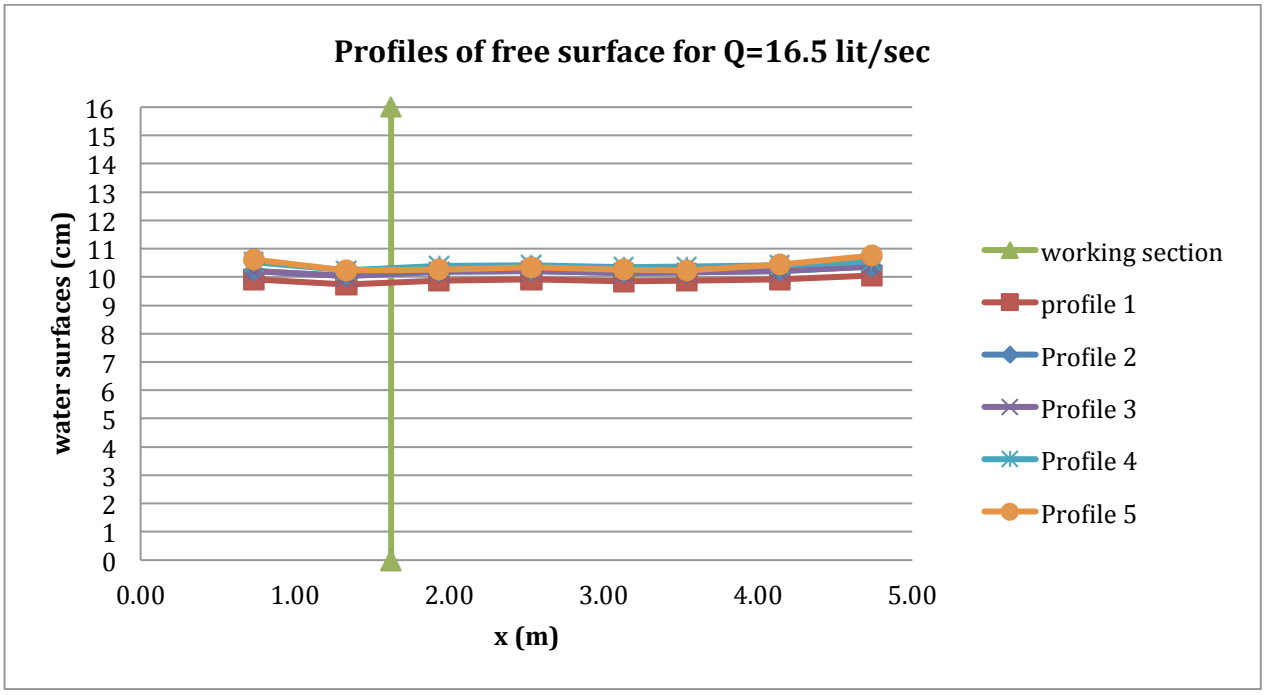

Fig.2.21

As it can be seen in this plot, we tried to keep the water depth as much as constant as possible and we had not sharp change in it.

2.4.3. Q-Qc Test

The objectives of this test, is:

1- Characterization of critical discharge $Q_{c,}$ this is important for us due to the fact that everything is referred to the hydrodynamic condition in comparison with critical one.
2- Characterization of feeding sediments in channel, using feeder, in case if we have desire to carry out live bed test, however we have not done this characterization.

By definition critical discharge is the discharge at which we will have incipient motion of sediment particles. However, definition of the threshold condition is quite uncertain. In this experiment we have applied definition used in recent years by other researchers in *Politecnico di Milano* namely; *Radice (2000), Teruzzi (2002) and Crotti (2005):*

$$\Phi = \frac{q_s}{\sqrt{g(s-1)d^3}}$$

$\Phi = Dimentionless\ sediment\ transport\ rate$

$q_s = transport\ rate\ per\ unit\ channel\ width$

$g = gravity\ acceleration\ \frac{m}{s^2}$

$d = particle\ dimension$

The critical thresholds corresponds to $\Phi = 5.7\times10^{-5}$, this value found by *Alessio Radice*, in principle; he had qualitative idea of incipient motion based on visual observation.

2.4.3.1. Test procedures

Basically, the Qs is measured by counting sediments passing over the object In order to apply formula… we should transfer it into the form that we can use in our experiment, hence:

$$\Phi = \frac{q_s}{\sqrt{g(s-1)d^3}} = \frac{Q_s}{B}\frac{1}{\sqrt{g\,(s-1)d^3}} = \frac{N\,W_g}{B\Delta t}\frac{1}{\sqrt{g(s-1)d^3}} \rightarrow N = \Phi\,\frac{B\Delta t}{W_g}\sqrt{g(s-1)d^2}$$

$Qs = Sediment\ discharge$

$B = Length\ of\ object\ that\ sediments\ pass\ over\ it$

$N = number\ of\ particles\ passing\ over\ the\ object$

$Wg = specific\ weight\ of\ the\ sediment\ particle$

$\Delta t = Reference\ time\ which\ is\ our\ choice$

The first step to start this test is to change one section of the channel to deep channel (Fig.2.22) and fill it with washed sands, and then we scrub the surface of the sediment tank.

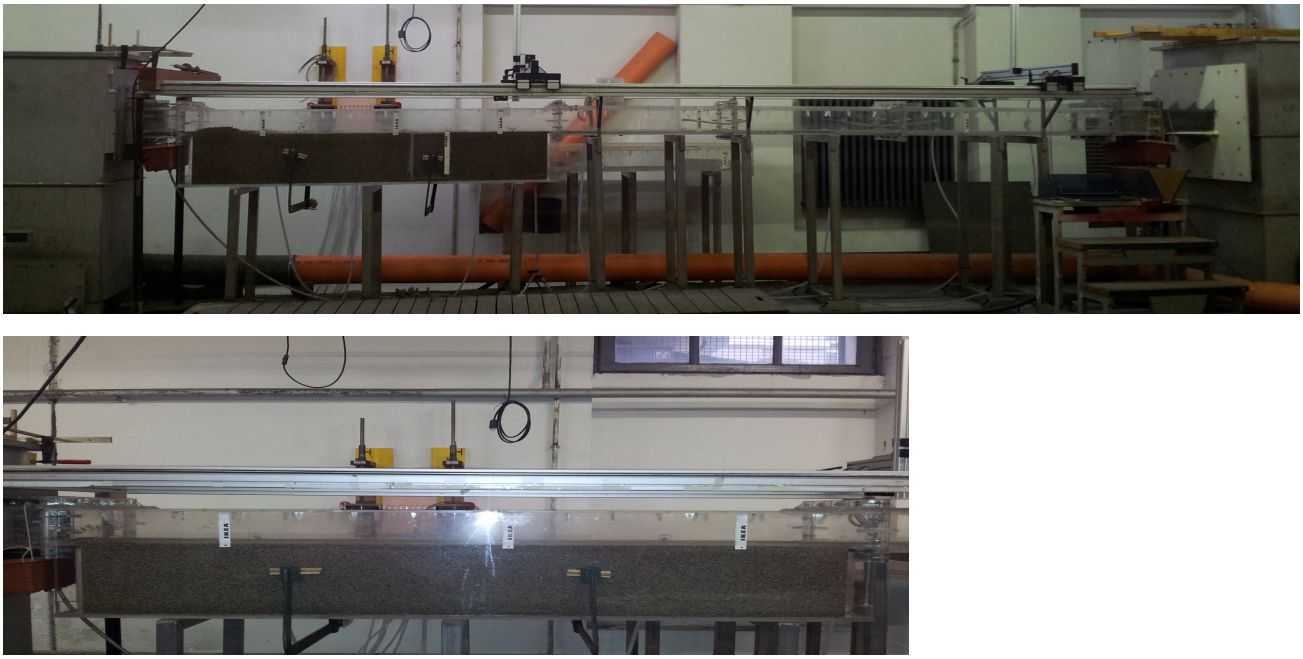

Fig.2.22

Afterwards we put an object (metal plate) with 8.4 cm length on to the movable bed (Fig.2.23), nearly 150 cm from downstream, where we want to put the abutment.

Fig.2.23

Next step is to run the channel flow, but in order to not to disturb bed sediments, we initially filled the sediment tank, using pipe with very low discharge. Subsequently we turned on channel starting from 0.4 Lit/sec, increasing it slightly while we adjust downstream boundary condition.

This procedure has been conducted for different discharges from 2.5 Lit/sec to 15.5 Lit/sec and for each value of discharge during time Δt we count number of particles passing over the yellow objet.

2.4.2.3.2. Profiles of free surface

For each test we have recorded water level in piezometers and value of discharge, hence we controlled water depth, which should be 10cm. All the tables and graphs related to this part of our experiment reported in the Annex…..

2.3.2.3. Results

Finally we came up with N-Q plot (Fig.2.24). Applying above formula …. We will find $N_{critical}$ corresponding to $\Phi_{critical}$:

	Radice (2000)	Teruzzi (2002)	Crotti (2005)	Davari (2012)
Φ_c	5.66E-05	5.66E-05	5.66E-05	5.66E-05
S-1	1.57	1.57	0.43	1.57
g (m/s^2)	9.81	9.81	9.81	9.81
d (mm)	5.00	1.90	3.60	0.90
d (m)	0.0050	0.0019	0.0036	0.0009
W_g (m^3)	6.54E-08	3.59E-09	2.44E-08	3.82E-10
B (cm)	10.0	8.4	8.4	8.4
B (m)	0.10	0.08	0.08	0.08
Δt (min)	15	5	8	0.67
Δt (s)	900	300	480	40
	108	129	41	53

Given the fact that, for different discharges we have different numbers, and knowing that our critical number is 53 we can find critical discharge corresponds to it (Table.2.5). It must be mentioned that, we repeated the test in two days in order to have more points in the plot.

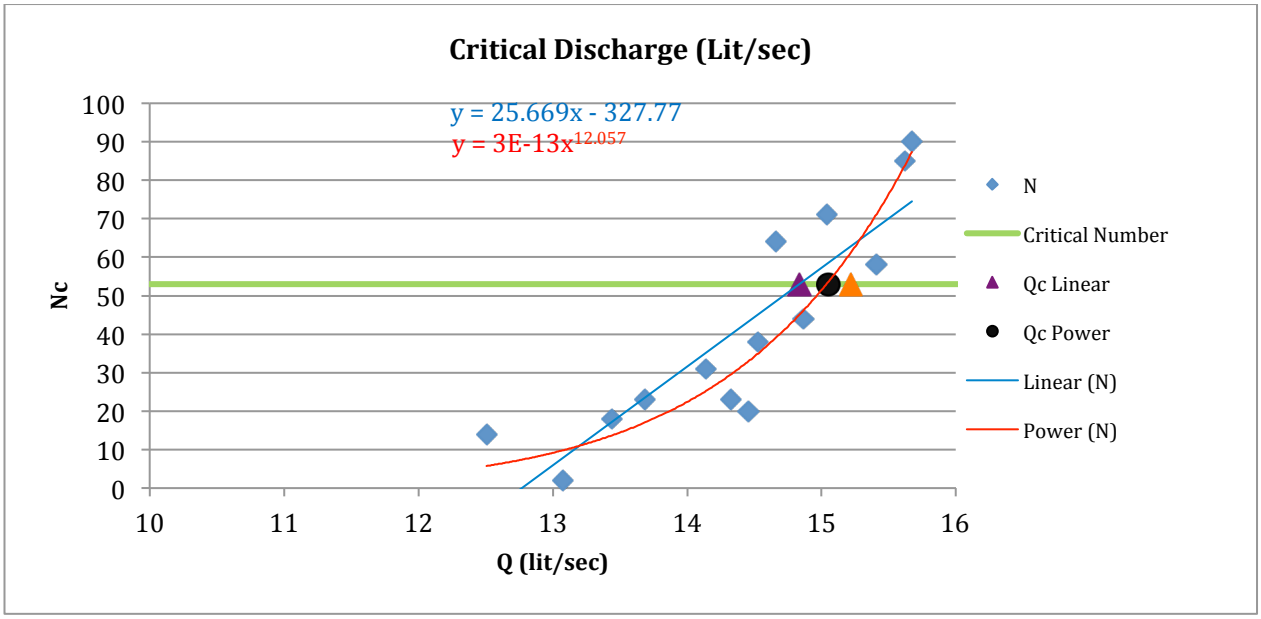

Fig.2.24.

Linear		Power		Ints Power and Linear	
Nc	Qc (Lit/sec)	Nc	Qc(Lit/sec)	Nc	Qc (Lit/sec)
53	14.83	53	15.05	52.9999	15.2

2.5 Abutments used in scour tests

The countermeasures are roughening elements, which are most promising and realizable. The abutment is made of two parts, the lower part being buried in the sediment bed and the upper part being installed to make the experiment start. The sketch below illustrates how the abutments are placed into the channel. Practically, the experiments have been run for two series of abutments shown in figure.2.25:

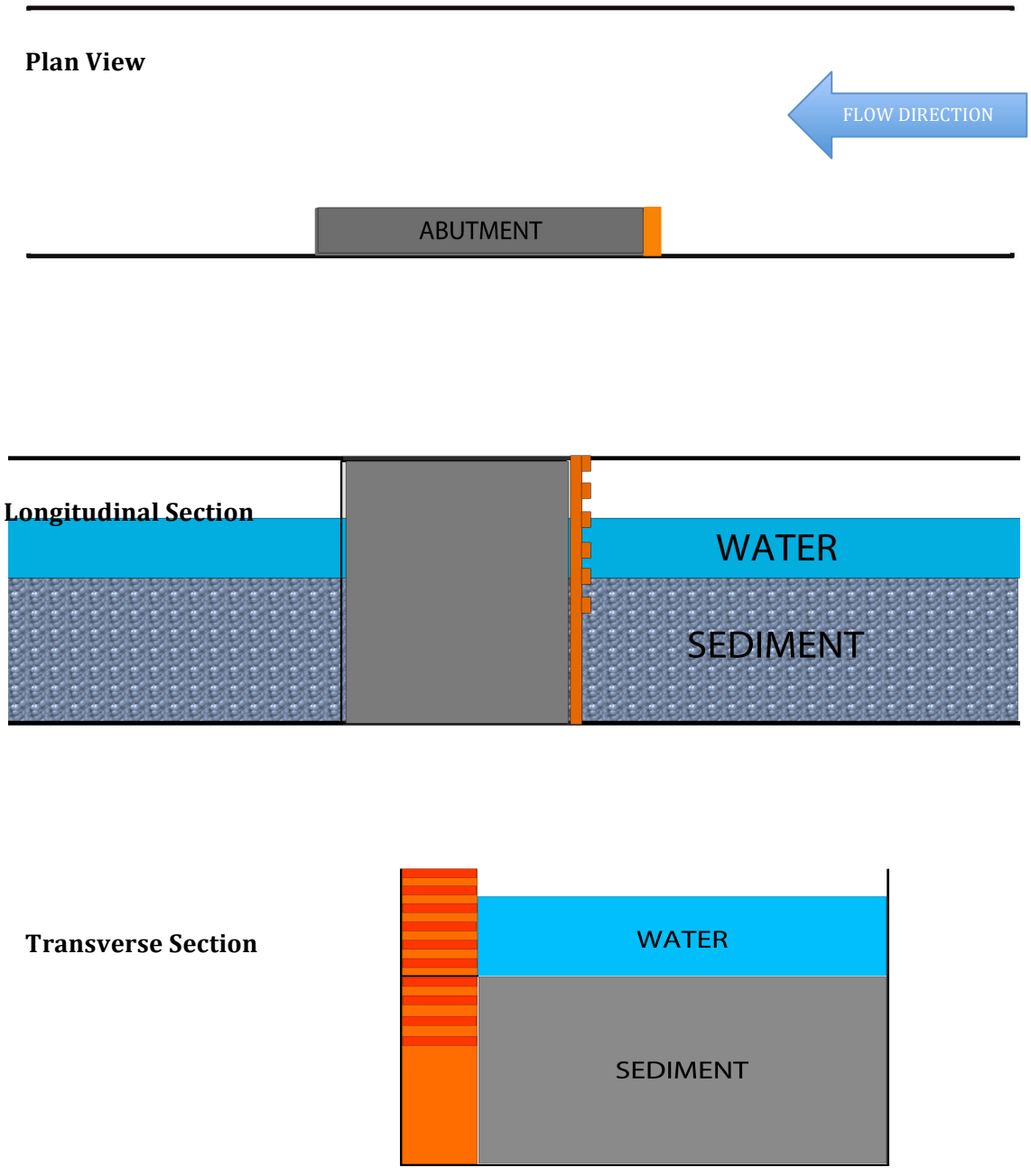

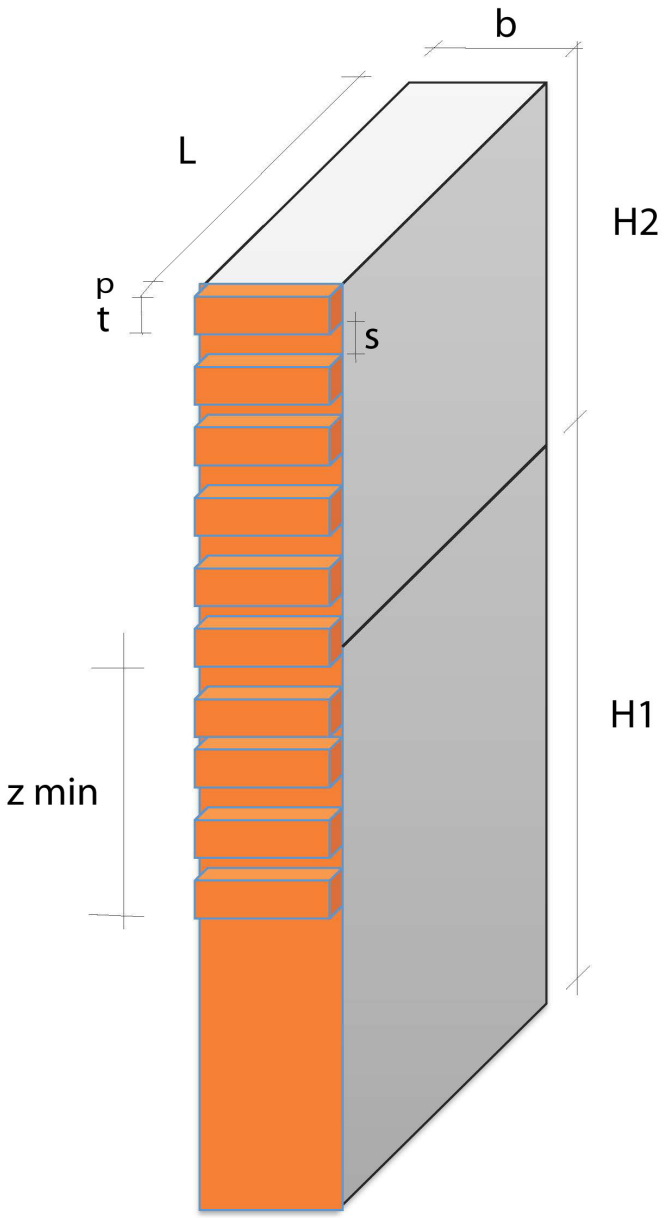

b= Abutment Width

t= Thickness of roughness element

p= protrusion of roughness element

s= Spacing between roughness element

z_{min}= minimum elevation of roughness elements (z_{min}=0 means that they are only above non-scoured level)

L= Abutment Length

H1= Height of Lower part

H2= Height of upper part

SERIE A								
Test	b (cm)	t (cm)	p (cm)	s (cm)	zmin (cm)	L (cm)	H1 (cm)	H2 (cm)
1	5	0	0	0	0	20	30	16
2	5	1	1	2	10	20	30	16
3	5	1	1	3	10	20	30	16
4	5	1	1	4	10	20	30	16
5	5	1	1	1	10	20	30	16

SERIE B								
Test	b (cm)	t (cm)	p (cm)	s (cm)	zmin (cm)	L (cm)	H1 (cm)	H2 (cm)
6	5	0	0	0	0	20	30	16
7	5	1	0.5	2	10	20	30	16
8	5	1	0.5	3	10	20	30	16
9	5	1	0.5	4	10	20	30	16
10	5	1	0.5	1	10	20	30	16

2.6. Trial Scour Test

This test has been done in order to understand the probable errors that may occur during test and to see which would be the best way to proceed our experiments. However before that it is needed to introduce the measurement tools that we have used in scour tests.

2.6.1.tools

In this section, I briefly introduce the tools that we have utilized to measure local scour depth or generally speaking to perform scour tests.

- Laser:

For surveying scour holes, a laser sensor mounted on a three-axes positioning system is used (Fig.2.26).

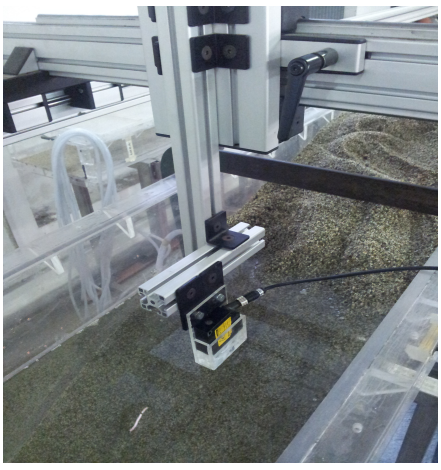

Fig.2.26

The laser works on a basis of triangulation principle and depending on the depth it sends a voltage to a special device, which shows the value in volts. This value can be further used in a formula, which converts volts into distance. A problem that sometimes occurs for the laser is if an air bubble appears at the place where the laser beam is located. Then the laser shows a red light, which means that there is an obstruction in the way of the beam and no possible measurement at this point can be taken. It should be mentioned that, Laser must be calibrated before performing the scour tests; indeed in the following section it is described how we calibrated this device.

To calibrate the Laser we have used a gauge shown in figure below. Sands cover one surface of this object and the other one is smooth. As it is seen in the figure… we draw some spots on both surfaces to be measured by Laser and by the particular gauge shown in figure.2.31. Totally, 18 points has been drawn on this object, 12 points on smooth surface and 8 points rough surface.

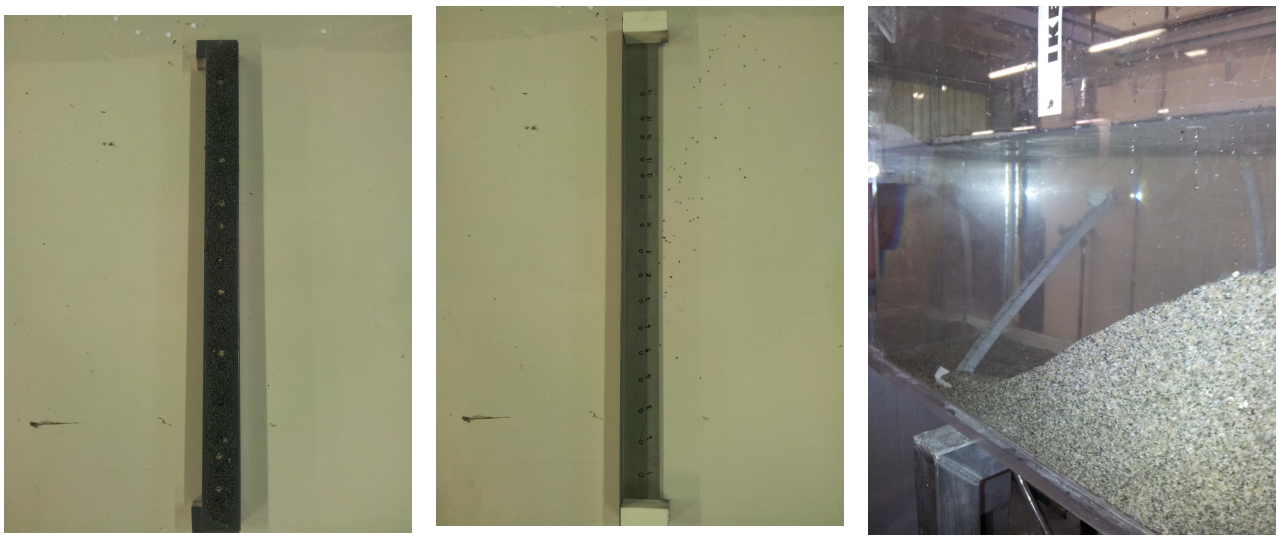

Fig.2.31. Object for calibration the laser (From left to right: Rough surface, smooth surface, position n the channel)

Initially, we filled the sediment tank by water, and then we put this object on it then the spots were measured both by laser and gauge to be compared.

We plot the measurements by gauge versus measurements by Laser in terms of voltage (Fig.2.32) and then we found the trend to be used to interpolate the values obtained by Laser (Table.2.6).

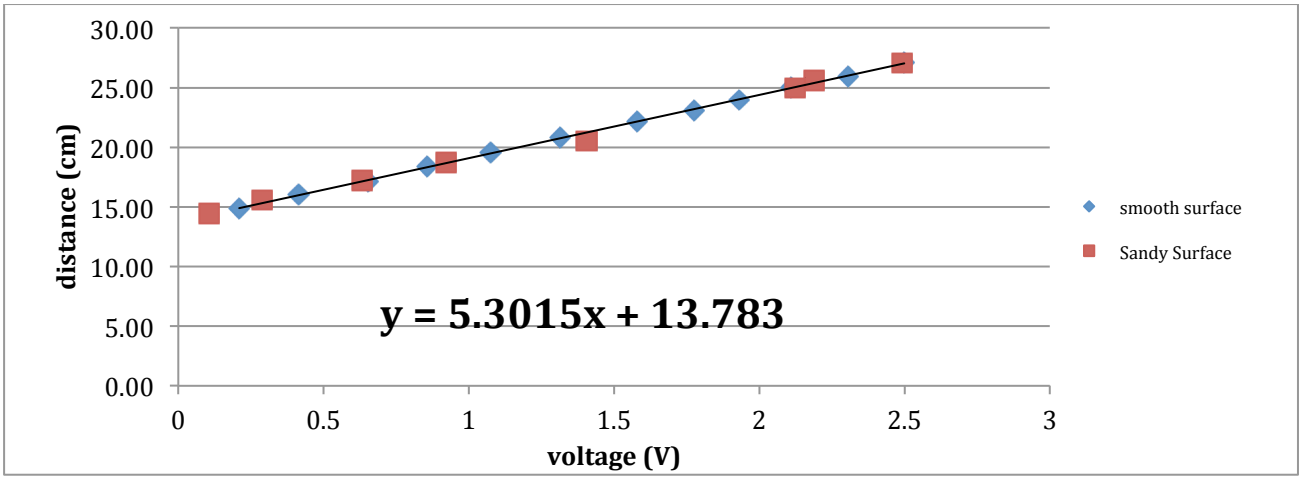

SMOOTH SURFACE					
No	Voltage	Distance Laser [cm]	Distance Gauge [cm]	Int Distance [cm]	Difference [cm]
1	2.499087	26.734	27.14	27.03	-0.112
2	2.303997	25.716	25.92	25.99	0.073
3	2.10804	24.693	25.03	24.95	-0.075
4	1.930903	23.768	23.96	24.02	0.056
5	1.77529	22.956	23.08	23.19	0.111
6	1.580659	21.939	22.15	22.16	0.009
7	1.314521	20.55	20.77	20.75	-0.022
8	1.075006	19.3	19.56	19.48	-0.081
9	0.857577	18.165	18.38	18.33	-0.054
10	0.652796	17.095	17.14	17.24	0.100
11	0.412924	15.843	16	15.97	-0.031
12	0.209725	14.782	14.91	14.89	-0.018
					OK

ROUGH SURFACE					
No	Voltage	Distance Laser [cm]	Distance Gauge [cm]	Int Distance [cm]	Difference [cm]
1	2.491	26.693	27.05	26.986	0.063
2	2.188	25.111	25.61	25.379	0.230
3	2.122	24.77	24.99	25.033	-0.043
4	1.405	21.027	20.53	21.232	-0.702
5	0.920	18.491	18.72	18.657	0.062
6	0.631	16.984	17.2	17.127	0.072
7	0.28	15.198	15.57	15.313	0.256
8	0.105	14.239	14.44	14.339	0.100
					OK

As it can be seen, the difference between two measurements in most cases are less than 1mm, therefore it can be concluded the value obtained by Laser are reliable

- Voltmeter:

  In order to check if Laser correctly does the measurement we used this device (Fig.2.27). In fact, we can see the vale of voltage that is registered on the software used for acquire this data, then we compare this value with the one that shows on the acquisition device, then if the voltages are different we should repeat measurement.

- Rulers:

  The scour holes depth at three points namely; at wall, at abutment nose and at downstream of abutment was measured manually using a ruler attached to the channels. The ruler was attached so that the "0" mark was at the initial level of the sediment bed (Fig.2.28).

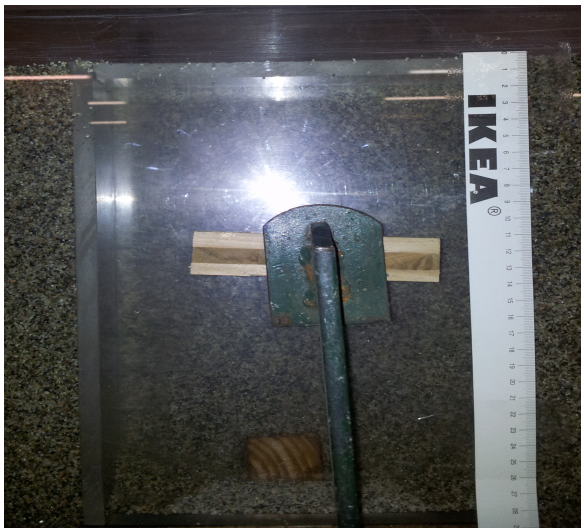

- Transparent pipe:

  In order to observe scour holes at abutment nose and point at downstream of the abutment we used this object (Fig.2.29)

-
-
-

- PC:

- In principal, the Laser sends the measurements to the acquisition device and subsequently this device send all the data to PC to be processed. We used " Visual Basic" program to process data.

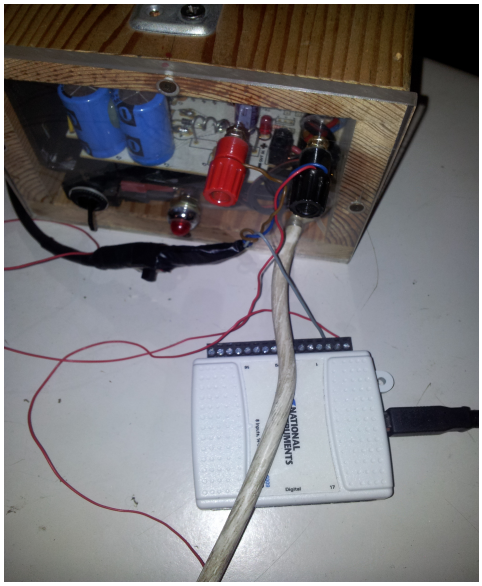

- Level:

This instrument has been used for leveling and calibration of the positioning system (Fig.2.30)

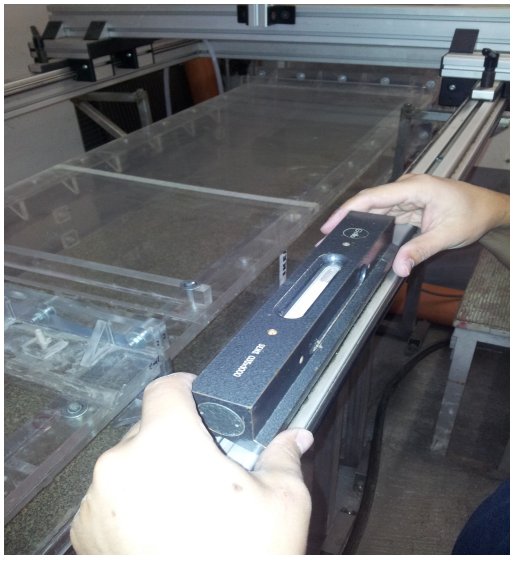

Fig.2.30

2.6.2 Scour Test procedure

- Place the abutment into channel; the abutment is placed at the left wall (Fig.2.32)

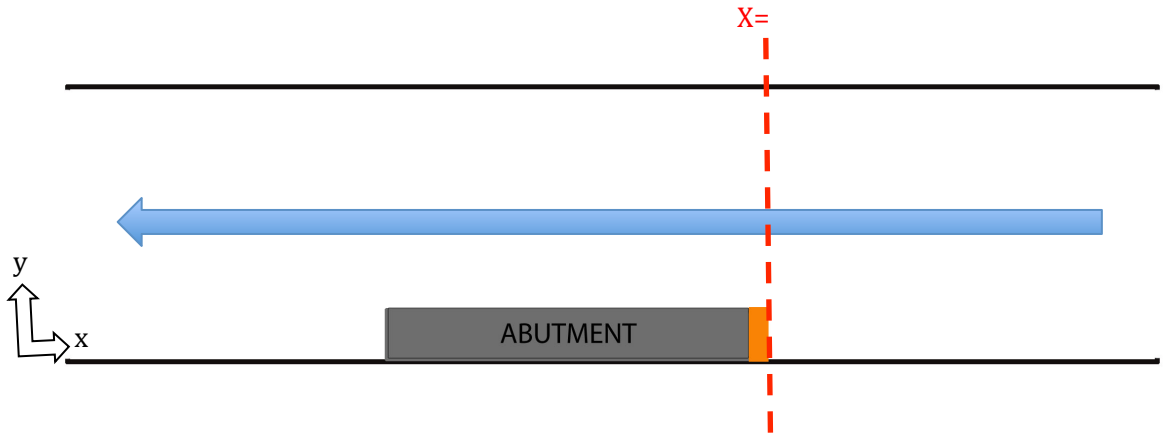

Fig.2.33

- Fill the tank by washed-sands till desired level.
- Put the clamps in order to avoid the channel to be deformed.
- Scrub the sediment surface by wooden oblique.
  What we concluded from trial test, was the fact that we should fill the tank a day before performing the test, due to the fact that, after filling the tank with water, sediment will settle down for some millimeters, hence for following test we replaced abutment and filled the tank a day before running the test and let the sediments to be settled down, the next day we refilled the tank and scrubbed the sediment surface.

- Try to fill channel (Sediment tank) slowly with water pipe, this should be done very carefully, not to disturb the sediment.
- Switch on the channel pump with very low rate discharge, approximately 0.4 Lit/sec.
- Increase discharge slightly while adjusting downstream boundary condition and water depth (10cm) till 14.8 Lit/sec, which is 99% critical discharge.
- After we observe that the water level is quite constant and we don't have dramatic change on it we can start putting the top part of the abutment while we have stopwatch in our hands and we record time and scour depth correspond to it, at three points (wall, nose and downstream part of abutment).
- Read water level in piezometers and discharge every 30 minutes in order to control the test condition.

-
- Take a survey of scour holes cross sections (Fig.2.34) after a certain time that we have decided to run the test.

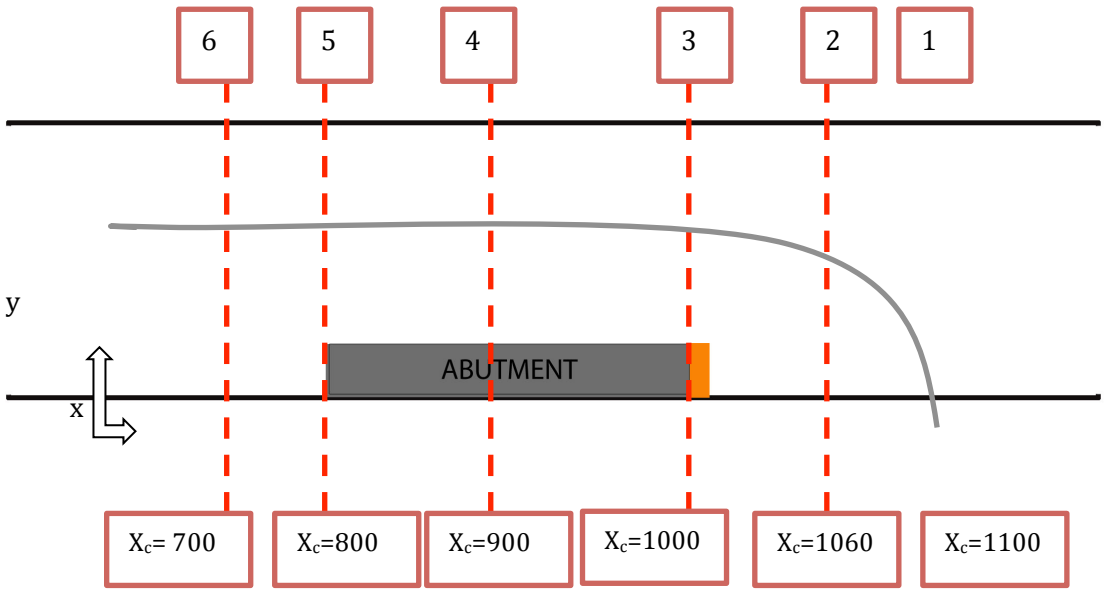

It should be noted, we run each test in two days, which in total we collect data for 7hours and half. The first day we pause test after 2h30 and made a survey, then in the second day, channel has been run for 5 hours and after that we made the second survey.

In order to pause the test, we declined discharge slightly down to 3Lit/sec while adjusting boundary condition and water level, then we took away the upper part of abutment to make a survey. In the next day to start again the test, we put back the removed part of abutment and then increased the discharge faintly up to 14.8 Lit/sec while adjusting boundary condition and water level.

This procedure was checked in a trial test, the experimental time for the trial test was 2h30'. This test has been carried out just to check the circumstances and to find which would be the best way to perform the whole experiments, in spite the fact that, we recorded the results of this test but they are not investigated and compared. The plots and tables related to this test is reported in Annex 2.

3. Scour Countermeasures Analysis:

In this section the results of our analysis for the countermeasures that we used is fully described. Initially, unprotected experiments are shown, with attention paid to experiment repeatability. Then, step by step, experiments presented individually and finally a synoptic observation is attempted. In the table 3.1. an overview of all tests and their parameters are reported:

	Test	b (cm)	t (cm)	p (cm)	s (cm)	zmin (cm)	Q (l/s)	Depth (cm)	Velocity (m/s)
SERIE A	1	5	0	0	0	0	14.7	10.65	0.345
	2	5	1	1	2		14.67	10.45	0.35
	3	5	1	1	3		14.7	10.4	0.355
	4	5	1	1	4		14.55	10.6	0.345
	5	5	1	1	1		14.61	10.6	0.34
SERIE B	6	5	0	0	0	0	14.65	10.5	0.35
	7	5	1	1	2		14.67	10.45	0.35
	8	5	1	1	3		14.72	10.4	0.355
	9	5	1	1	4		14.65	10.5	0.35
	10	5	1	1	1		14.62	10.6	0.345

3.1. Unprotected Abutments:

In the first experiment an unprotected abutment as an obstacle was used. This experiment has repeated for both series, in order to be compared and verify the repeatability. The experiment procedure was exactly the same as in the trial test expressed in chapter 2.

3.1.2. Scour Depth with time:

During the tests, the scour depth was continuously measured at 3 points namely; at abutment wall (poin1), abutment nose (point2), downstream corner of abutment (Fig3.1). As mentioned previously scour depth was measured using rulers stacked to these points.it can be noted that, the test condition in terms of discharge and water depth was controlled by measuring water level in the piezometers and reading discharge, all the graph and tables are reported in the annex.
If we consider the channel as reference the location of these points are (in mm)
:

W		N		D	
Xc	Yc	Xc	Yc	Xc	Yc
1000	0	1000	50	800	50

Fig.31

The temporal variations of the scour depth at the three points for both tests are reported in Figure 3.2. Need to mention that, logarithmic trend is what is typically seen in this kind of experiments.

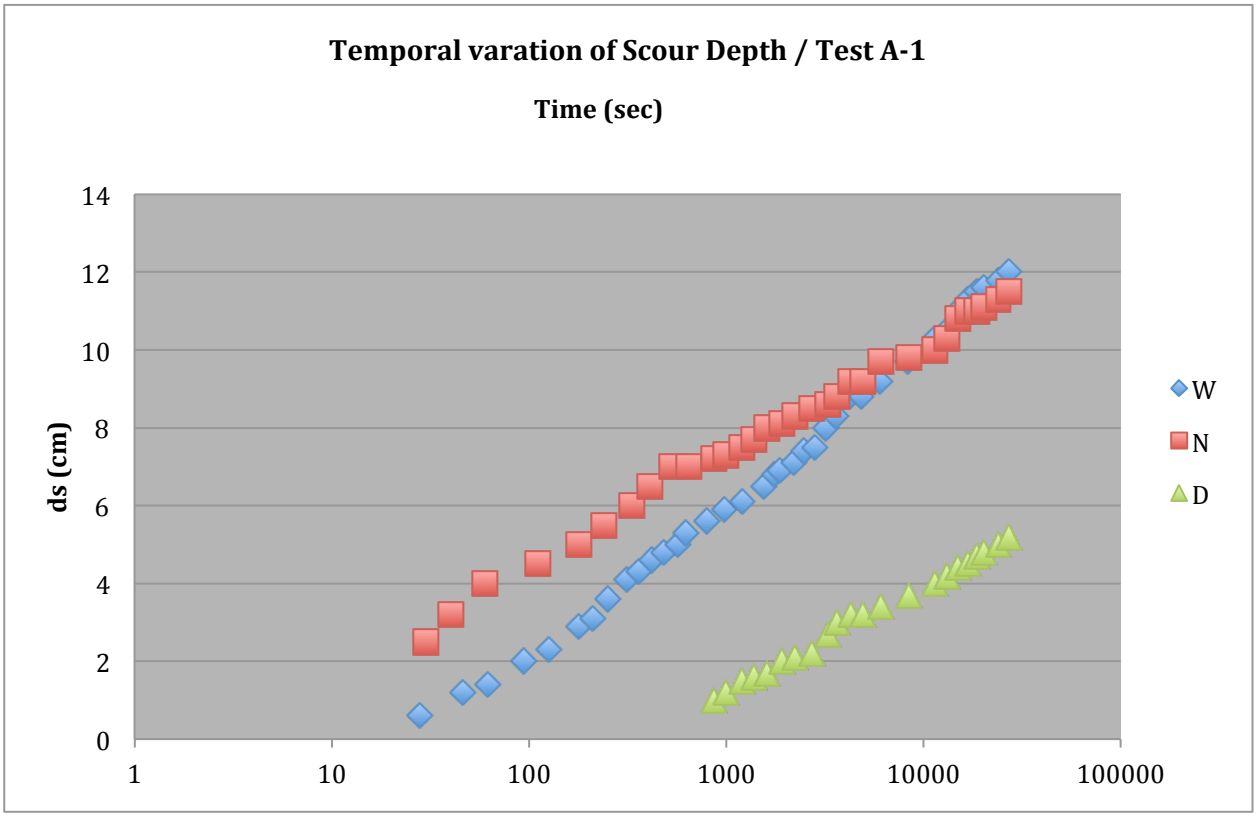

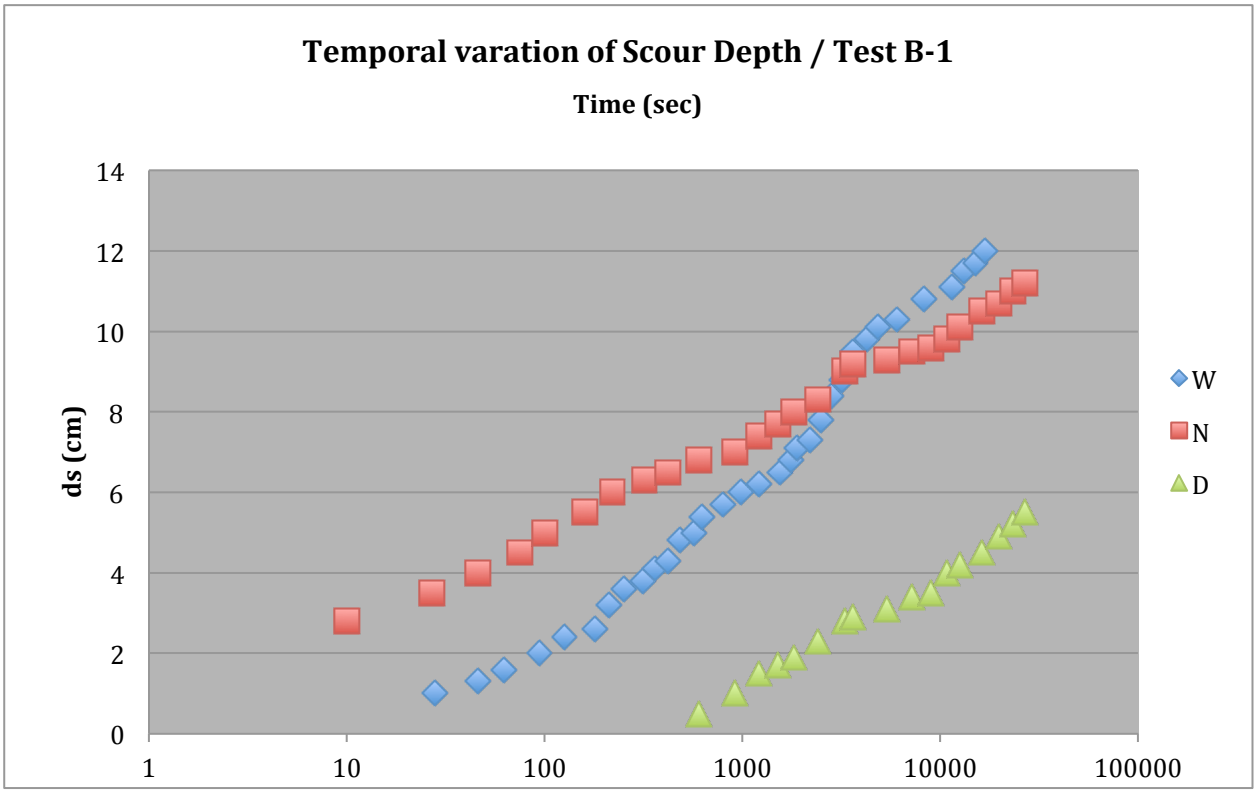

Fig.3.2

As it can be seen from the plot, in the first stage of the test the scour has a sharp rise at flume wall and nose, whereas the scour at down stream corner has started after 10 minute. After a certain time the scouring velocity decreases and the graph shows a gentle slop. At the end of this experiment, the maximum scour occurred at abutment wall that is 12 cm, in spite the fact that before this stage the scour was greater at abutment nose. As a matter of fact, the scour at nose and at wall converge and cross each other at certain point and after that we can observe deeper scour at wall. In other words, if at the start the score holes depth is deeper at the abutment nose, but in time, maximum depth moves from nose to wall. This can be logically explained by the motion of the sediments, since at the wall the scour hole does not receive any sediments from upstream but in the meantime scour hole at the nose receives particles that are passing by from the scour hole at the wall. As the scour hole increases, the principle vortex weakens, which results in a smaller scouring intensity at the nose.

From Fig.3.2 the maximum scour depth after 1 hour was about 8.3 cm at the abutment wall and 8.8 cm at the nose so the 1 hour mark can be assumed the time when the scour hole started to move from the nose to the wall. At the end of Test 1, after 7 hours and 30 minutes the maximum scour depth reached 12 cm at the abutments wall, 11.2 cm at the abutments nose and 5.2 cm at the downstream corner of abutment, hence the difference between nose and flume wall points was roughly 0.8 cm.

As far as repeatability is concerned, we can note that the trends in both tests are the same and this can be verified from figure 3.3 to 3.5.

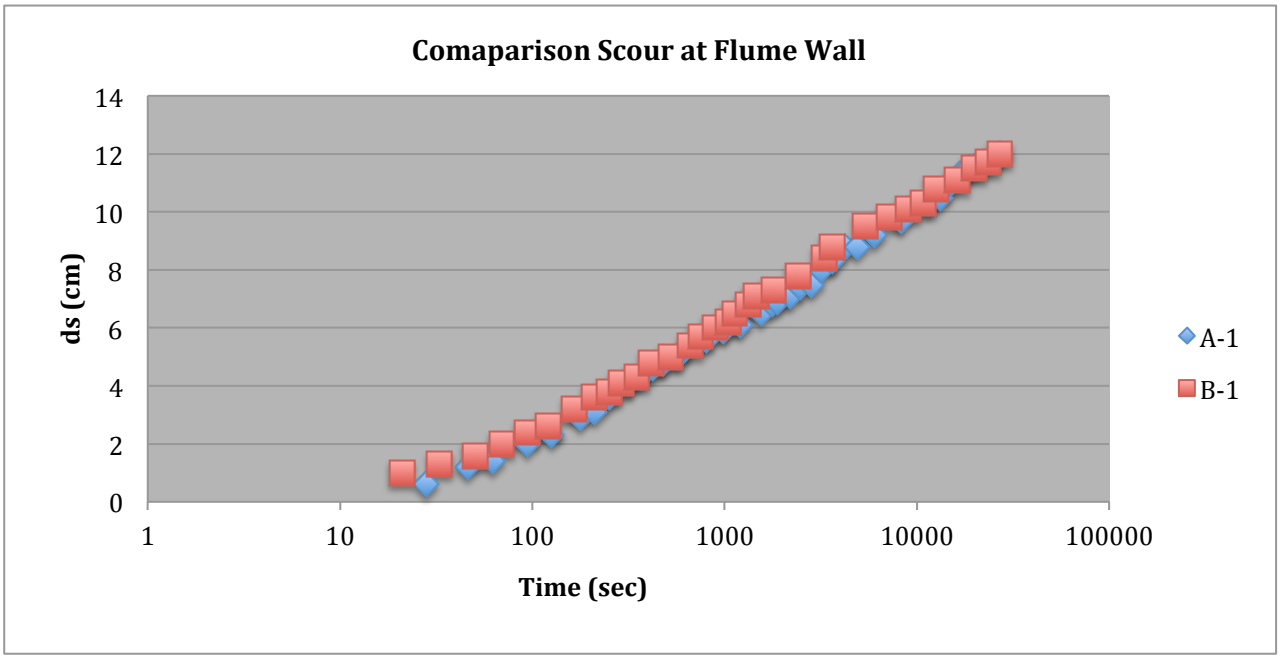

Fig.3.3

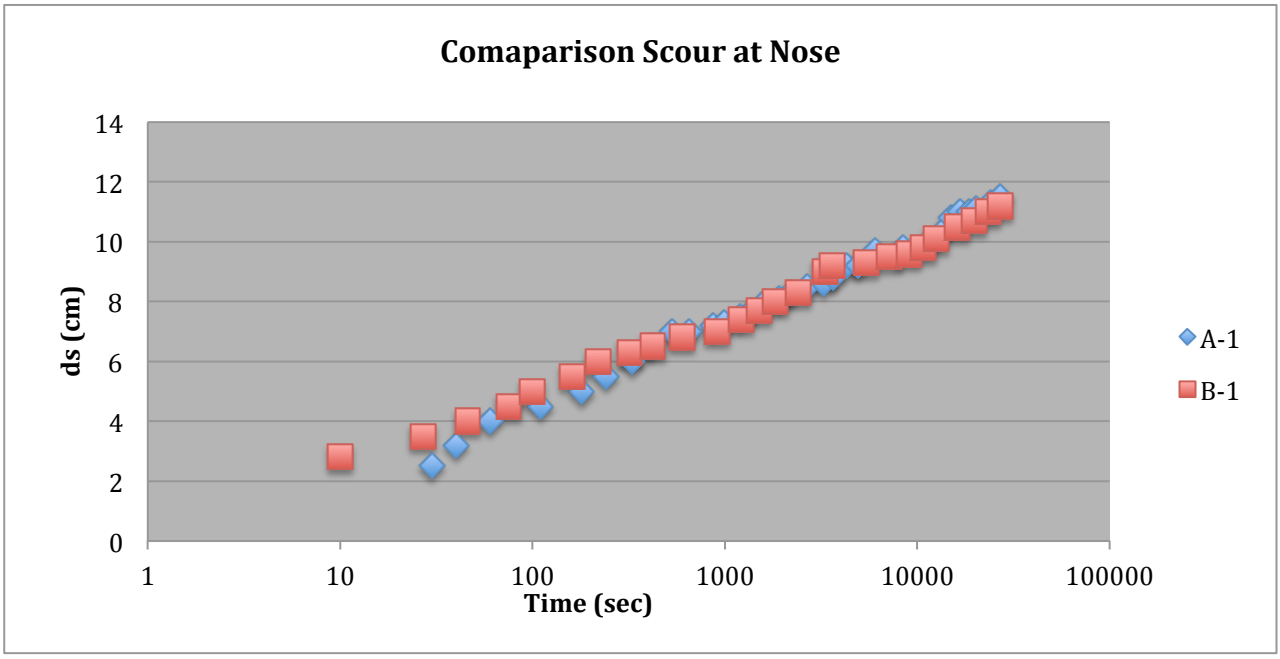

Fig.3.4

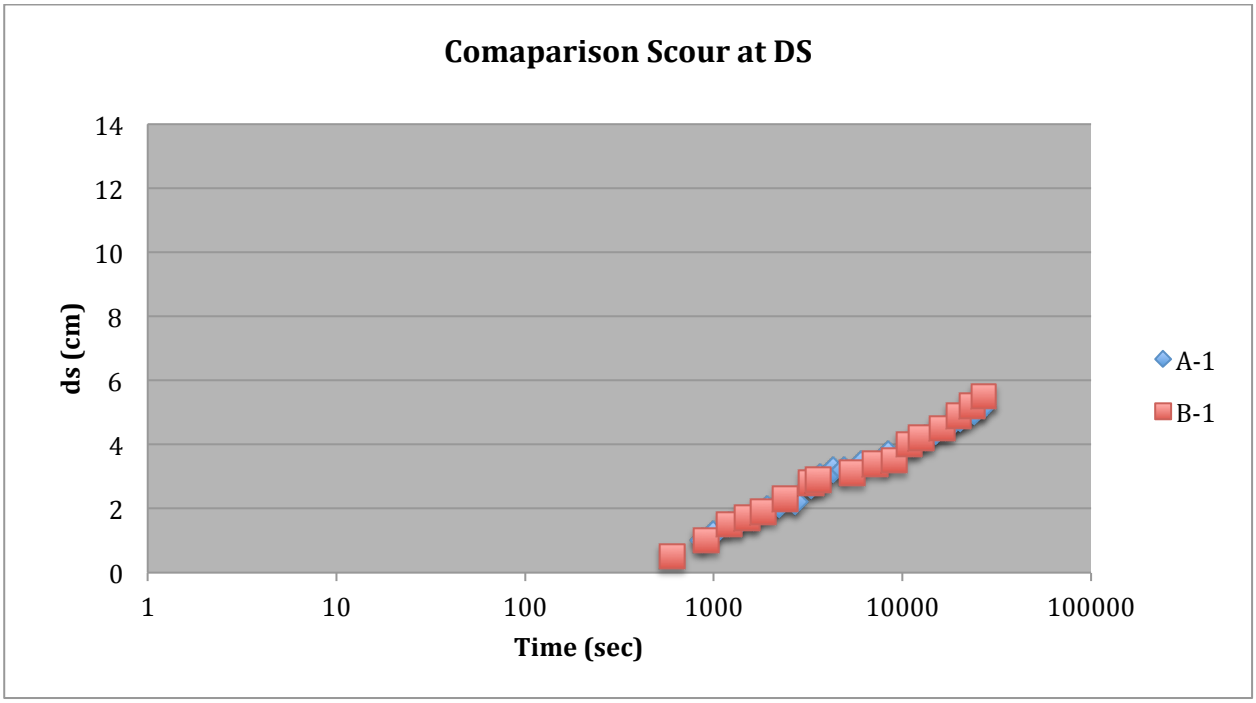

Fig.3.5

Having looked at this graph we can see, the trend remain the same in both tests, although there are some changed in few points. At the end of experiments, the scour at nose and wall is the same for both tests but scour at down stream point in test B-1 is a bit deeper. However, to my understanding, we can say in general the repeatability is fully satisfactory.

3.2. Effect of protection:

3.2.1. Description of the Abutments:

As it is shown in figure.2.25 the abutments that we have used in this experiment have two parts that can be separated (mentioned before). Basically, the vertical wooden wall was attached to the abutment by screws, therefore in order to perform each test we just needed to change this wall. The properties of abutment utilized in each test are reported in table.3.1.

The experiment procedure was exactly the same as in the previous tests.

3.2.2. Scour Depth with time:

3.2.2.1 Scour Depth with time for Series A:

Also during the scour tests with the countermeasures, the scour depth was continuously measured near the abutment (points W, N and D in Figure 3.1). The temporal variation of the scour depth at the three points for test A-2 is reported in Figure.3.6. In the first stage of the test the same events as in the previous experiment occurred. If at the start the scour hole at the abutments nose is deeper, then in time the scouring at the nose weakens and the scour hole becomes evenly deep both at the nose and at the abutments wall, which can be seen in Fig.3.6. and approximately at the end of experiment they converge each other and scour at wall become even greater. But the difference with the unprotected abutment is that, the convergence happen nearly at the end of experiment, not 1 hour after starting and then, the maximum value of scour at nose is 10 cm and

at wall is 10.2 cm, which can be concluded that, not only there is 1.2cm reduction of scour at nose and 1.8 at wall but also the difference between scour at two points is decline to 0.2, that could be due to the fact that, the roughness element weakens the down flow.

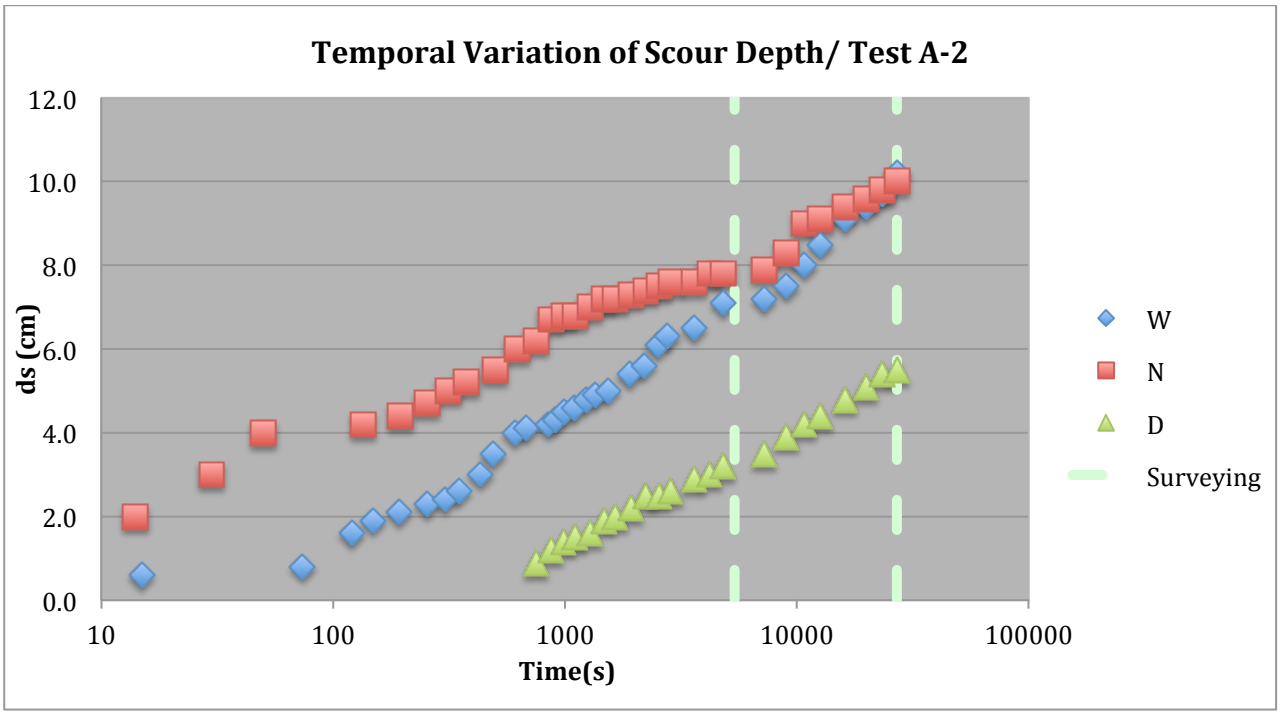

Fig.3.6

Interestingly, at downstream point scour starts after 10 minute, moreover at this point we cannot observe remarkable change. We may consider that, we are using local scour countermeasures and this point I quite far from the protections.

As it is noted before, we have surveyed the scour hole for 6 sections at experimental time of 2h30' and 7h30' that will be reported in annex.

The first protected abutment has 2cm space between two roughening element with protrusion of roughening element equal to 1 cm. Subsequently, for the first series of test we kept the same protrusion but we changed the space between element to see how our results will be changed.

The temporal variation of scour depth for this series of our experiments are shown below:

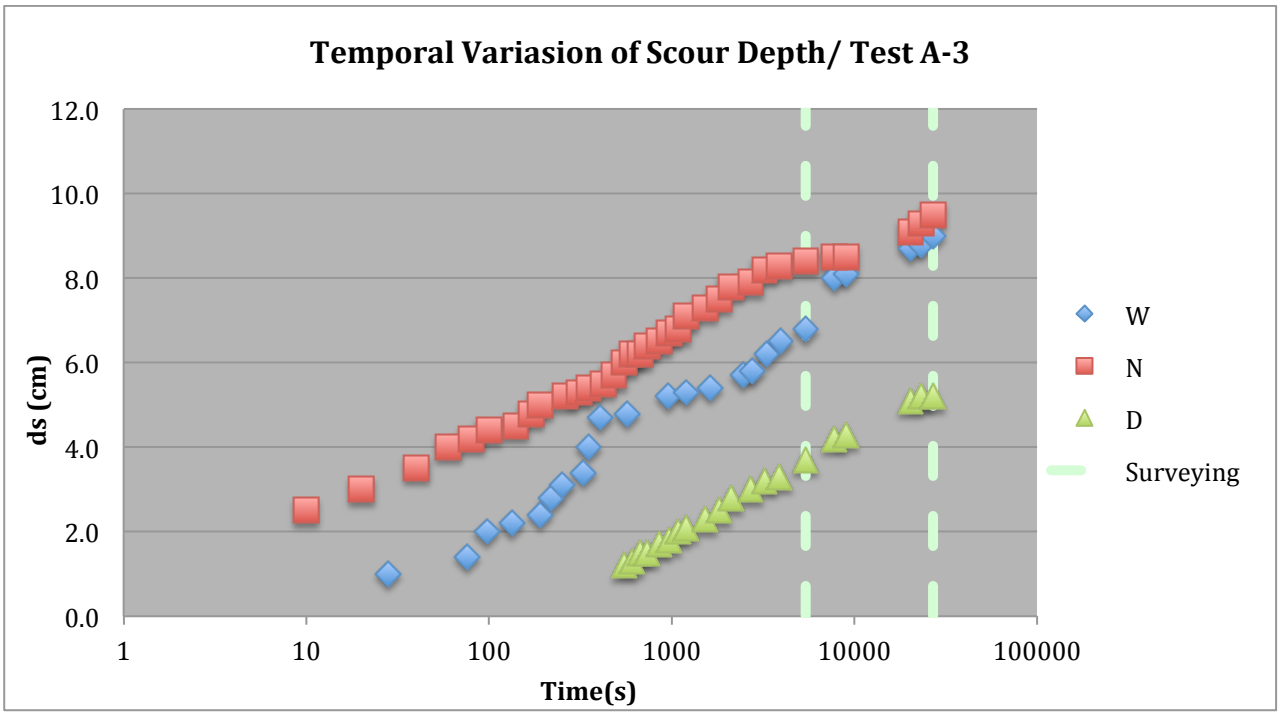

Fig.3.7

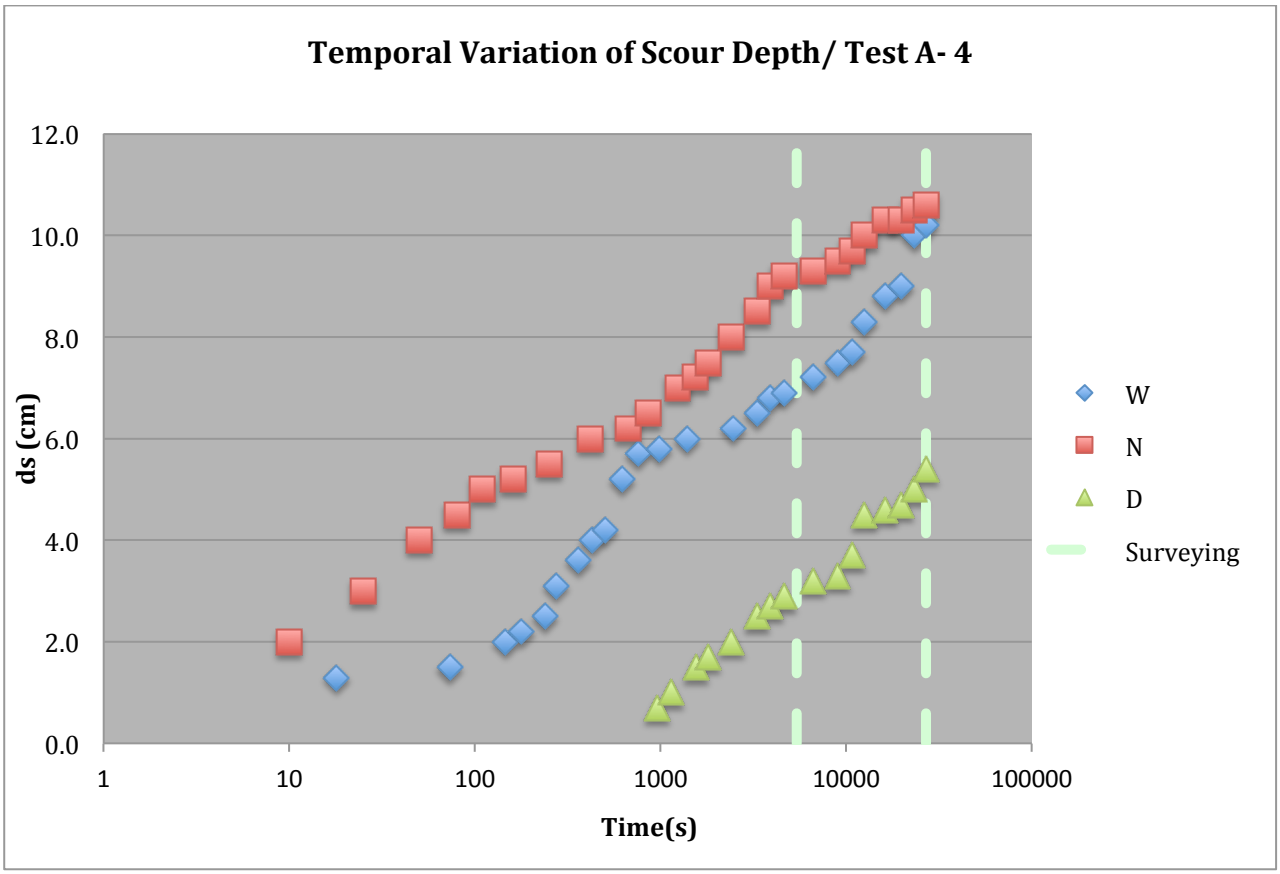

Fig.3.8

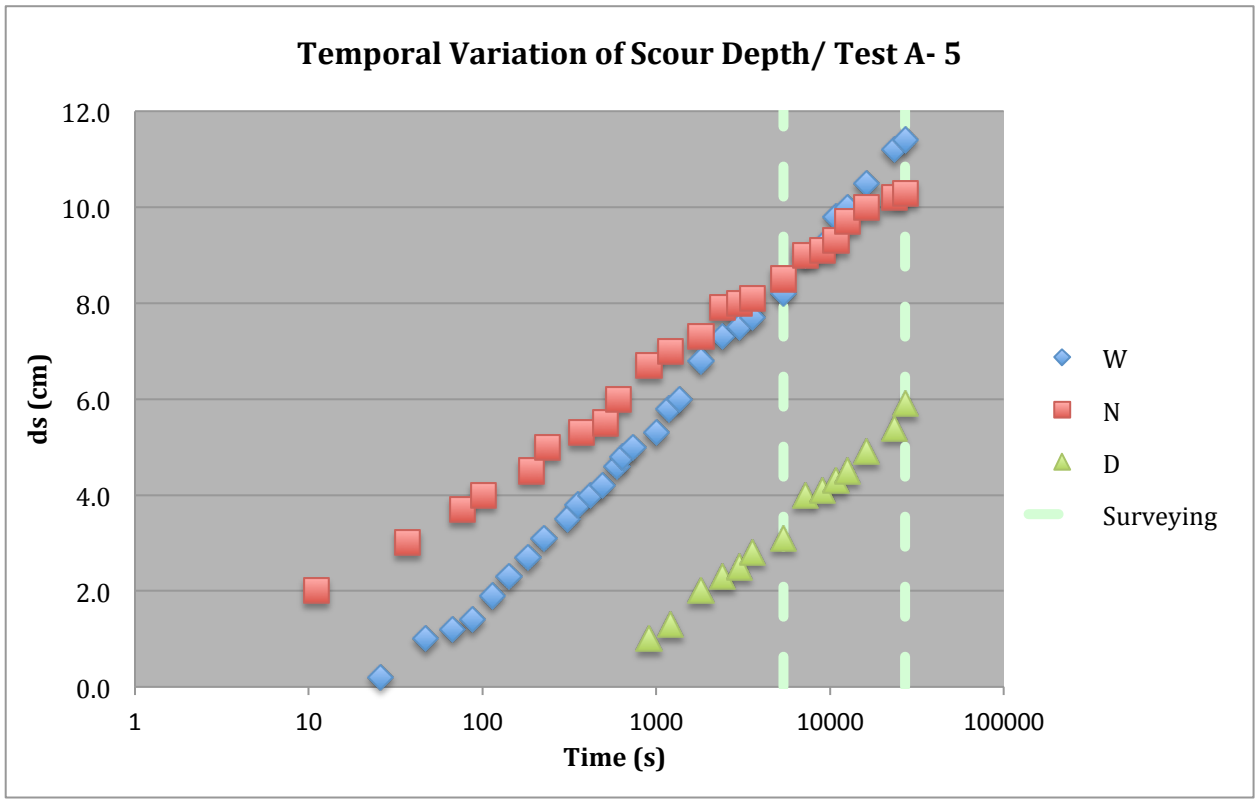

Fig.3.9

As it is obvious from these plots, the trend is quite the same for all tests instead of test A-5, in the mentioned test we can see similar behavior as unprotected test, scour at nose and abutment cross each other earlier than other tests but later than unprotected test. Indeed, the experimental campaign was designed in such a way to arrive at spacing so small, that the upstream face of the abutment would result in a new one shifted upstream. So it is reasonable that, for the lowest spacing we arrive at this effect.

In comparison with unprotected test, in which these two lines cross each other just 1h after experiment starts whereas in test A-5 this happen around 4h30 after test begins with the value of 9cm in both points.

Comparisons of scour depth at each point for all tests are plotted in fig 3.10 to 3.12.

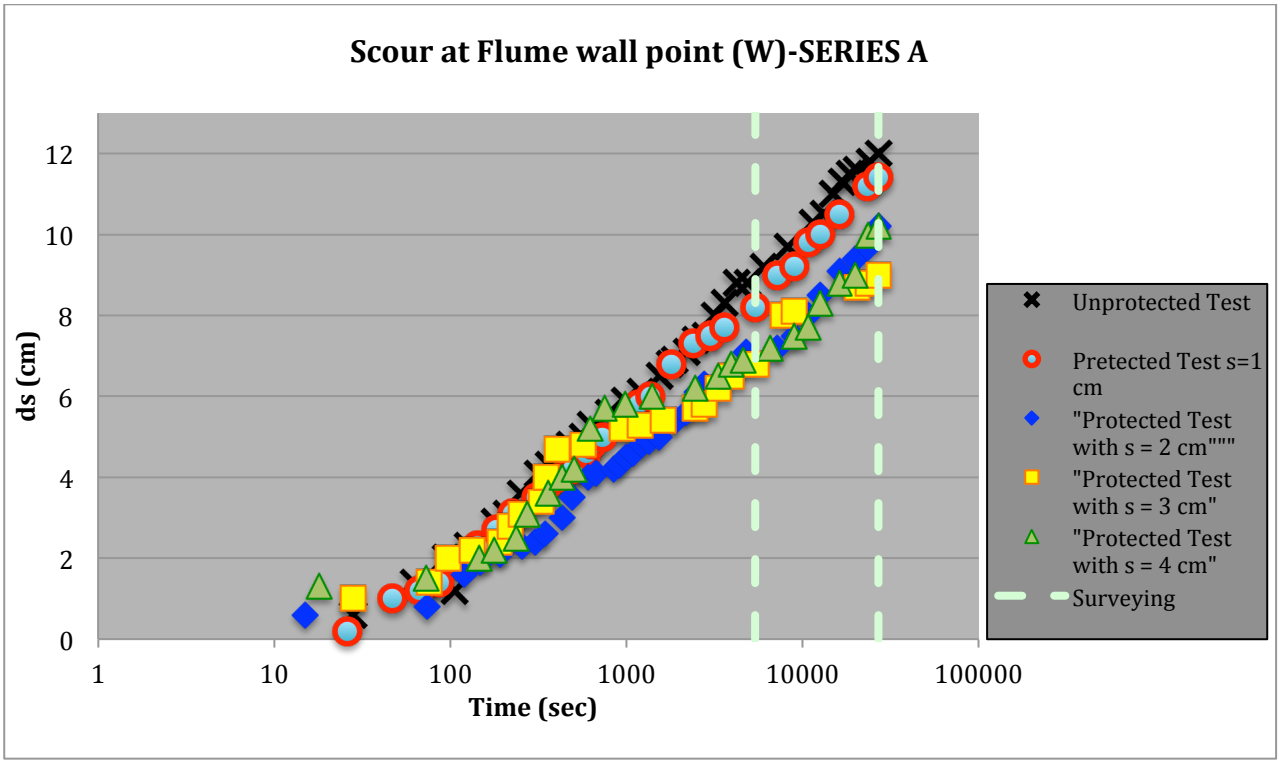

Fig.3.10

Referring to Fig.3.10 we can conclude that, the best behavior at the end of experiment at flume wall is presented by abutment with s=3 cm with maximum scour depth equal to 9cm. As it is said before the abutment with s=1 has similar behavior of unprotected test and we can notice the reduction at this point for this test is not significant. Interestingly, this abutment has shown good behavior just at the beginning of the test, and we can see the minimum scour depth is belonged to this test. On the opposite at this stage the maximum scour depth is presented by abutment with s=4 cm.

Nearly, in the middle of the experiment (3h30'), the best behavior is shown also by abutment with s=3cm.

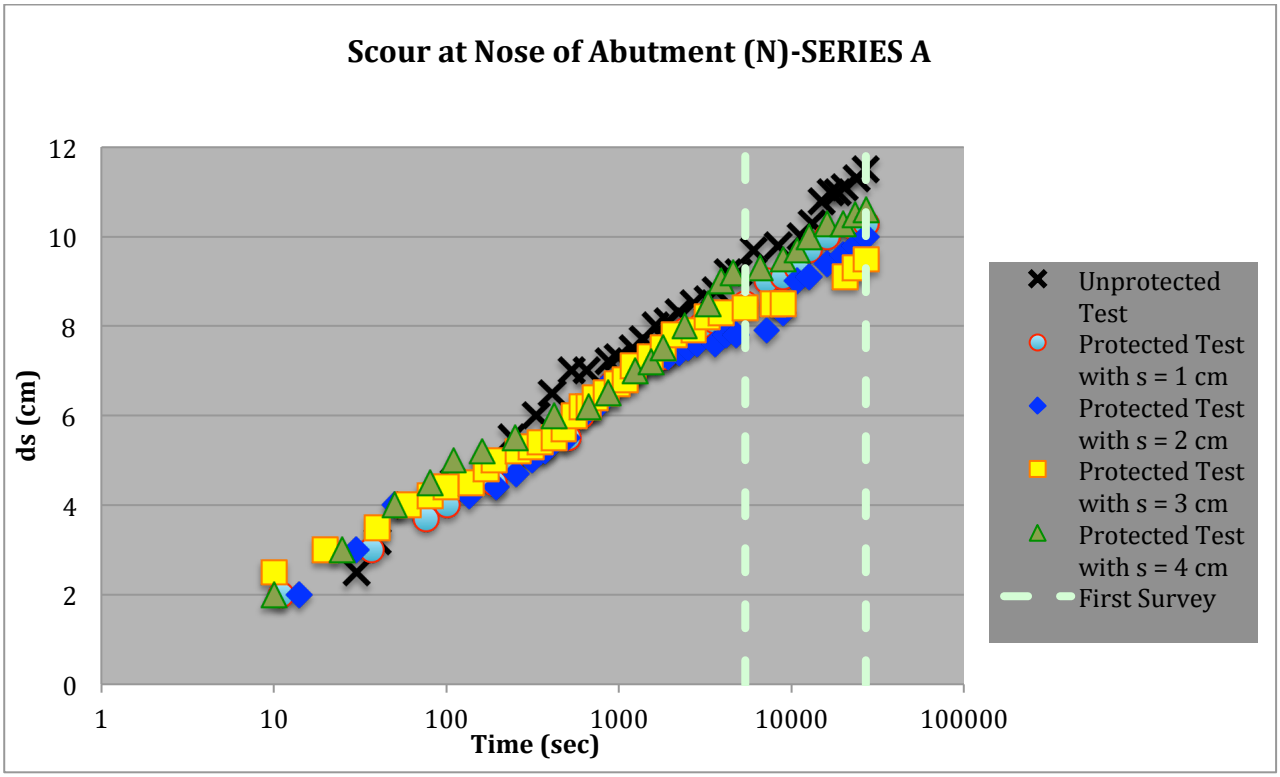

Fig.3.11

At this point also, we have less scour depth for abutment with s=3cm at the end of experimental time with the value of 9.5cm however the worst performance at start is belonged to this abutment. Surprisingly, despite the fact that we have expected to see maximum depth at wall, here the behavior is more confused. However, as also discussed on the paper by *Radice A, O Lauva (2010) On flow-altering countermeasures for scour at vertical-wall abutment,* these roughening elements have poor effect in protecting the nose.

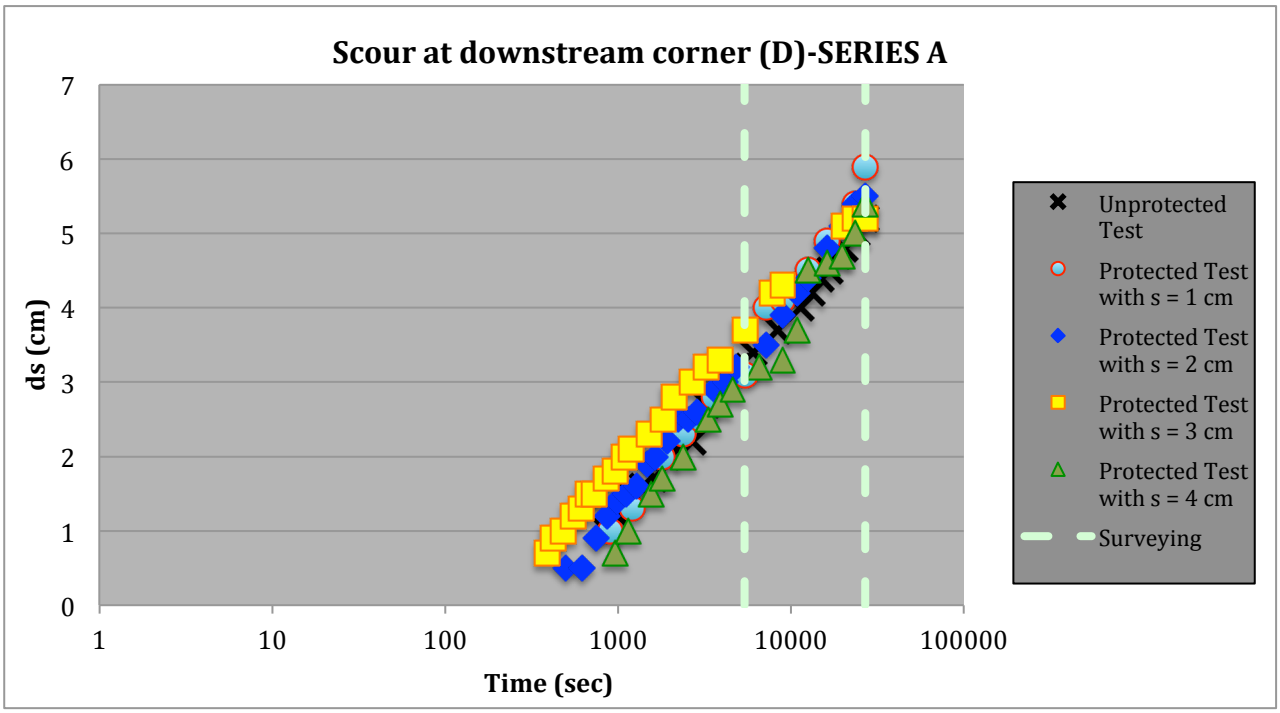

Fig.3.12

Nevertheless, there is no significant reduction of scour at this point but, again we see that, the minimum scour depth is happened for abutment with s=3 at the end of experiment which is equal to 5.2 cm and with respect to the unprotected abutment there is little change. The maximum scour at this point happen for abutment with s=1 which is equal to 5.9cm that prove not only there is no reduction at scour depth but also is deeper with compare to unprotected abutment.

3.2.2.2 Scour Depth with time for Series B:

In this part of our experiments, we tried to change not only spaces between roughening element but also we change the protrusion of roughening element to 0.5cm to see how the result will be changed. From figure 3.13 to 3.16 the variation of scour with time for each tests of this series are presented.

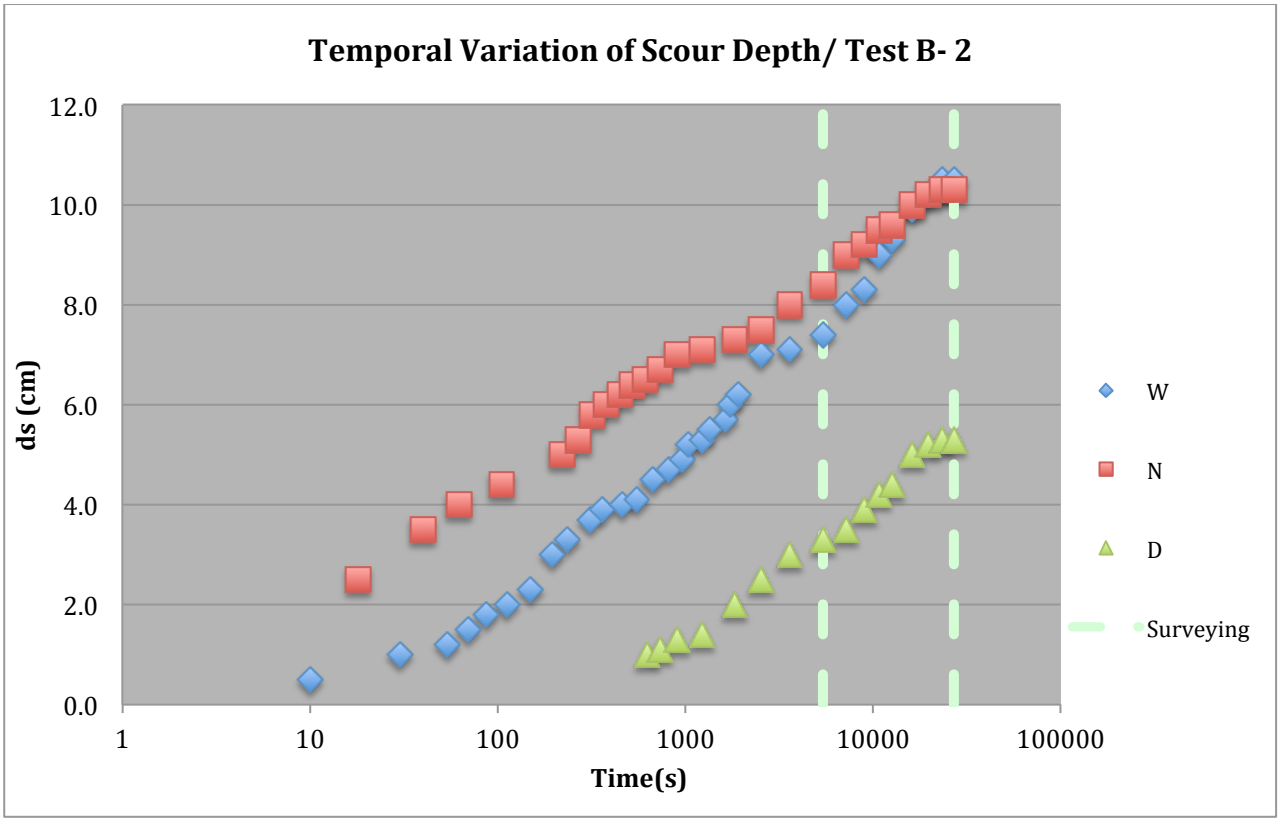

Fig.3.13

Having watched at this graph, we can see that scour at nose and at wall converge and cross each other 4h30' after the experiment starts and reach to 9cm at both points. Compare to test A-2 the time that 2 lines meet each other decreased for about 2 hours whereas the scour depth for test A-2 at this point is equal to 9.8cm.

As we expected, the maximum scour depth occur at wall that reach to 10.5 at wall, which is 0.3mm deeper than test A-2. Equally it happened for all tests, at the first stage the scour at nose rise dramatically at abutment nose but in time weakens and moves to abutment wall.

Also for this test, we cannot observe significant reduction at down stream corner of the abutment.

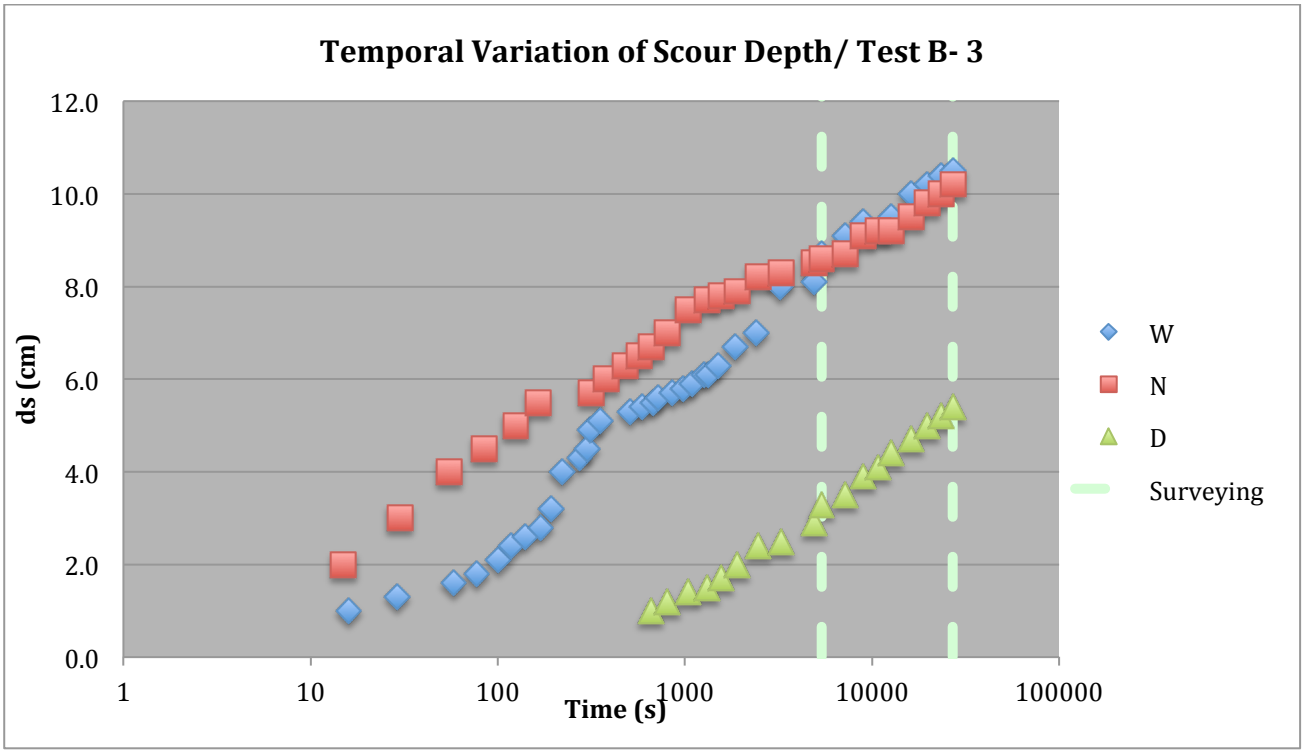

Fig.3.14

As apposed to test A-3 in which the value of scour at wall never reach to scour at nose even at the end of process, in this test these two line cross each other much earlier than test B-2 nearly 2h30' after tests starts and hit 8.5cm in both points. In comparison with test B-2 the maximum scour depth remains the same, which is equal to 10.5cm, but it is deeper with respect to the test A-3. Moreover no reduction at downstream corner of abutment.

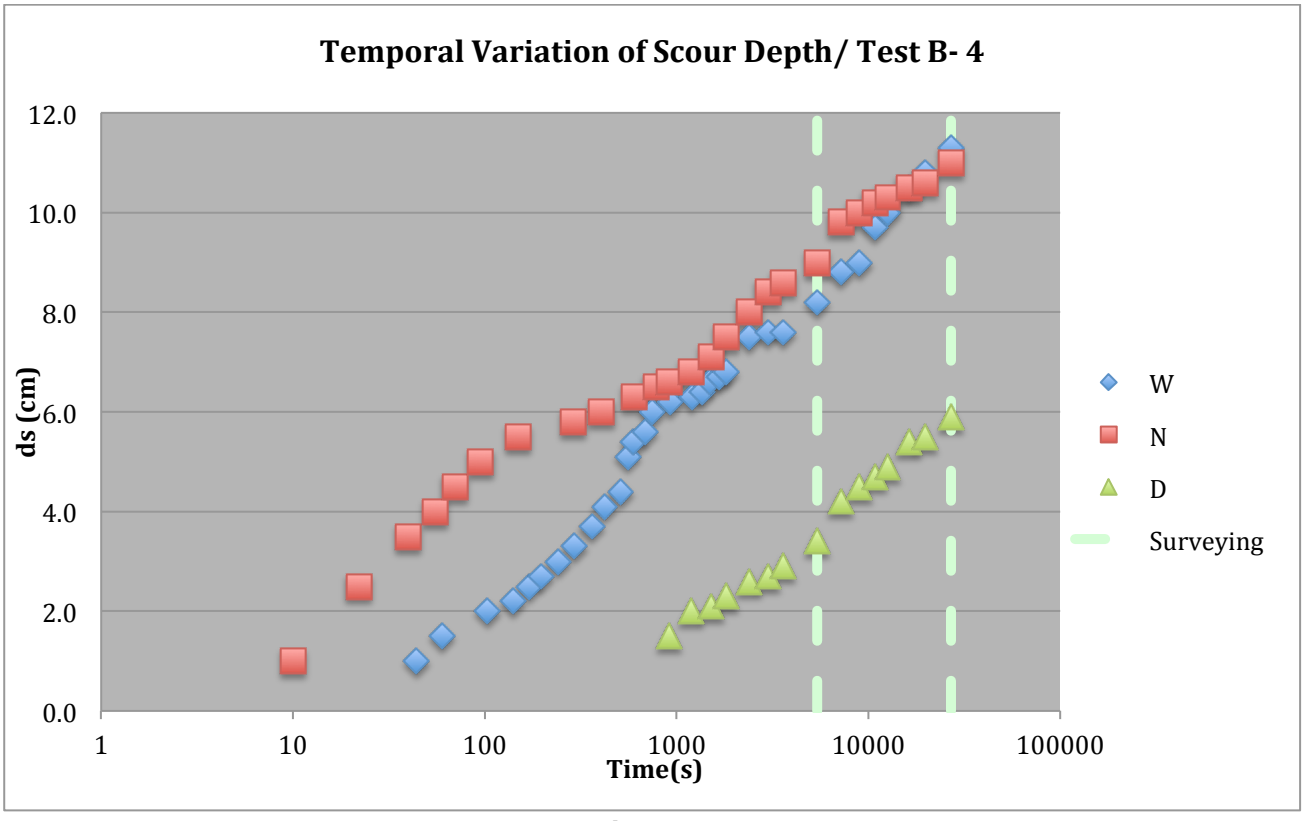

Fig.3.15

In this test, two lines (W and N) cross each other almost in the middle stage of the experiment, but as it is expected the maximum scour occur at wall that reach 11.3cm whereas in test A-4 maximum scour occur at nose with the value of 10.6 cm. Interestingly enough, not only there is no reduction at downstream corner with respect to the unprotected abutment but also the plot illustrates an slight increase of scour at this point for this test.

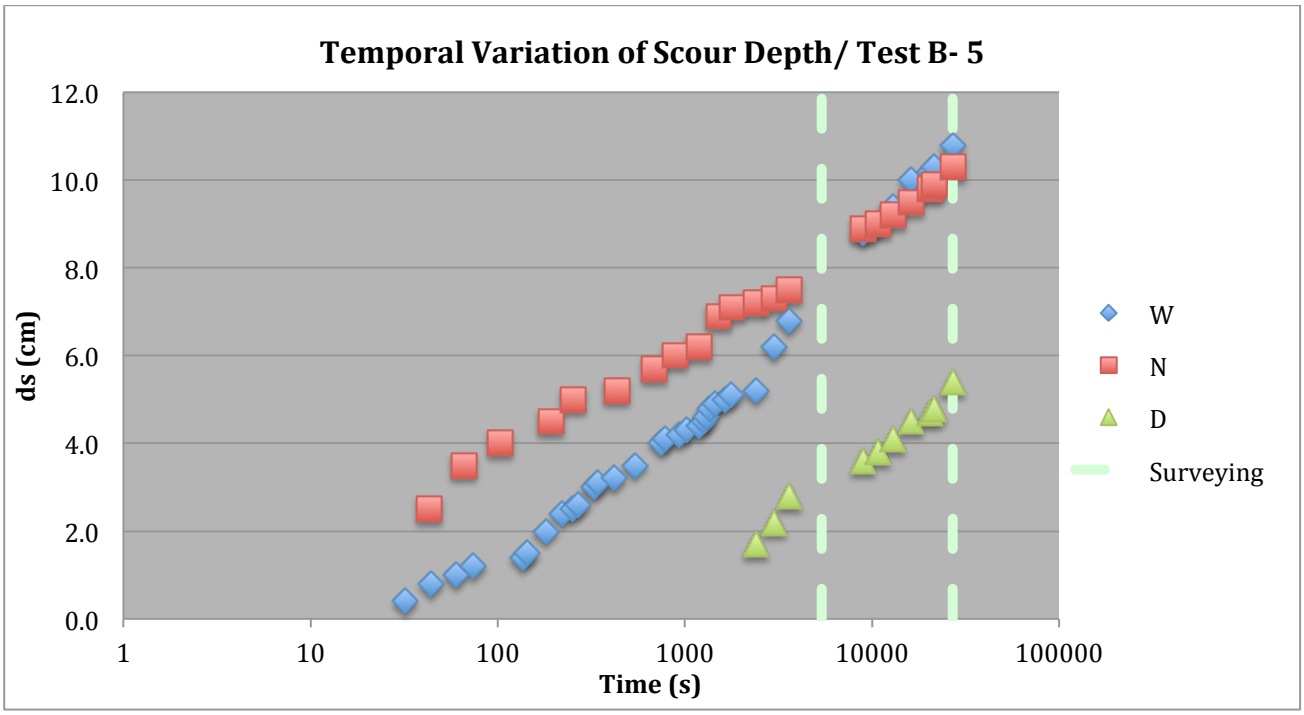

Fig.3.16

In this test, we can see the same behavior as other tests of this series. Obviously the maximum scour is related to flume wall of abutment that reaches 10.8cm, which compare to test A-5 is reduced by 0.8cm however scour at nose is almost the same with respect to test A-5 with the value of 10.2cm. Again, no reduction at downstream point presented.

Comparisons of scour depth at each point for all tests are plotted in fig 3.16 to 3.18.

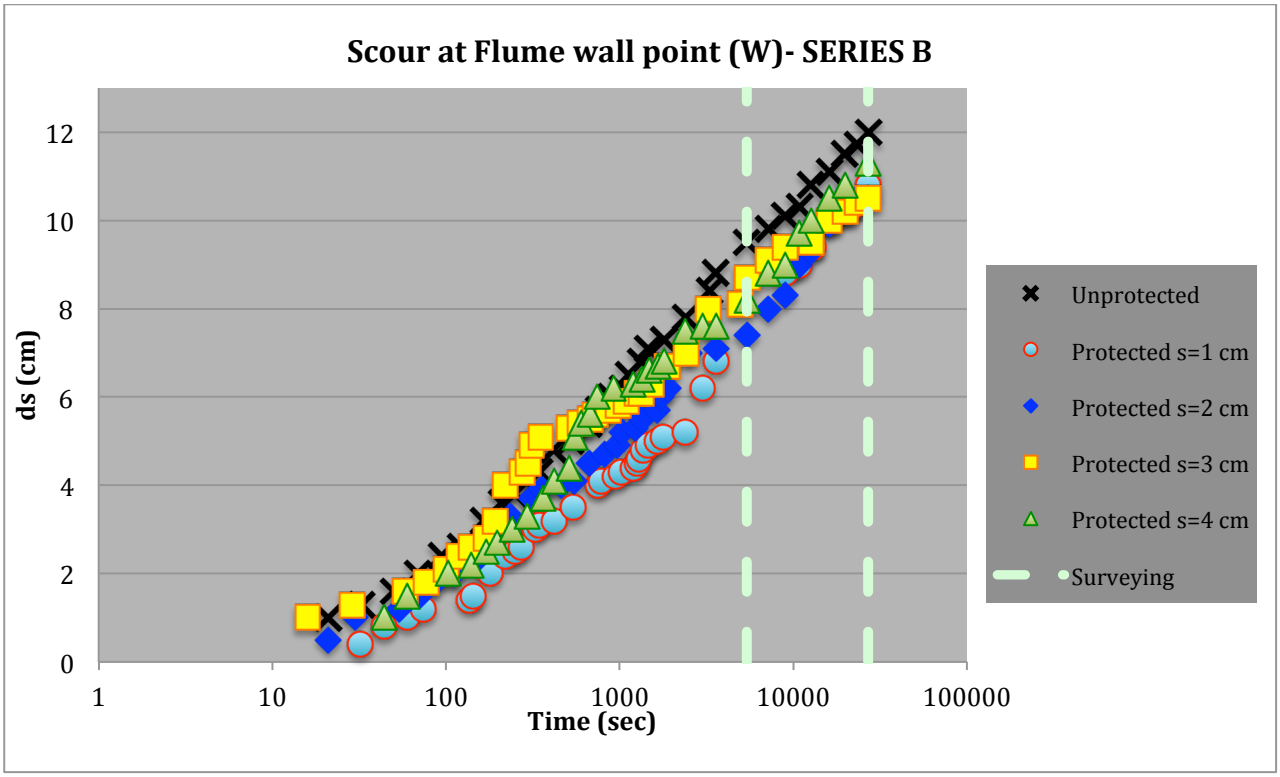

Fig.3.16

Considering Fig.3.16 we can conclude that, similarly in this series of tests the best behavior at the end of experiment at flume wall is presented by abutment with s=3 cm with maximum scour depth equal to 10.5cm which is 1.5cm greater than abutment with p=1cm. On the opposite at the beginning of the experiment the maximum scour depth is occurred in this abutment and the minimum scour occurred at abutment with s=1cm. Moreover, in the middle of the experiment (3h30'), the best behavior is shown also by abutment with s=3cm.

For this series the abutment with s=4 has relatively similar behavior of unprotected abutment and the reduction in scour is not remarkable. Interestingly, the abutment with s=1cm has shown not only good behavior just at the beginning of the test but also the value of scour at the end of experiment is reduced by 1.2cm whereas for the similar case in series A the reduction was not meaningful, we can see the minimum scour depth just at the beginning of the experiment is belonged to this test.

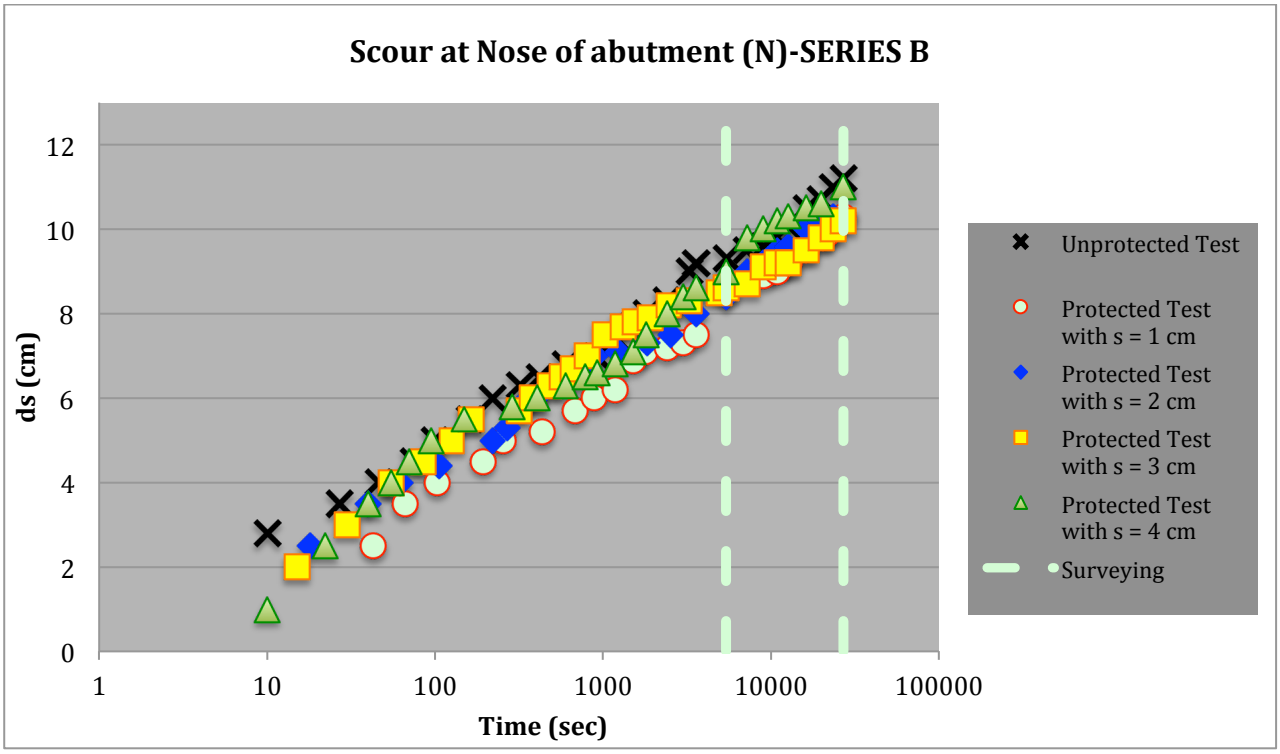

Fig.3.16

At this point , we have less scour depth for abutment with s=3cm at the end of experimental time with the value of 10.2 cm which is 0.7cm deeper than the one in series A however the worst performance just at start is belonged to this abutment. What is quite interesting in this series of tests, is the fact that the abutment with s=1cm and p=0.5 shows good behavior opposite to the abutment with the same space but p=1cm. At the end of experiment we can see the same value of scour depth for this test. Moreover if we compare the whole trend we can conclude this test has more effect on scour reduction than the others.

Similarly to what happened at abutment wall, the worse behavior at the beginning of the experiment is also belong to test A-3.

Having looked at figures 3.15 and 3.16, we can note the maximum depth is occurred at flume wall of the abutments, as it was expected.

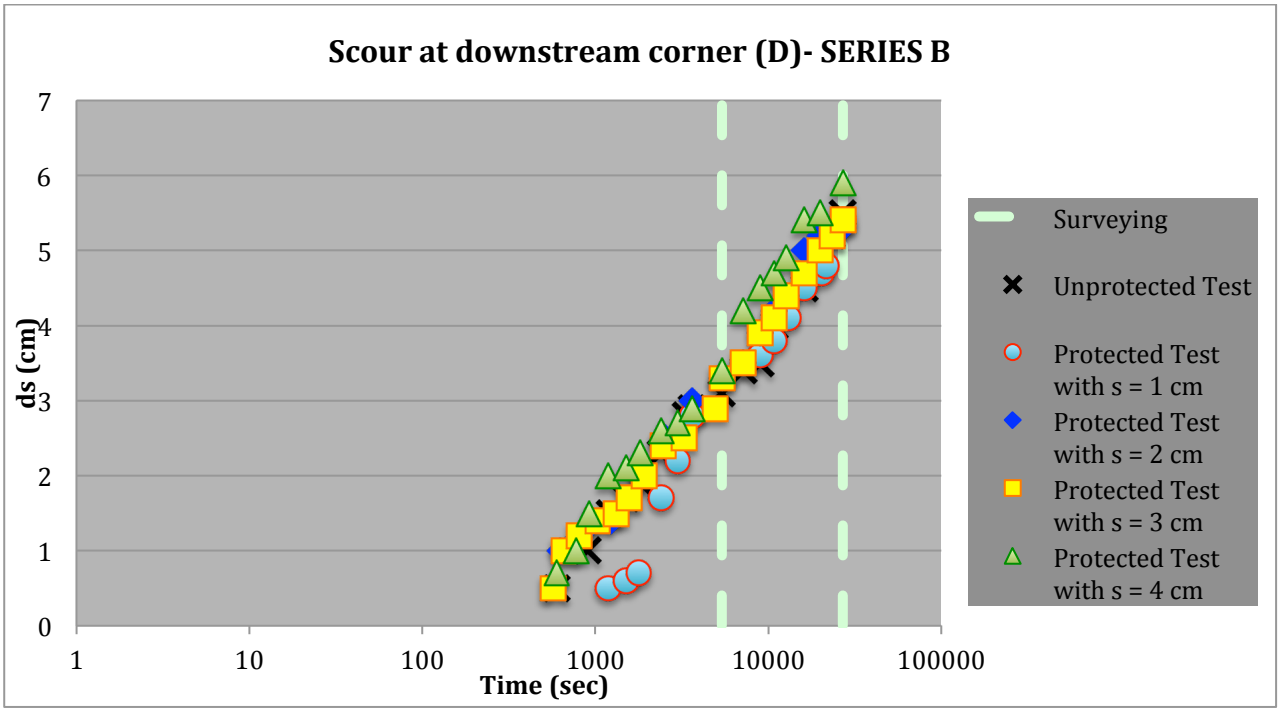

Fig.3.16

Nevertheless, there is no significant reduction of scour at this point but, again we see that, the minimum scour depth is happened for abutment with s=3 at the end of experiment which is equal to 5.2 cm and with respect to the unprotected abutment there is slight change. The maximum scour at this point happen for abutment with s=4 which is equal to 5.9cm, take into account this happened with s=1 for series A proves not only there is no reduction at scour depth but also is deeper with compare to unprotected abutment.

Mentioning, in test with s=1cm we can see a considerable delay of scour at this point which can be interesting.

3.4. Scour depth with respect to the space between elements

In this section, the effect of protections with regards to space between roughening elements is studied for both series; the reference time is chosen in three different stages, namely at beginning of the test, at roughly middle of the experiment and at the end of experiment. Noted that, the scour depth and space between elements are normalized with respect to the abutment width (b).

The results are presented in following figures.

3.4.1. Scour Depth vs. Space at Nose (N):

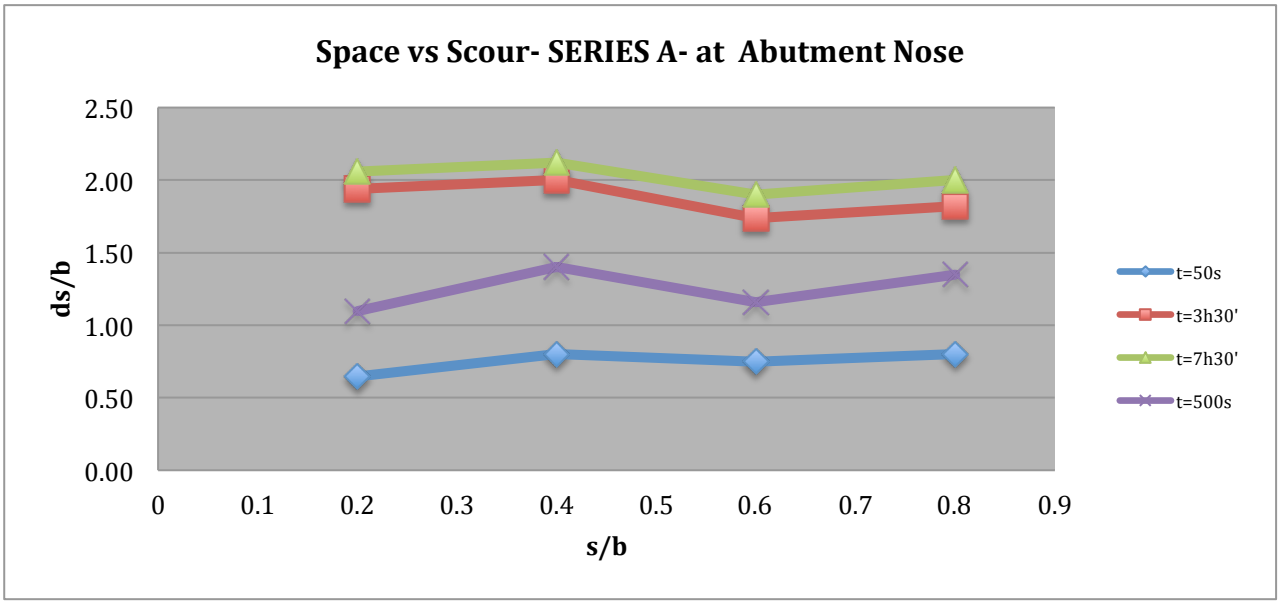

Looking at this plot, we can conclude that at the beginning the best behavior is represented by lower space, however at the middle stage and at the end of experiment, the minimum scour depth at nose occur for the abutment with s=3.

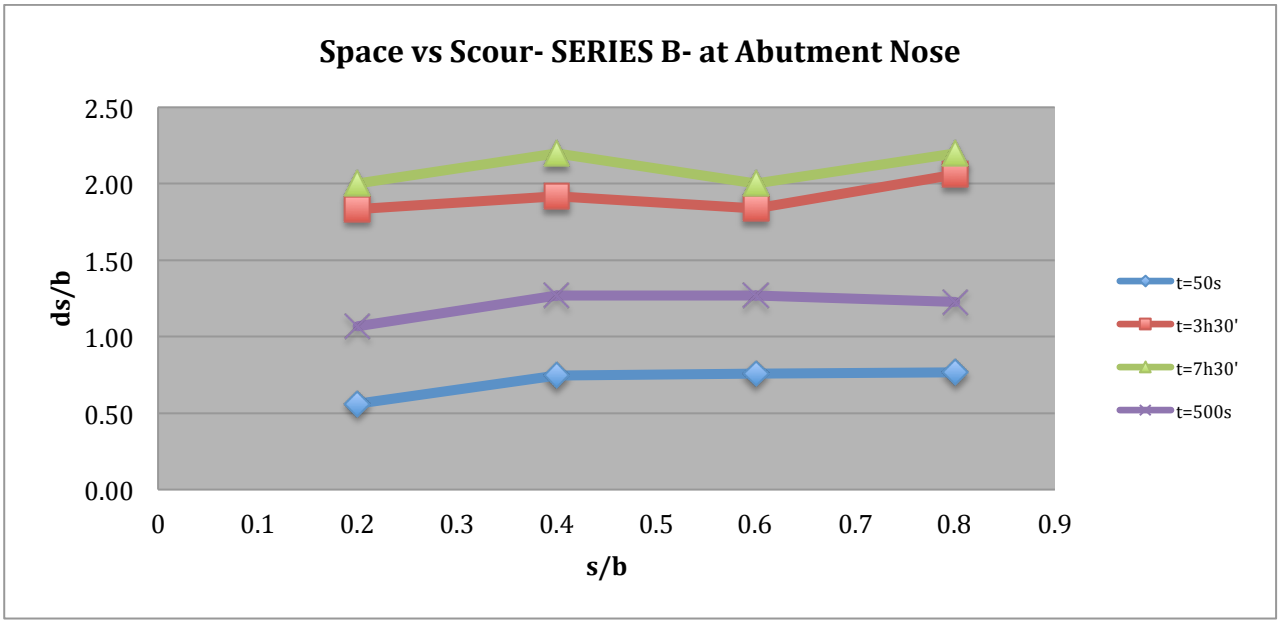

For these series we can see also the similar tendency as series A.

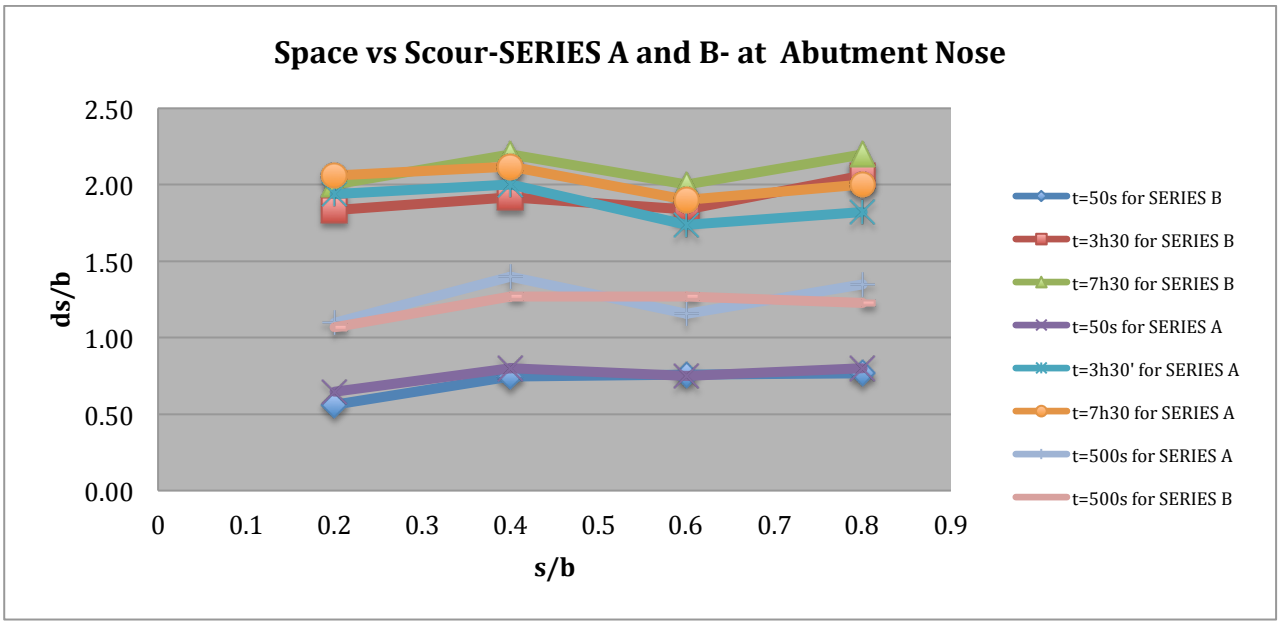

Looking at this plot, it can be concluded that at the beginning of the test, both series show almost same behavior, just scour for series A is a bit greater which is not notable. In principal, we can observe less scour for the abutment wit s=3cm in both series, yet at the end of experiment and also at the middle stage the scour is deeper for series B at this point.

Briefly, the reduction of scour depth at abutment nose is more in abutment with s=3cm and p=1cm.

3.4.2. Scour Depth vs. Space at Wall (W):

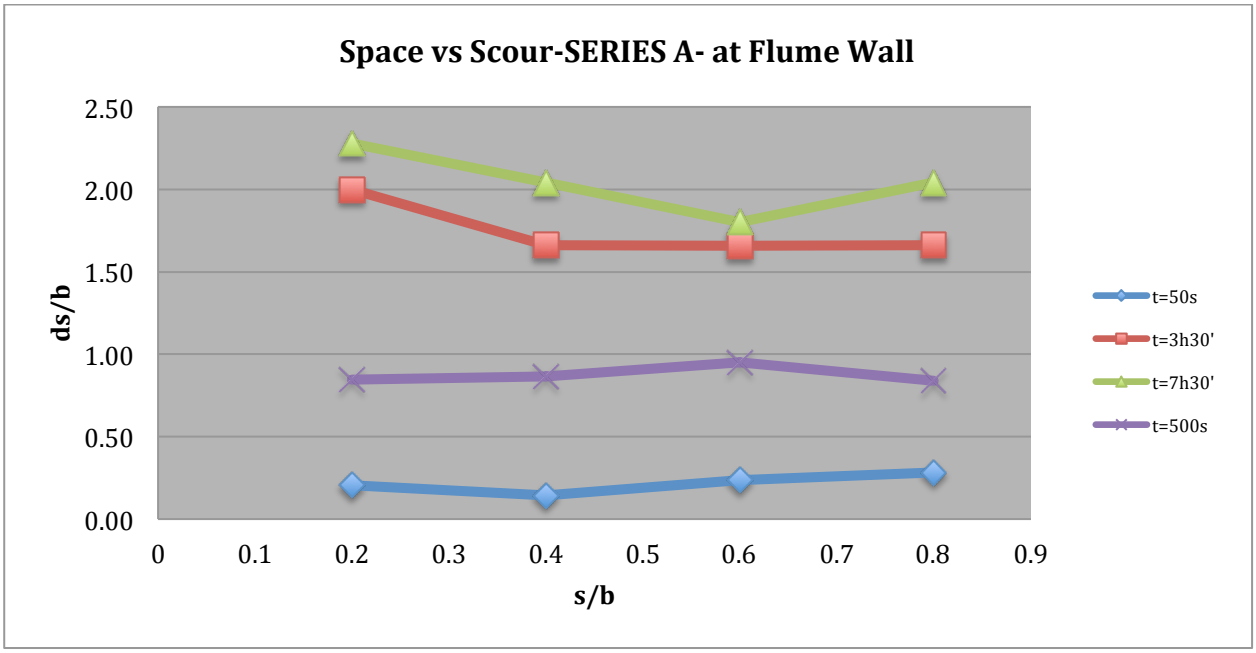

Having examined this plot, it can be said, despite the fact that, the trend at the first stage is not perfectly constant but the changes are not significant and all abutments behave similarly.

Plus the fact that, at final stage, at this point also the best behavior is shown by the abutment with s=3cm, however in the middle of experiment except test A-2 the other tests have roughly same scour depth.

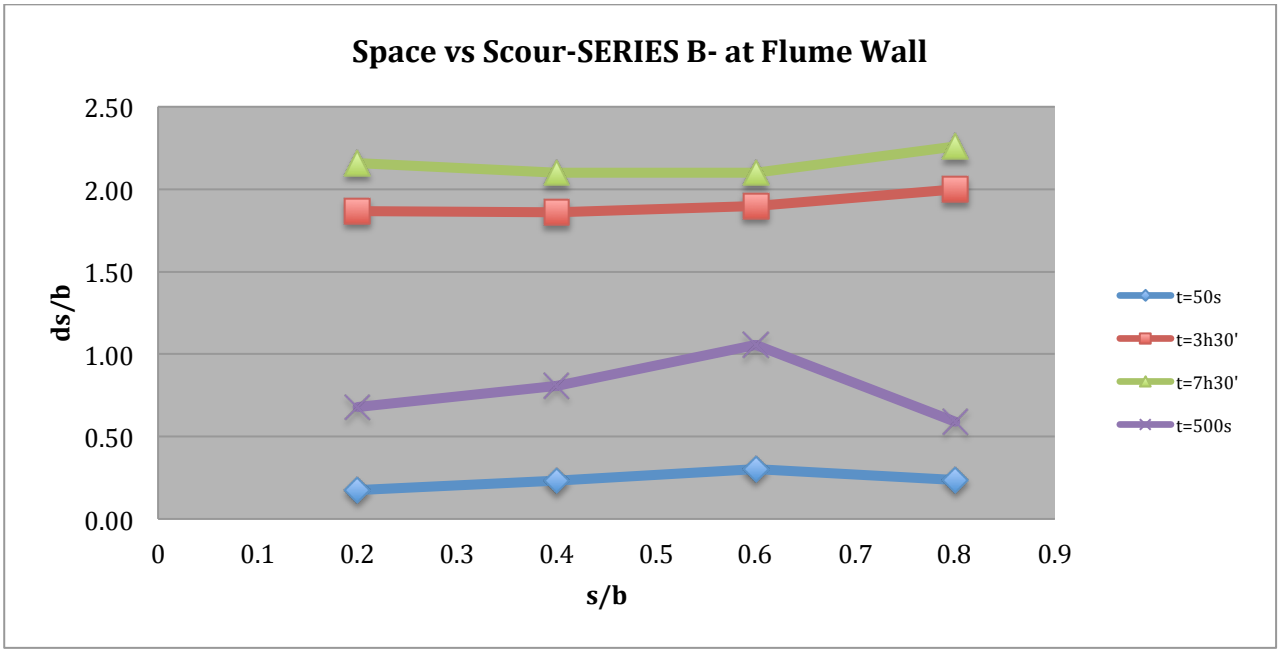

For this series, abutment with s=2cm and s=3cm have same scour depth at the end of experiment, but at the first stage the maximum value of scour happened for abutment with s=3cm.

Interestingly, in the middle of the experiment both abutments have roughly similar scour depth.

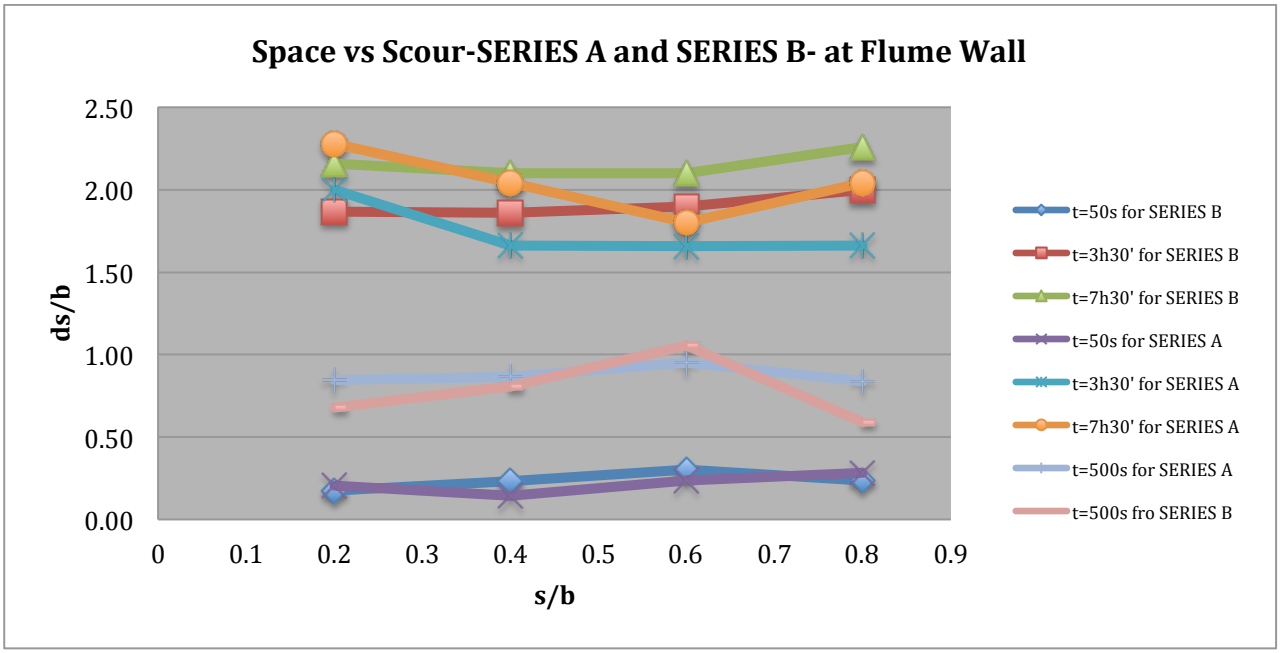

Looking at this plot, it can be concluded that at the beginning of the test, both series show almost same behavior at this point same as abutment nose, just scour for series A is a bit greater which is not remarkable. Clearly, we can observe less scour for the abutment wit s=3cm in both series at the end of process, yet at this stage and also at the middle stage the scour is deeper for series B at this point.

As a conclusion, the reduction of scour depth at flume wall of abutment is more in abutment with s=3cm and p=1cm.

3.4.3. Scour Depth vs. Space at Downstream Corner of Abutment (D):

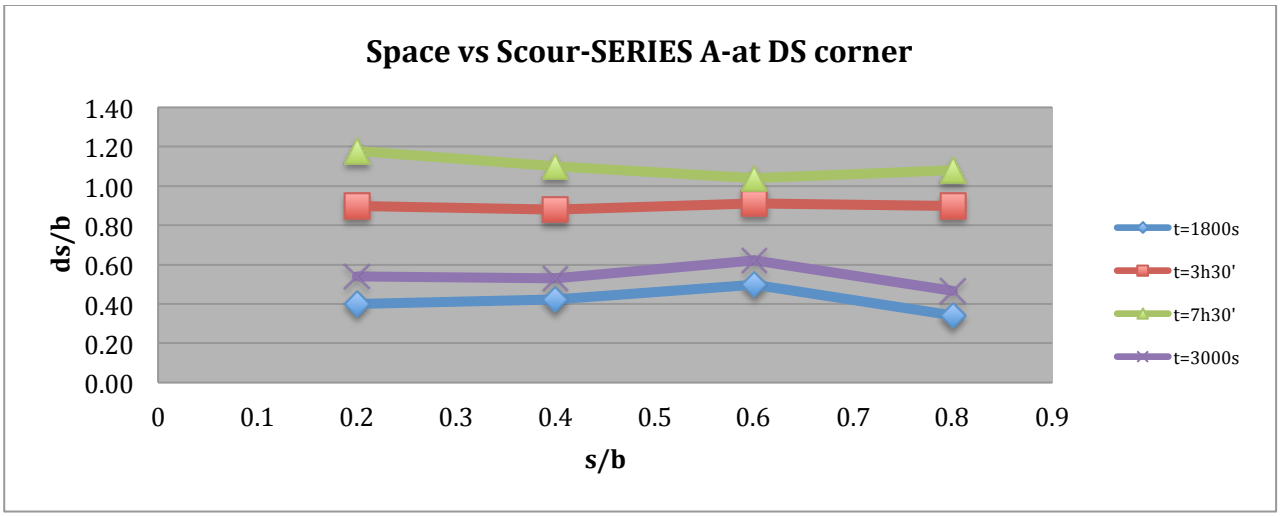

Referring to this plot, it can be understood, at the first stage the abutment with s=3cm shows different behavior in comparison with the other tests, in which the scour is quite greater.

Subsequently, in the end of experiment, at this point also, the abutment with s=3cm shows the best behavior; nevertheless in the middle of experiment except test A-2 the other tests have roughly same scour depth.

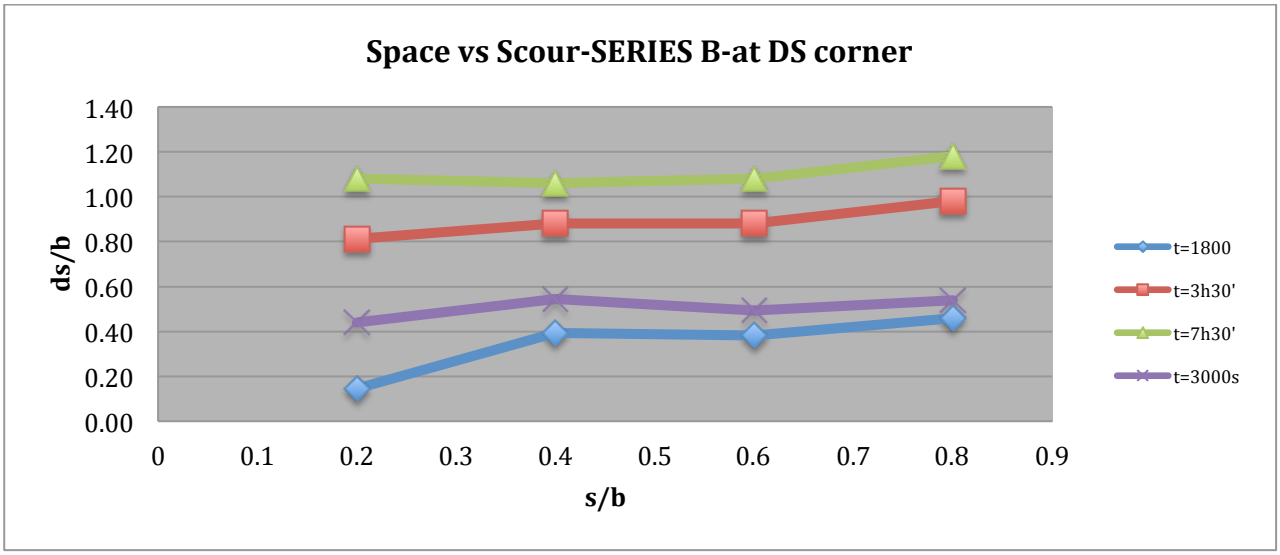

For this series, abutment with s=2cm and s=3cm have quite same scour depth at the end of experiment, however scour is slightly higher in the abutment with s=3cm.

Although at all the stages the maximum value of scour happened for abutment with s=4cm. As it can be seen test B-5 shows a good behavior at the beginning of the experiment. In general we can conclude, for this series at this point the best behavior is represented by the abutment with s=1cm.

Comparing all tests in both series at this point, it can be concluded that at the beginning of the test, there is a enormous difference in scour value in test A-5 and B-5. As a conclusion, the reduction of scour depth at down stream corner is more in abutment with s=1cm and p=0.5cm.

3.5. Percentage of reduction found:

In the following, I presented the percentage of reduction with respect to the unprotected abutment in scour hole at three points mentioned previously for three different stages, one just at the beginning of the experiment, one at the middle of experiment and one at the end of experiment.

At time= 50 sec

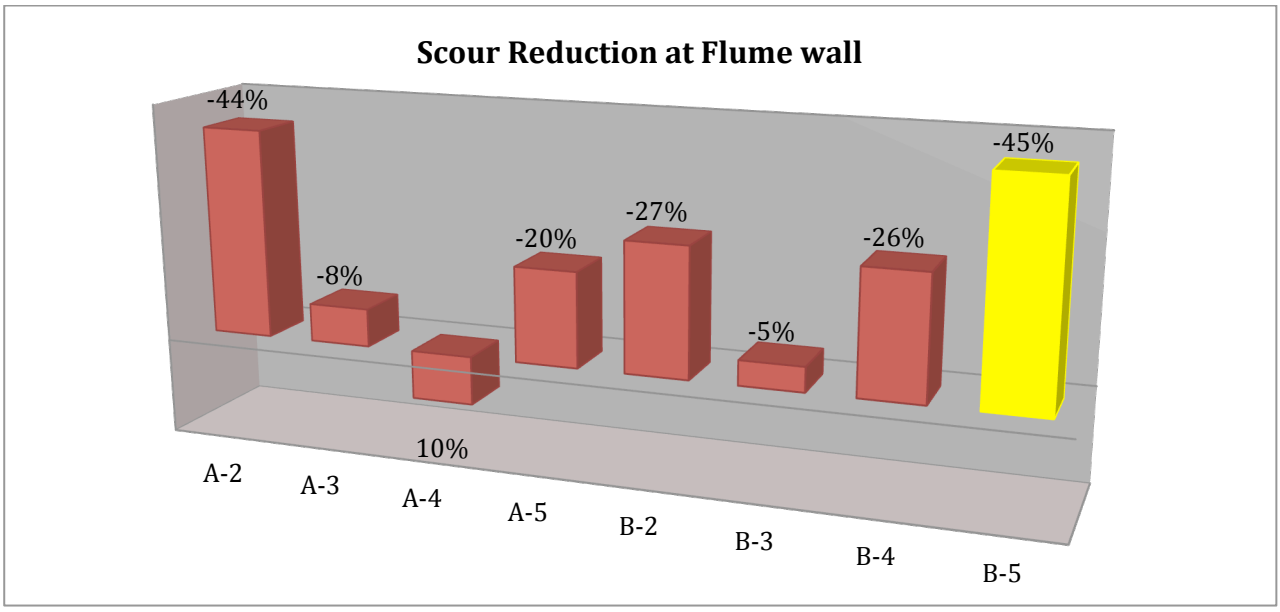

At time= 3h30′

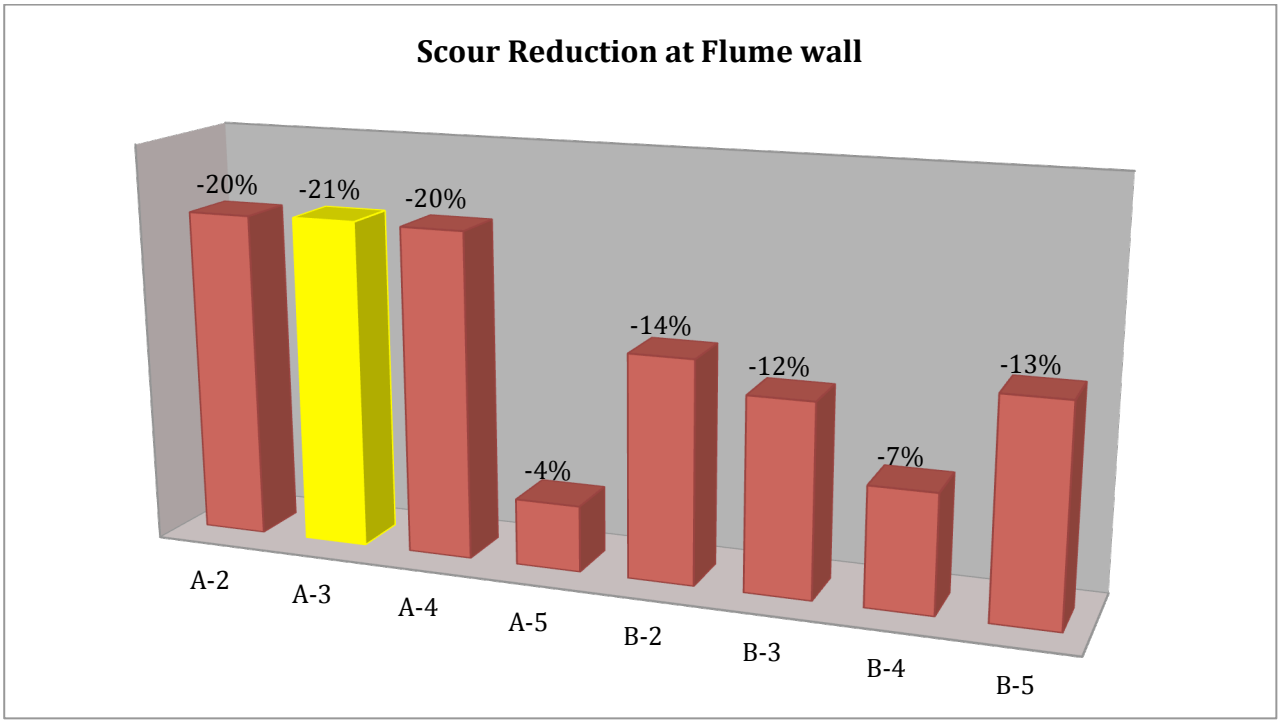

At time= 7h30'

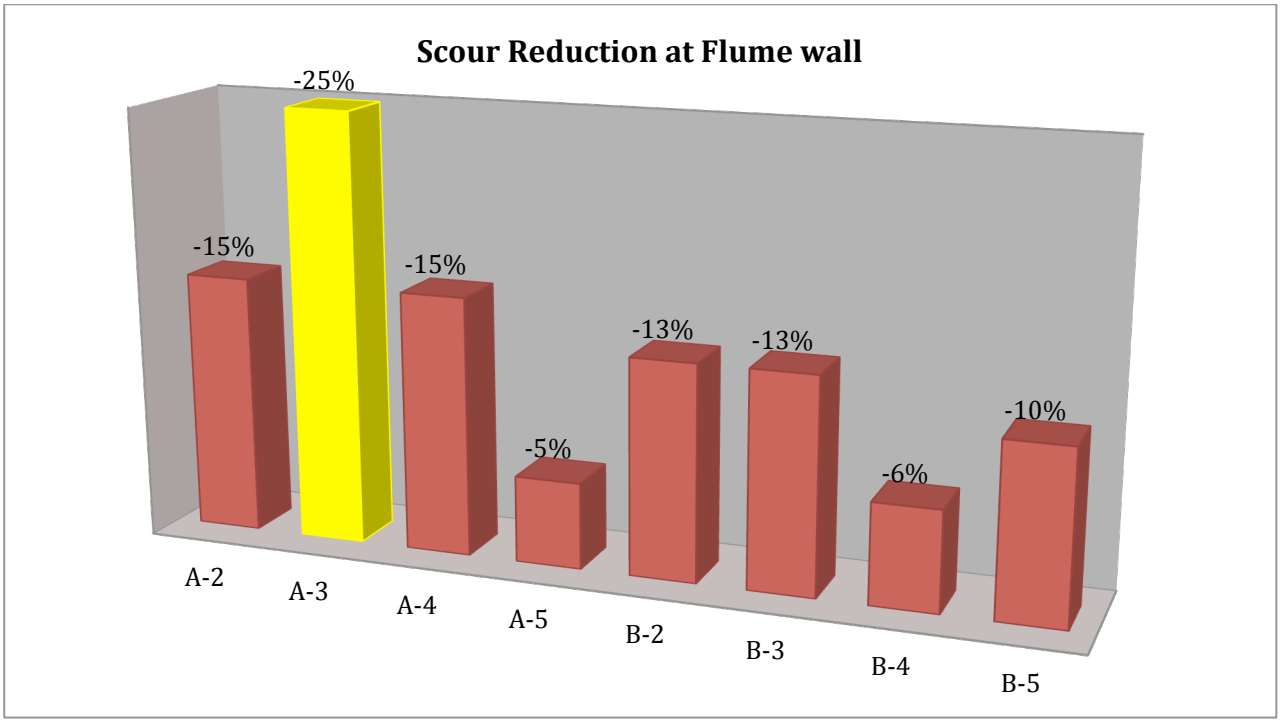

Having looked at this graphs, what it all comes down to is that, at this point (W) the abutment with s=3cm and p=1cm has reacted better that the other abutments, despite the fact that we can see abutment with s=1cm and p=0.5 has better behavior at the beginning of the experiment. My conclusion is that for this point we can say the best abutment is with s=3cm and p=1cm.

At time= 50 sec

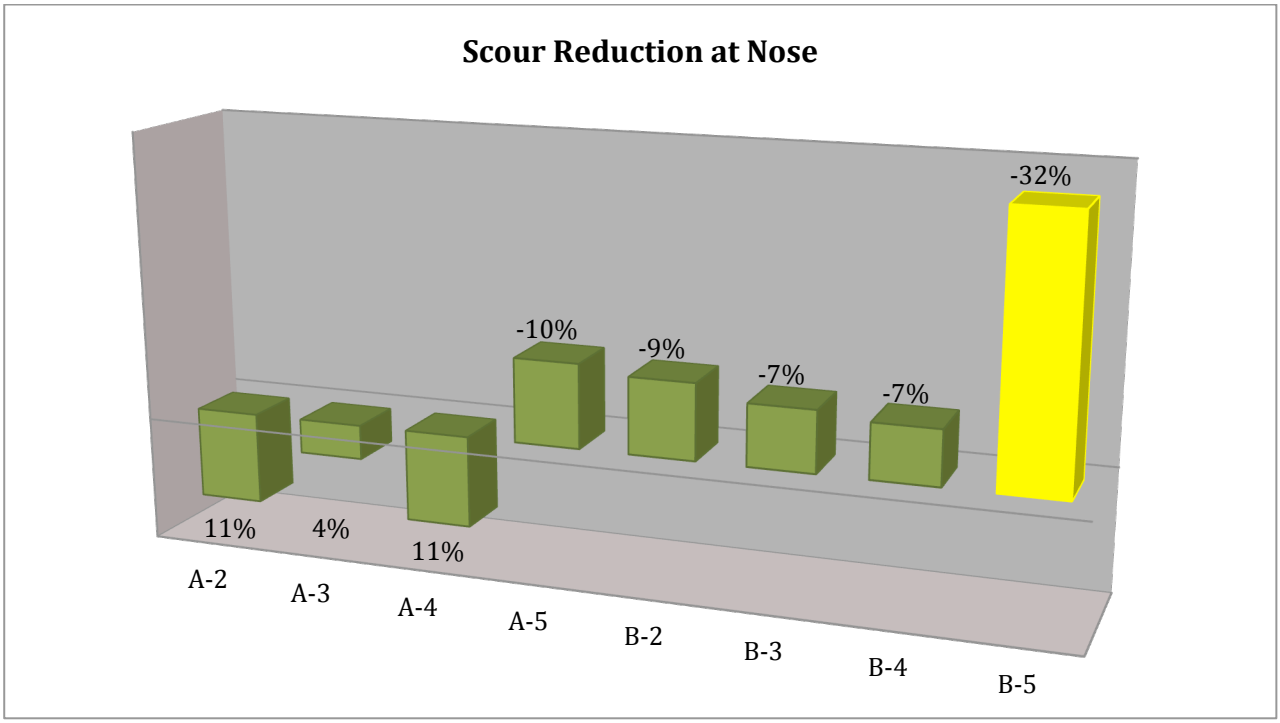

At time=3h30′

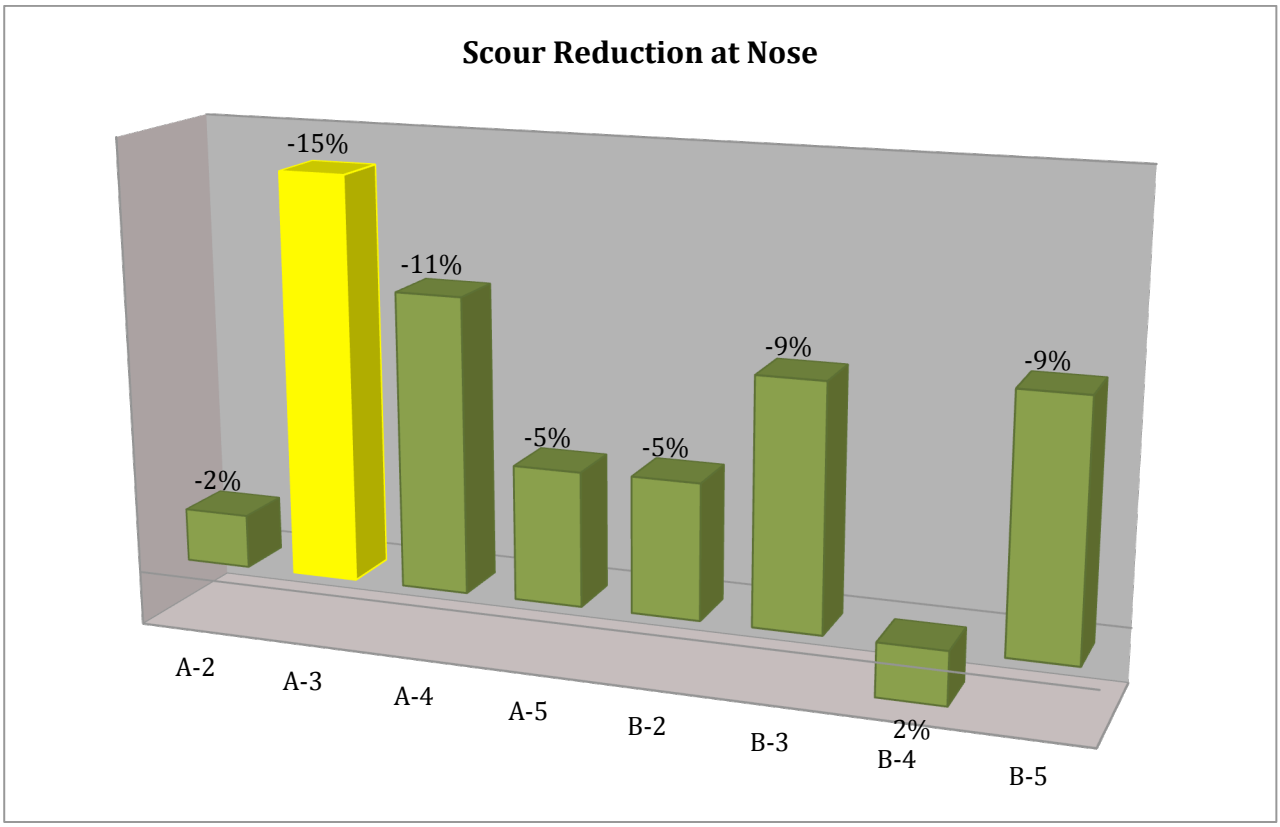

At time=7h30′

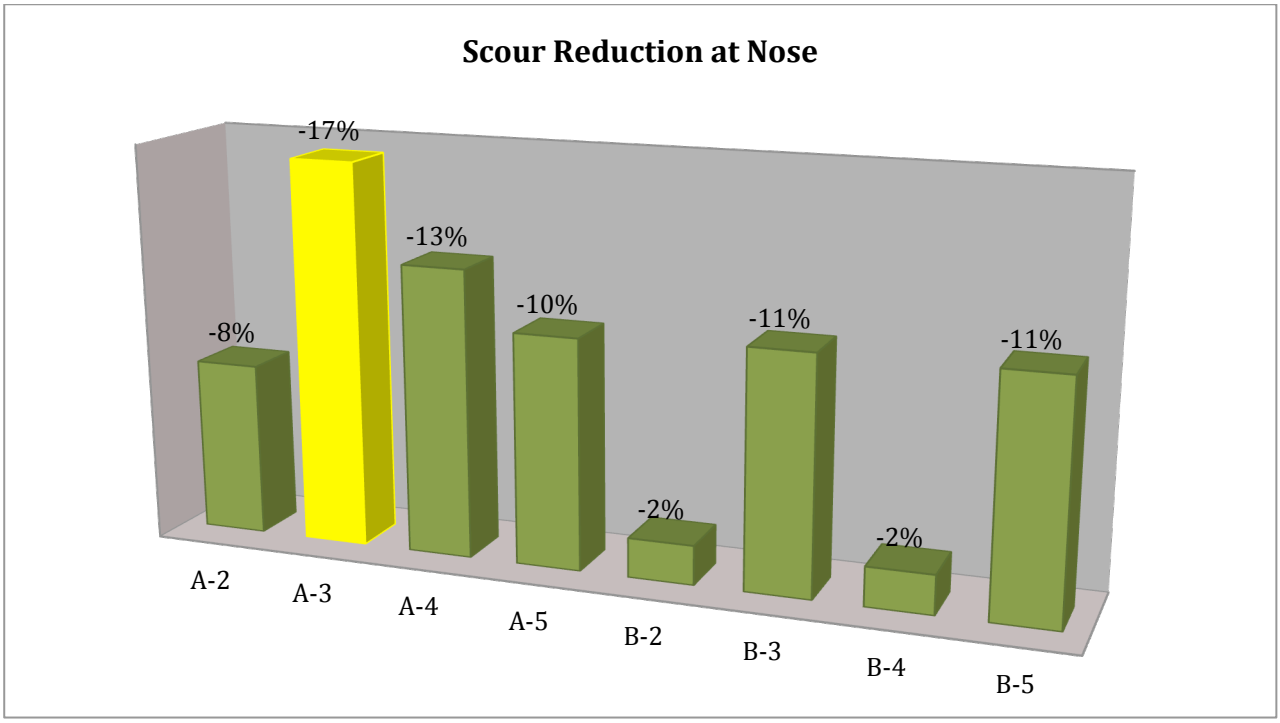

Obviously, for this point also we can observe among all abutments, the one with p=1cm and s=3cm has the maximum reduction at the middle and final stage however, similarly to what we have seen at flume wall, the maximum reduction at the beginning of the experiment is belonged

to abutment with s=1cm and p=0.5cm. My understanding is that, also for this point I have to say the best choice would be the abutment with s=3cm and p=1cm.

At time=30'

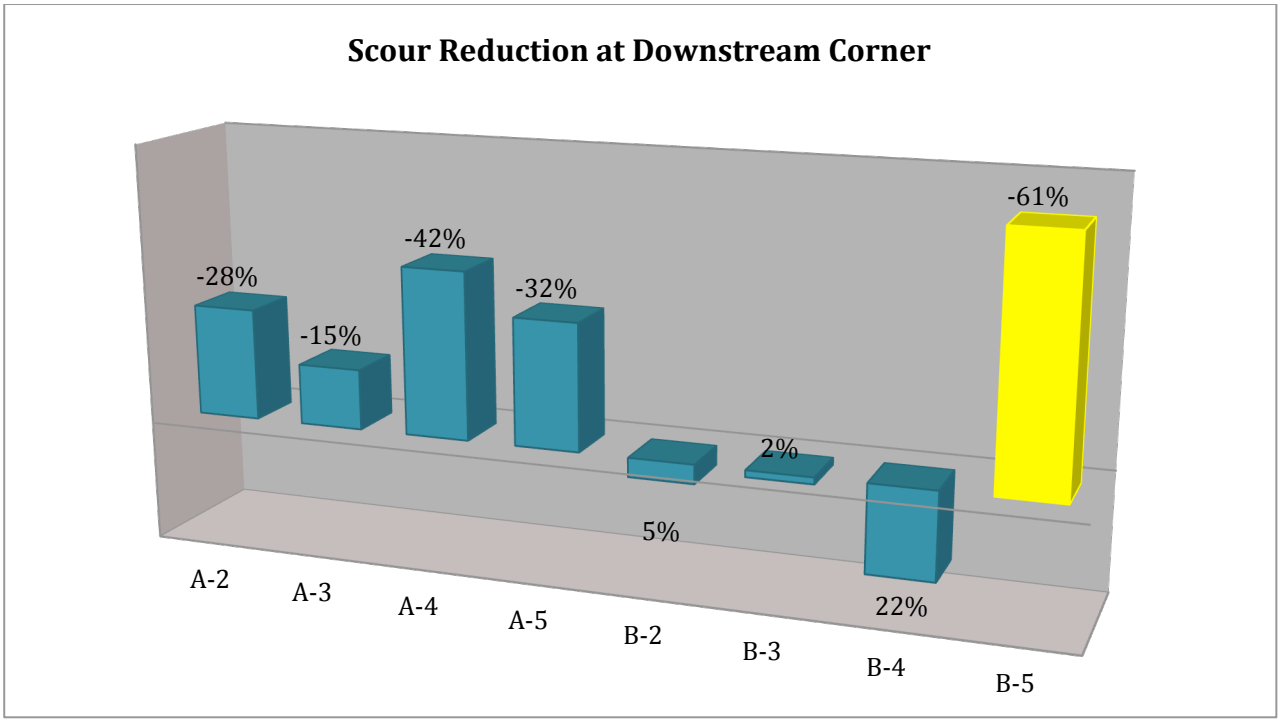

At time=3h30'

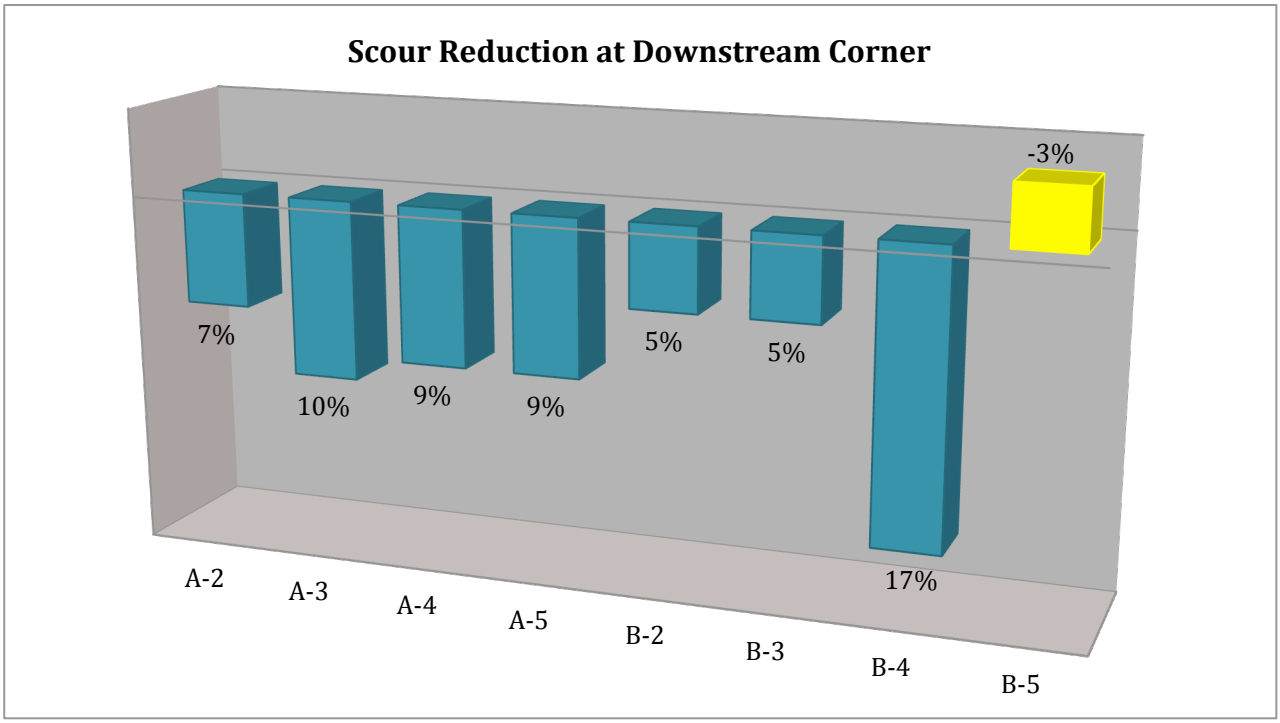

At time=7h30'

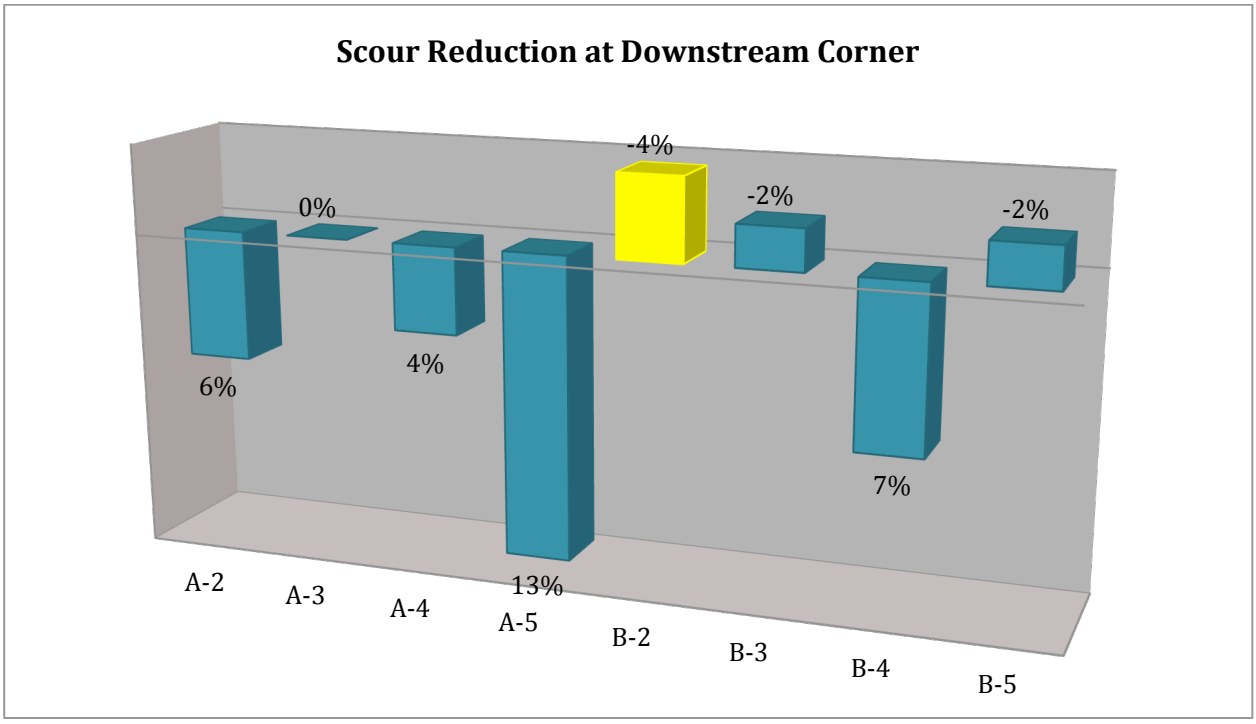

As it is also mentioned previously, at this point we cannot see remarkable reduction in scour depth at middle and final stage, however we may consider that we are using local countermeasure and y=this point is quite far from it.

Having gone through the above plots, we can come to the conclusion that as far as local scour is concerned, it would be fair a safe assumption to say that, among the protected abutment that we have used, the maximum reduction at the end of experiment can be seen using abutment with p=1cm and s=3cm with 25% and 17% reduction at flume wall and nose of abutment respectively, therefore my recommendation through the countermeasures that we have used would be using roughening elements with protrusion equal to 1cm and 3cm space between them, need to be mentioned that the scale factor of our model is 50, therefore when it comes to the real case;

b		t		s		p	
Model (cm)	Prototype (m)	Model (cm)	Prototype (m)	Model (cm)	Prototype (m)	Model (cm)	Prototype (m)
5	2.5	1	0.5	3	1.5	1	0.5

Conclusions

Scour is a natural phenomenon caused by the erosive action of flowing stream on alluvial beds. It may occur as a result of natural changes of flow in the channel, as part of longer-term morphological changes to the river, or through man's activities, such as building structures in the channel or dredging material from the bed. If the depth of scour becomes significant, the foundations' stability may be endangered, with a consequent risk of the structure suffering damage or failure. Failure of bridges due to scour at their foundations, which consist of abutments and piers, is a common occurrence. Bridge scour is one of the three main causes of bridge failure. It has been estimated that 60% of all bridge failures result from scour and other hydraulic related causes.

Basically there are two ways in protecting the bridge structures from scouring; those are bed armoring and flow altering techniques. Bed armoring technique helps protect the area where scour takes place and has the ability to withstand high shear stresses during high flow events, so the bed armoring technique does not affect the flow. The flow altering techniques work to alter the flow alignment to transfer the scour potential away from the vicinity of bridge abutments.

This work is intended to be a contribution to the field of scouring problems at the bridge structures. The aim of the work was to analyze how the scour hole reacts to different kinds of protected abutments. These experiments were done in the Hydraulic laboratory of Politecnico di Milano.

In order to run the main tests namely scour tests, initially it was needed to calibrate the channel and calibrate the piezometers, to arrive at the possibility to reliably measure water depths. Afterwards, we performed some preliminary test, for instance, velocity measurements to see how the flow is distributed along the channel on the fixed bed and free surface channel, plus Q-Qc test in order to find the critical discharge for the chosen water depth. This test were also conducted on free surface channel but in movable bed. It is important to know the threshold discharge for the channel since most of the literature frameworks of the scour process refer to a stage parameter in terms of flow intensity compared with the critical one. For example, it is frequently recalled that the scour depth is maximum for critical conditions, while it is lower for clear-water (discharge lower than critical) and live-bed (discharge higher than critical) conditions. It should be mentioned that we aborted to process data related to the velocity measurement test due to the fact that the instrument DOP was not working properly and we had errors in our results.

As far as scour countermeasures is concerned, the experimental program involved 10 runs, including 2 different series of protected abutment. The tests were conducted on free surface channel, under clear-water condition. The protection chosen was represented by elements roughening the upstream face of the abutment, characterized by a protrusion, a thickness and spacing. In each experimental series, thickness and protrusion were kept the same and the spacing was changed. This choice in designing the experimental campaigns stems from the fact that a spacing with minimum induced scour is expected, since for large spacing the elements will have small effect on the down flow and for very small spacing the elements would just result in a new abutment face shifted upstream. The roughening elements were not put for the entire depth of the abutment, but only down to a submergence equal to the water depth, in an attempt to pay attention to feasibility of the systems. In the first series of our experiments, we used thickness equal to 1cm and protrusion of 1cm; for the second series, we repeated the test with unprotected

abutment in order to satisfy the repeatability of the previous test with unprotected abutment, subsequently we kept the same thickness of elements but we decreased the protrusion to 0.5 cm.

As it is mentioned, we controlled the experimental condition in terms of water depth and flow discharge, having looked at the plots and tables related to water free surface profiles which are reported in Annex 2 we can conclude during this campaign we could maintain the stationary flow condition reasonably, and we didn't have significant fluctuation in water free surface level and discharges.

The experiment with protected abutment with s=3cm and p=1 cm showed a good scour reduction both at wall and at abutment nose at the final stage of the experiment. Basically, the reduction of 25% and 17% at these points respectively, can be observed at this abutment. To my understanding, this abutment was the most successful one in the experimental campaign of the abutments. If one considers a scaling factor to reality of, for example, 50, this value when transferred to reality will be:

b		t		s		p	
Model (cm)	Prototype (m)	Model (cm)	Prototype (m)	Model (cm)	Prototype (m)	Model (cm)	Prototype (m)
5	2.5	1	0.5	3	1.5	1	0.5

Since there has been a phenomenological interest in this field for the last decades between scientists all over the world it is worth the efforts to explore more aspects of scour reduction at bridge constructions to gain more knowledge, analyze the problems and propose new solutions for the engineers.

References

Lauva O. (2012). " An Experimental Analysis of the Scour Process at Unprotected and Protected Bridge Structures," Internship Research Project presented to the *University of Politecnico di Milano, at Milan, Italy.*

Bruce W. Melville (1997) Pier and Abutment Scour: Integrated Approach, *Journal of Hydraulic Engineering, Vol. 123, No. 2.*

Chanson, H. (2004) The Hydraulics of Open Channel Flow: An Introduction, Second edition. Elsevier Butterworth-Heinemann.

Chiew, Y. M. (1995). "Mechanics of riprap failure at bridge piers." J. *Hydraul. Eng., 121_9_, 635–643.*

Chiew, Y. M., and Lim, F. H. (2000). "Failure behavior of riprap layer at bridge piers under live-bed conditions*." J. Hydraul. Eng., 126(1), 43–55.*

Chiew, Y.-M. (2004). "Local scour and riprap stability at bridge piers in a degrading channel." *J. Hydraul. Eng., 130(3), 218–226.*

Dongol, D. M. S. (1994). "Local scour at bridge abutments." *Rep. No. 544, School of Engineering., The Univ of Auckland, New Zealand.*

Gill, M. A. (1972). "Erosion of sand beds around spur dikes." *J. Hydr. Div., ASCE, 98(9), 1587-1602.*

Hannah, C. R. (1978) Scour at Pile Groups. *Res. Rep. No. 28-3, Civ. Engrg. Dept., Univ. of Canterbury, Christchurch, New Zealand.*

Kandasamy, J. K. (1989). "Abutment scour." *Report No. 458, School of Engineering, University of Auckland, Auckland, New Zealand.*

Kumar V., Kittur G. Ranga Raju, and Nandana Vittal (1999) Reduction of Local Scour Around Bridge Piers Using Slots and Collars, *Journal of Hydraulic Engineering, Vol. 125, No. 12.*

Kwan, T. F. (1984). "Study of abutment scour*." Report No. 328, School of Engineering, University of*

Auckland, Auckland, New Zealand.

Kwan, T. F. (1988). "A study of abutment scour." *Report No. 451, School of Engineering, University of Auckland, Auckland, New Zealand.*

Lagasse, P. F., Zevenbergen, L. W., Schall, J. D., and Clopper, P. E. (2001). "Bridge scour and stream instability countermeasures." *HEC23 FHWA NHI 01–003, Federal Highway Administration, U.S. Dept. of Transportation, Washington, D.C.*

Li Hua, Brian D. Barkdoll, M.ASCE, Roger Kuhnle, and Carlos Alonso (2006) Parallel Walls as an Abutment Scour Countermeasure, *Journal of Hydraulic Engineering, Vol. 132, No. 5.*

Melville, B. W. (1992) Local Scour at Bridge Abutments, *Journal of Hydraulic Engineering, Vol. 118, No.4.*

Melville, B., Ballegooy, S., Coleman, S., and Barkdoll, B. (2006a). "Countermeasure toe protection at spill-through abutments." *J. Hydraul. Eng., 132(3), 235–245.*

Richardson, E. V., and Davis, S. R. (1995). "Evaluating scour at bridges." *Hydraulic Engineering Circular*

No. 18 (HEC-18). Rep. No. FHWAIP- 90-017:204, FHWA, Washington, D.C.

Shen, H. W., Schneider, V. R., and Karaki, S. S. (1966). Mechanics of local scour. *U.S. Department of Commerce, Nat. Bureau of Standards, Inst. for Appl. Technol.*

Tey, C. B. (1984). "Local scour at bridge abutments." *Report No. 329, School of Engineering, University of Auckland, Auckland, New Zealand.*

Wong, W. H. (1982). "Scour at bridge abutments." *Report No. 275, School of Engineering, University of Auckland, Auckland, New Zealand.*

Zarrati, A. R., Nazariha M.; and Mashahir M. B. (2006) Reduction of Local Scour in the Vicinity of Bridge Pier Groups Using Collars and Riprap, *Journal of Hydraulic Engineering, Vol. 132, No. 2,*

Radice A, O Lauva. (2010) On flow-altering countermeasures for scour at vertical-wall abutment, *Politecnico di Milano*

Annex 1
(Diary)

DAY	TYPE OF ACTIVITY	Q (l/s)	Water Depth (cm)	V (m/s)	X from DS (m)
Jul-12					
23	Clean flow configurator and system it				
	Set up DS boundary condition using wood cover				
	First test calibration of the channel	6	10	0.15	
24	Measurement of channel bed elevation				
	Calibration of the piezometers				
25	Start measuring velocity profiles	16	10	0.4	1.63
					2.69
					3.77
Sep-12					
10	Velocity Measurements	8	10	0.2	
		12	10	0.3	1.63
					2.69
					3.77
11	Velocity Measurements	10	10	0.25	1.63
					2.69
					3.77
		14	10	0.35	1.63
					2.69
					3.77
28	Stop Velocity Measurements				
	Redo The previous test due to achieving not reasonable results	10	10	0.25	
Oct-12					
1	Repetition of Velocity Measurements				
2	Replace the deep channel				

8	Calibration of the positioning system and first calibration of the Laser				
9	Start Q-Qc Test	2.5	10.1	0.06	
		4.2	9.9	0.11	
		6	10.2	0.15	
		8.3	10.2	0.20	
		10.2	10.1	0.25	
		12.5	10.3	0.30	
		14.4	10.4	0.35	
		15	10.1	0.37	
		15.6	10.2	0.38	
11	Repeat Q-Qc test for different discharges	6.96	10.2	0.17	
		10.27	10.3	0.25	
		12.37	10.1	0.31	
		13.07	10.2	0.32	
		13.44	10.4	0.32	
		14.14	10.1	0.35	
		14.66	10.3	0.36	
		14.32	10.4	0.34	
		14.52	10.6	0.34	
		14.87	10.1	0.37	
		15.67	10.1	0.39	
		15.41	10.3	0.37	
		13.69	10.4	0.33	
12	Second Calibration of the Laser				
17	Trial Scour test	14.76	10.4	0.35	
29	Test A-1	14.65	10.7	0.34	
30	Test A-1	14.75	10.6	0.35	

	Nov-12				
7	Test A-2	14.65	10.4	0.35	
8	Test A-2	14.69	10.5	0.35	
12	Test A-3	14.68	10.3	0.36	
13	Test A-3	14.73	10.5	0.35	
	Jan-13				
24	Test A-4	14.48	10.7	0.34	
25	Test A-4	14.56	10.5	0.35	
	Feb-13				
6	Test B-1	14.56	10.5	0.35	
7	Test B-1	14.68	10.5	0.35	
14	Test B-2	14.65	10.4	0.35	
15	Test B-3	14.69	10.5	0.35	
19	Test B-3	14.68	10.3	0.36	
20	Test B-3	14.73	10.5	0.35	
27	Test B-4	14.67	10.6	0.35	
28	Test B-4	14.62	10.4	0.35	
	Mar-13				
12	Test A-5	14.62	10.6	0.34	
13	Test A-5	14.6	10.6	0.34	
19	Test B-5	14.62	10.7	0.34	
20	Test B-5	14.62	10.5	0.35	

Annex 2

in this Annex an example of the tables and graphs related to each test is presented. The All tables and plots are given in CD

Water Profiles related to Velocity Measurements Tests

Q=8 l/s

Time 11:38 am										
Profile 1										
Q (l/s)		Piezometers	1	2	3	4	5	6	7	8
1	7.910	x (m)	0.73	1.34	1.94	2.53	3.13	3.54	4.14	4.74
2	7.890	Reading (cm)	104.0	103.8	103.9	103.9	103.9	103.9	103.9	103.8
3	7.780	Bed, actual (cm)	96.0	96.3	96.3	96.3	96.3	96.4	96.2	95.9
4	7.960	Depth, actual (cm)	8.0	7.5	7.6	7.6	7.6	7.5	7.7	7.9
5	7.920	Bed, interp (cm)	96.2	96.3	96.2	96.2	96.3	96.2	96.2	96.1
6	7.930	Depth, interp (cm)	7.8	7.5	7.7	7.7	7.6	7.7	7.7	7.7
7	7.900									
8	7.780									
9	7.770									
10	7.840									
Average	**7.87**									

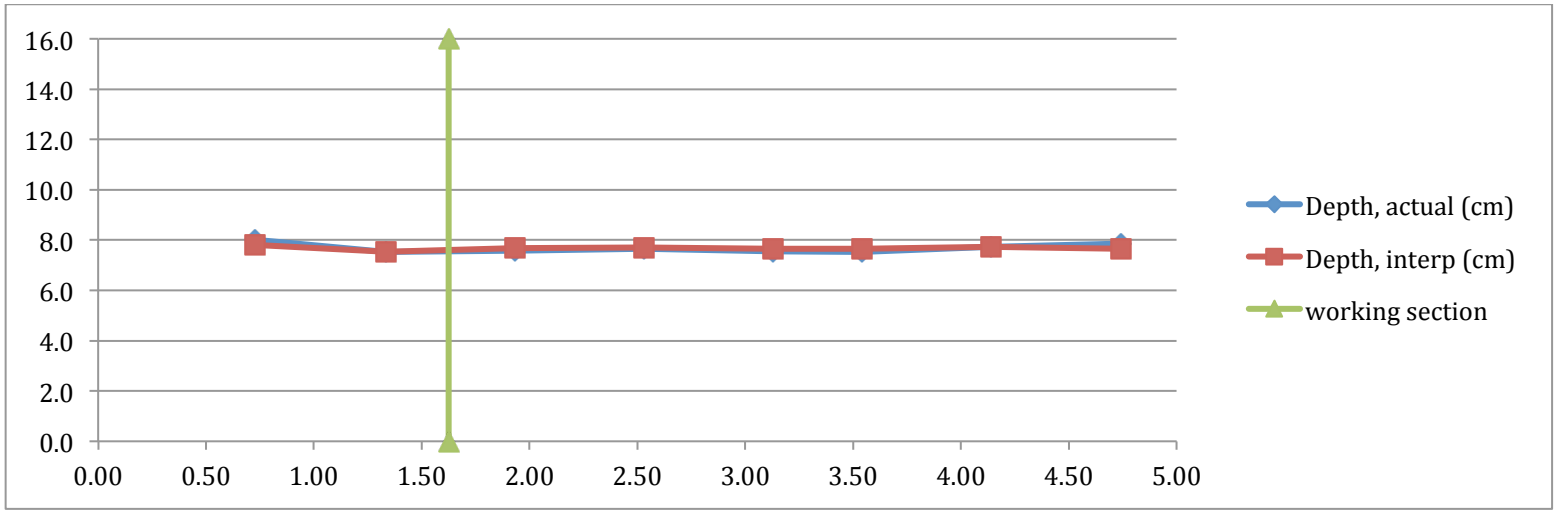

Water Profiles related to Q-Qc Test

Time 11:30 am										
Profile 1										
Q (l/s)		Piezo	1	2	3	4	5	6	7	8
1	2.430	x (m)	0.73	1.34	1.94	2.53	3.13	3.54	4.14	4.74
2	2.480	Reading (cm)	106.4	106.4	106.4	106.4	106.3	106.3	106.3	106.3
3	2.450	Bed, actual (cm)	96.0	96.3	96.3	96.3	96.3	96.4	96.2	95.9
4	2.440	depth, actual (cm)	10.4	10.1	10.1	10.1	10.0	9.9	10.1	10.4
5	2.430	Bed, interp (cm)	96.2	96.3	96.2	96.2	96.3	96.2	96.2	96.1
6	2.490	depth, interp (cm)	10.2	10.1	10.2	10.2	10.0	10.1	10.1	10.2
7	2.460									
8	2.410									
9	2.460									
10	2.450									
Average	**2.45**									

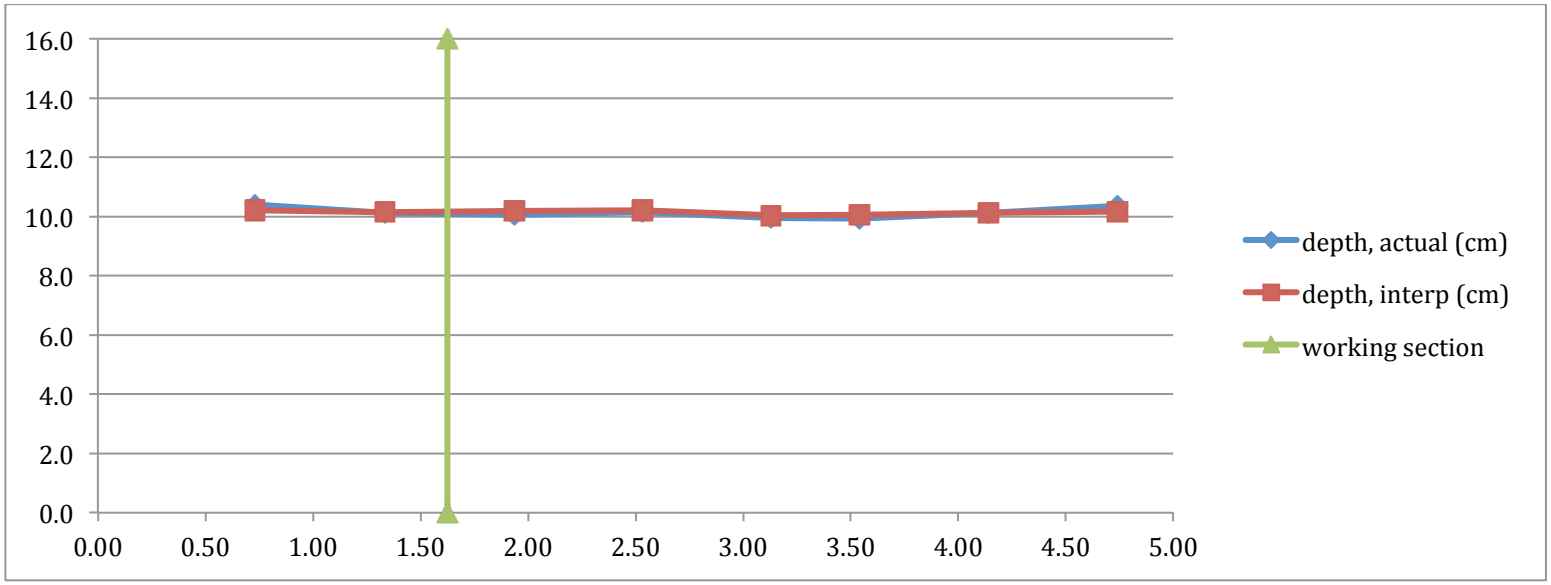

Cross Sections

Series A

Trial Test

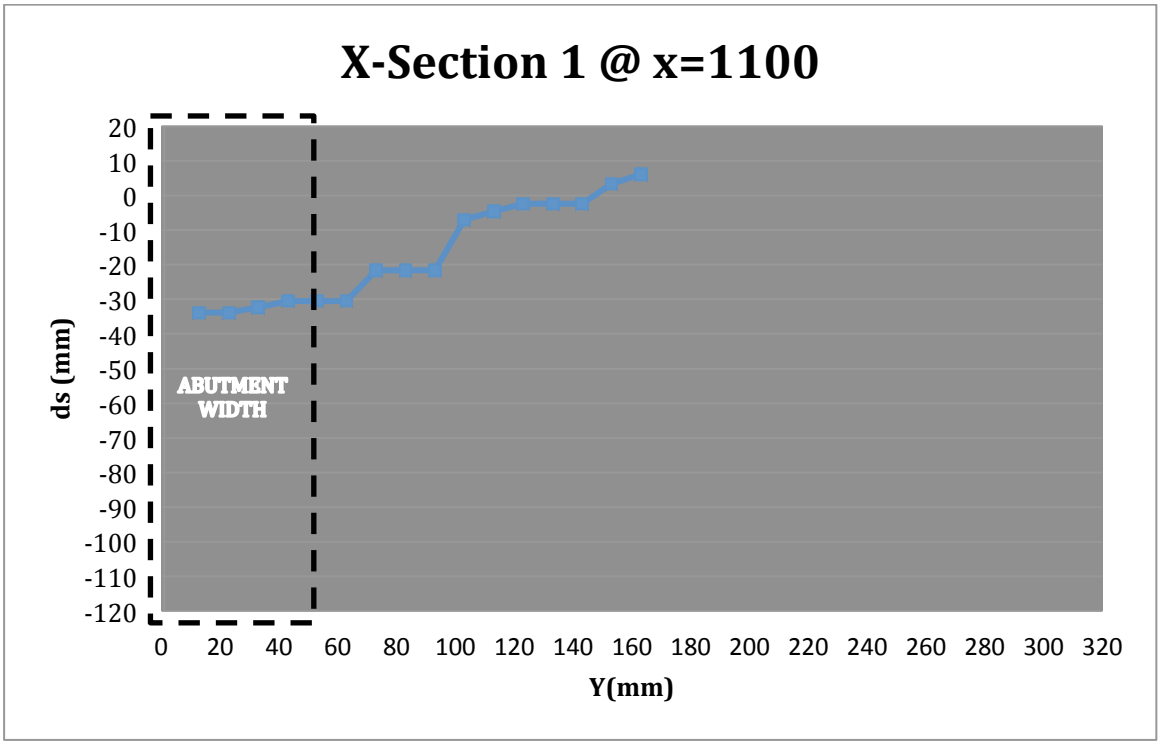
X-Section 1 @ x=1100
ds (mm)
20
10
0
-10
-20
-30
-40
-50
-60
-70
-80
-90
-100
-110
-120
ABUTMENT WIDTH
0 20 40 60 80 100 120 140 160 180 200 220 240 260 280 300 320
Y(mm)

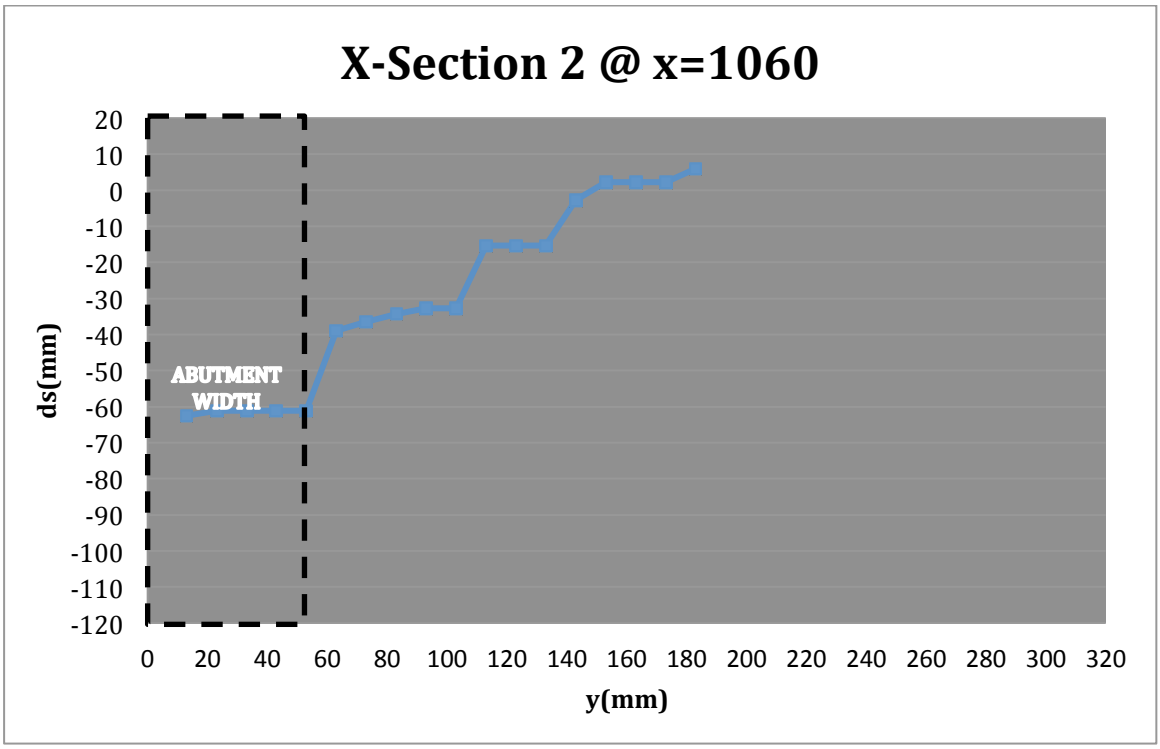
X-Section 2 @ x=1060
ds(mm)
20
10
0
-10
-20
-30
-40
-50
-60
-70
-80
-90
-100
-110
-120
ABUTMENT WIDTH
0 20 40 60 80 100 120 140 160 180 200 220 240 260 280 300 320
y(mm)

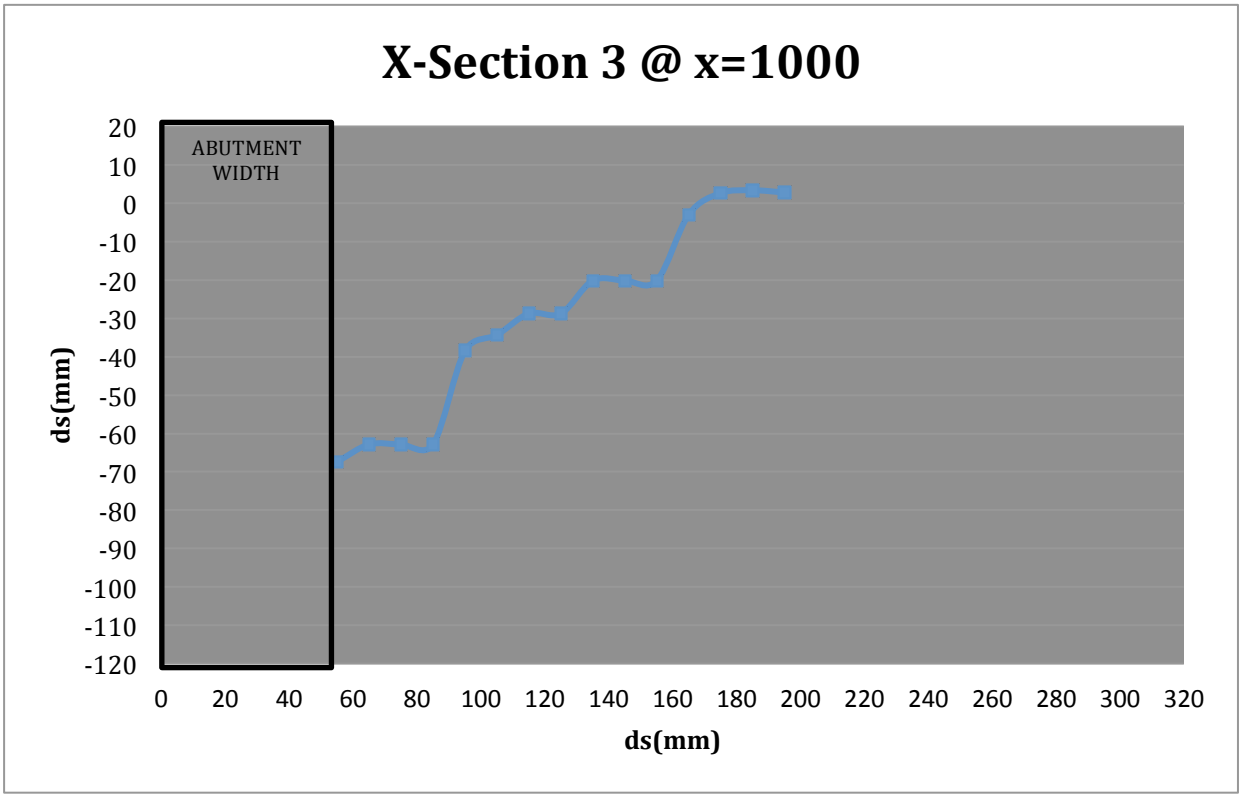
X-Section 3 @ x=1000
ABUTMENT WIDTH
ds(mm)
20
10
0
-10
-20
-30
-40
-50
-60
-70
-80
-90
-100
-110
-120
0
20
40
60
80
100
120
140
160
180
200
220
240
260
280
300
320
ds(mm)

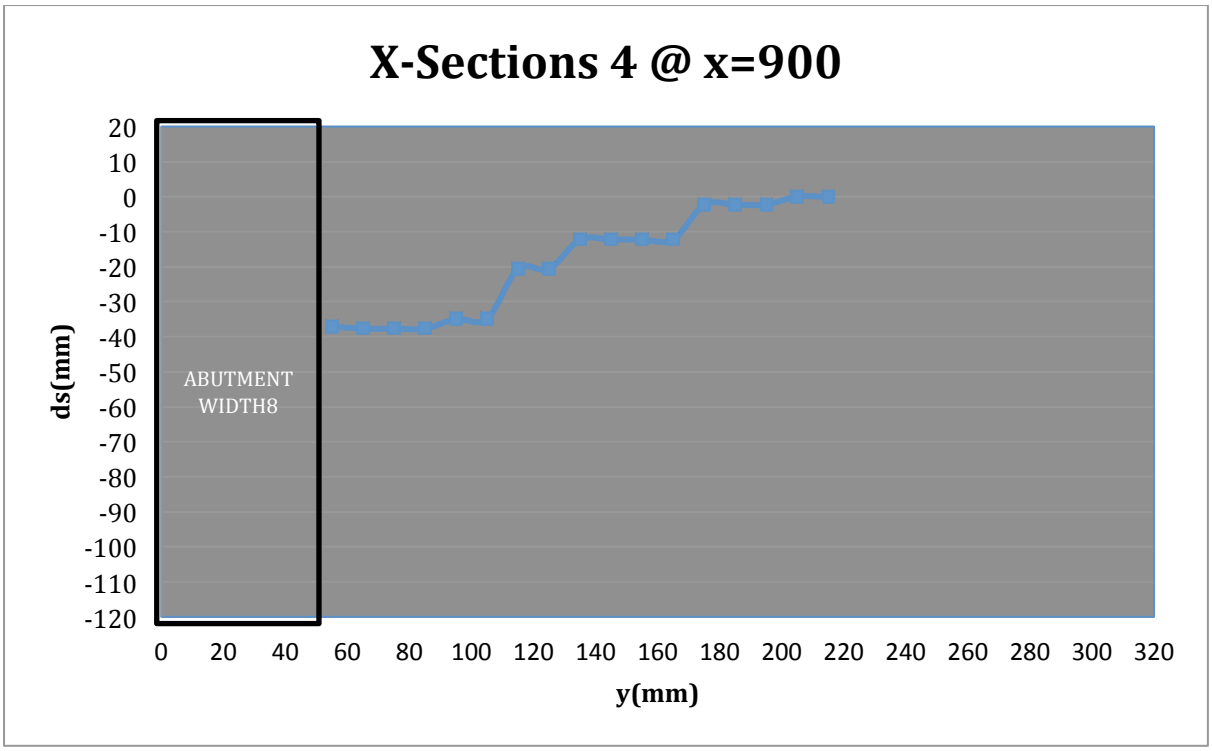
X-Sections 4 @ x=900
ABUTMENT WIDTH8
ds(mm)
20
10
0
-10
-20
-30
-40
-50
-60
-70
-80
-90
-100
-110
-120
0
20
40
60
80
100
120
140
160
180
200
220
240
260
280
300
320
y(mm)

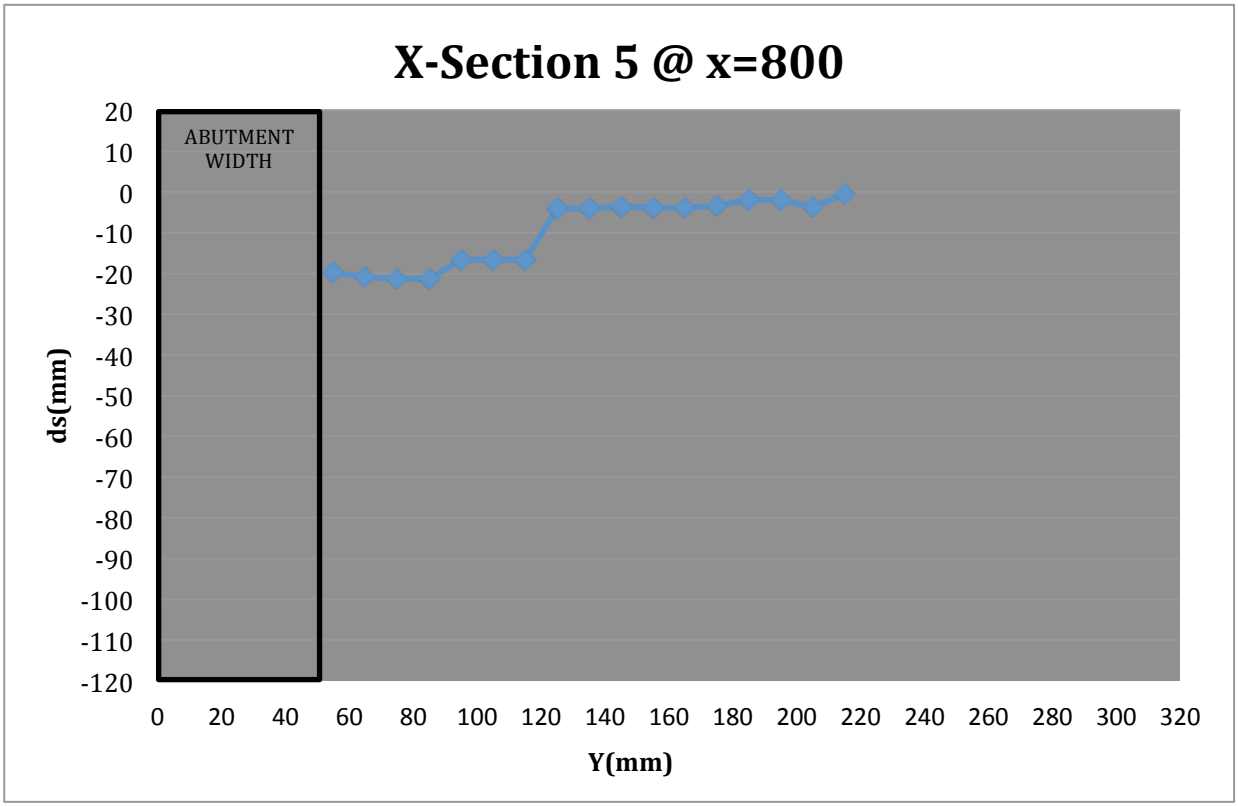
X-Section 5 @ x=800
ABUTMENT WIDTH
ds(mm)
20
10
0
-10
-20
-30
-40
-50
-60
-70
-80
-90
-100
-110
-120
0
20
40
60
80
100
120
140
160
180
200
220
240
260
280
300
320
Y(mm)

Trial Test

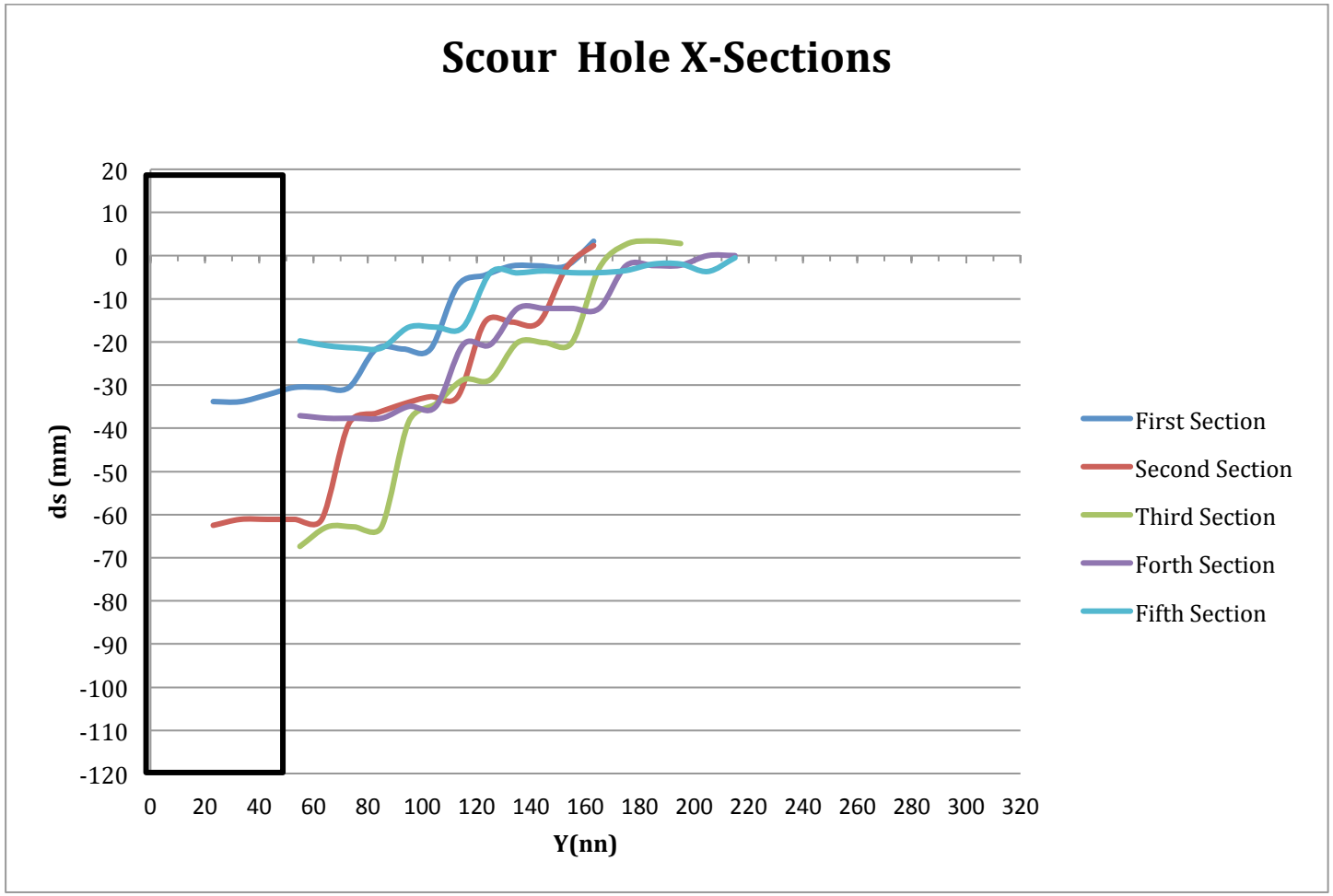
Scour Hole X-Sections
ds (mm)
20
10
0
-10
-20
-30
-40
-50
-60
-70
-80
-90
-100
-110
-120
0
20
40
60
80
100
120
140
160
180
200
220
240
260
280
300
320
Y(nn)
First Section
Second Section
Third Section
Forth Section
Fifth Section

Cross Sections

Series B

Test B-1 First Survey

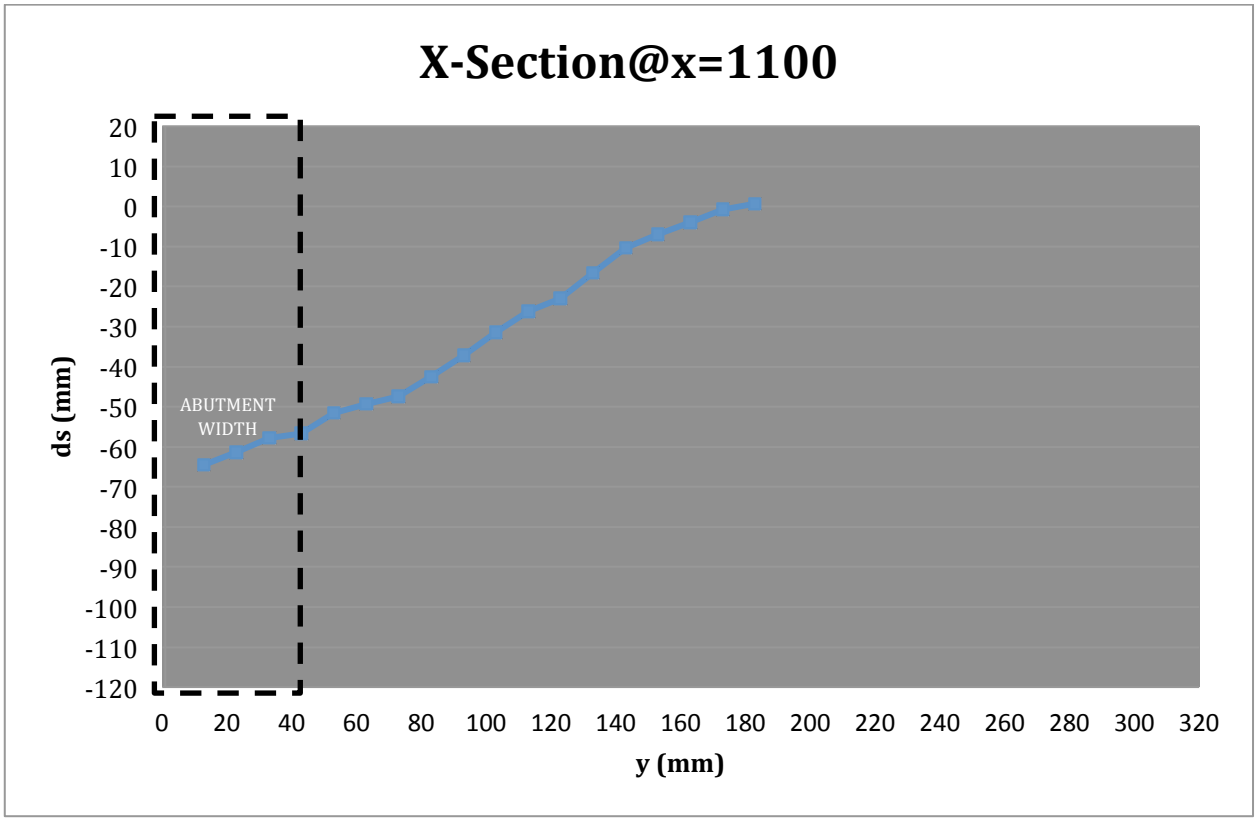

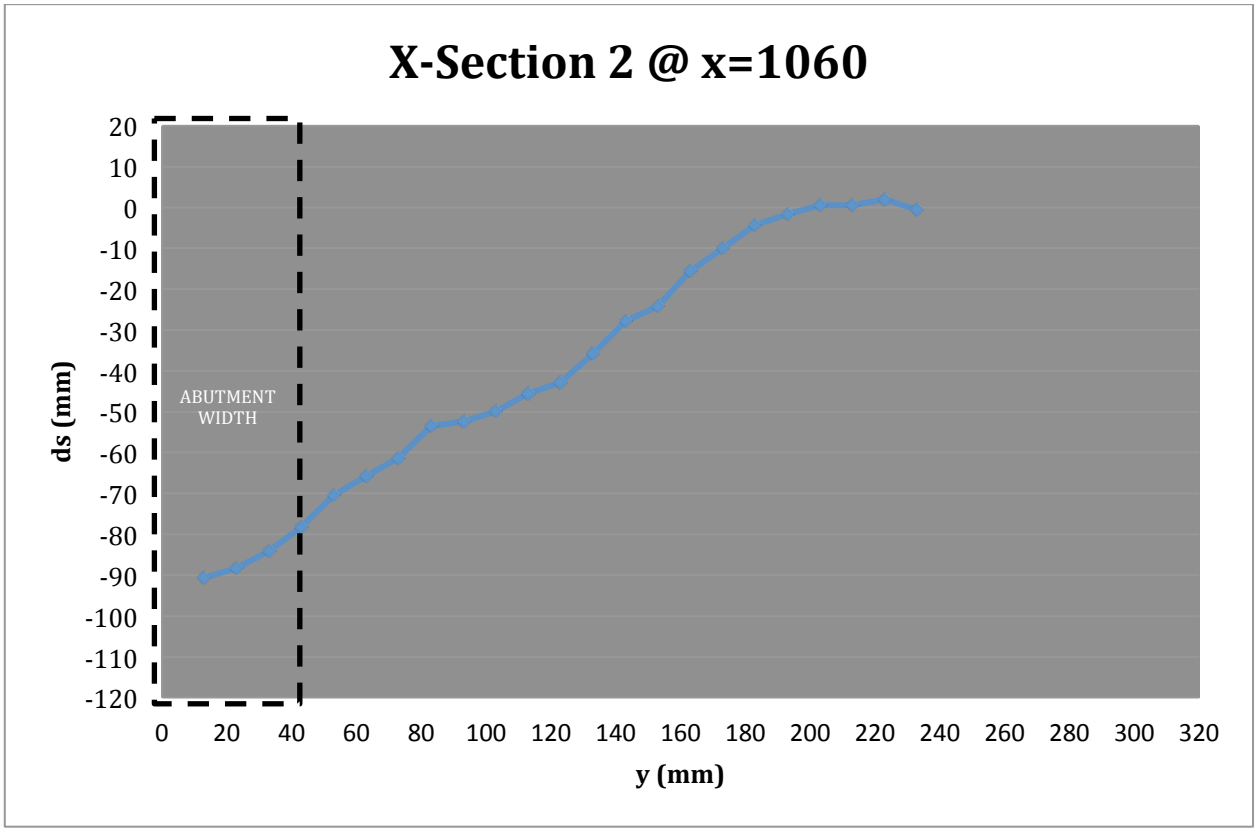

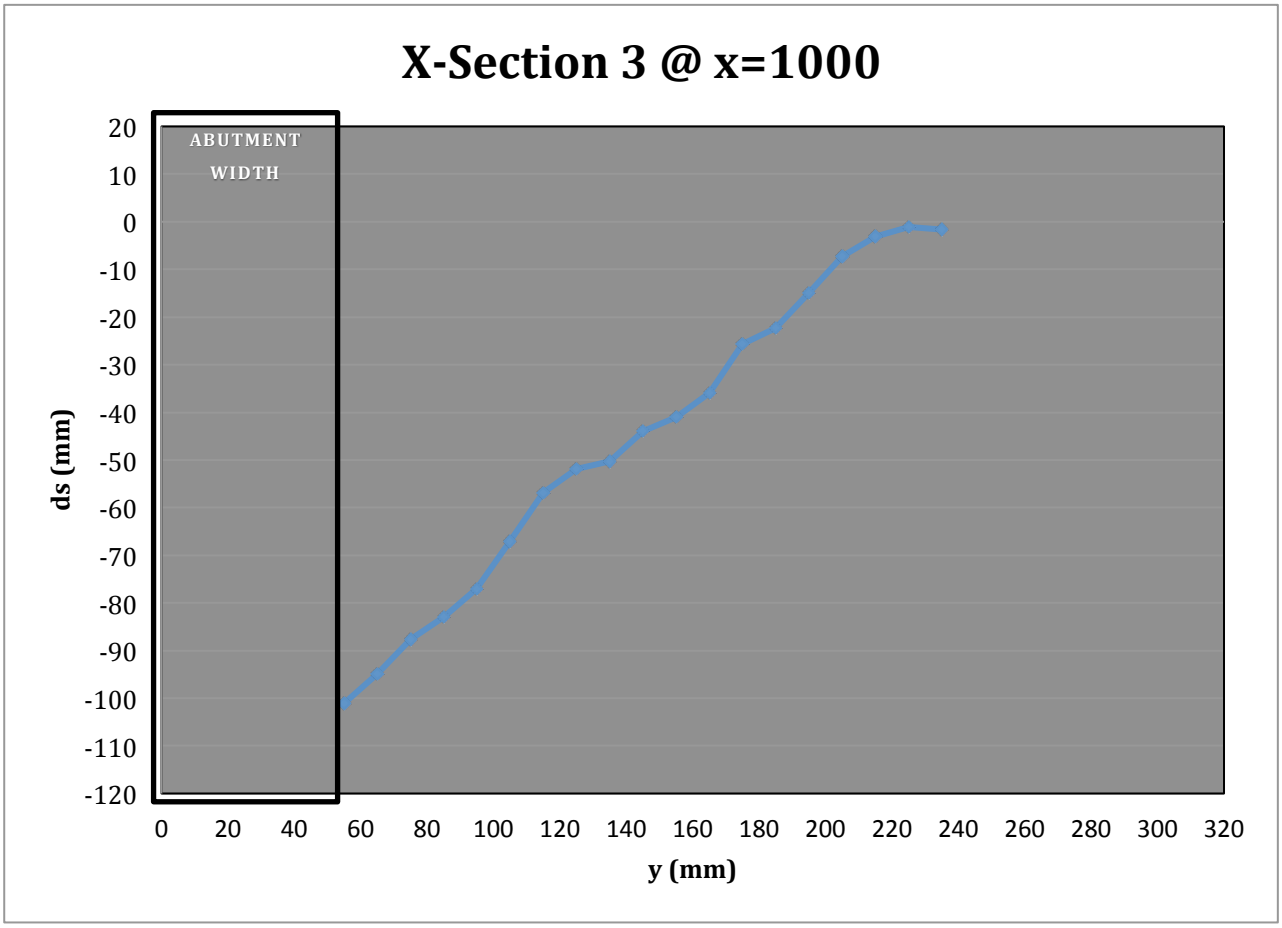
X-Section 3 @ x=1000
ABUTMENT WIDTH
ds (mm)
y (mm)
20
10
0
-10
-20
-30
-40
-50
-60
-70
-80
-90
-100
-110
-120
0
20
40
60
80
100
120
140
160
180
200
220
240
260
280
300
320

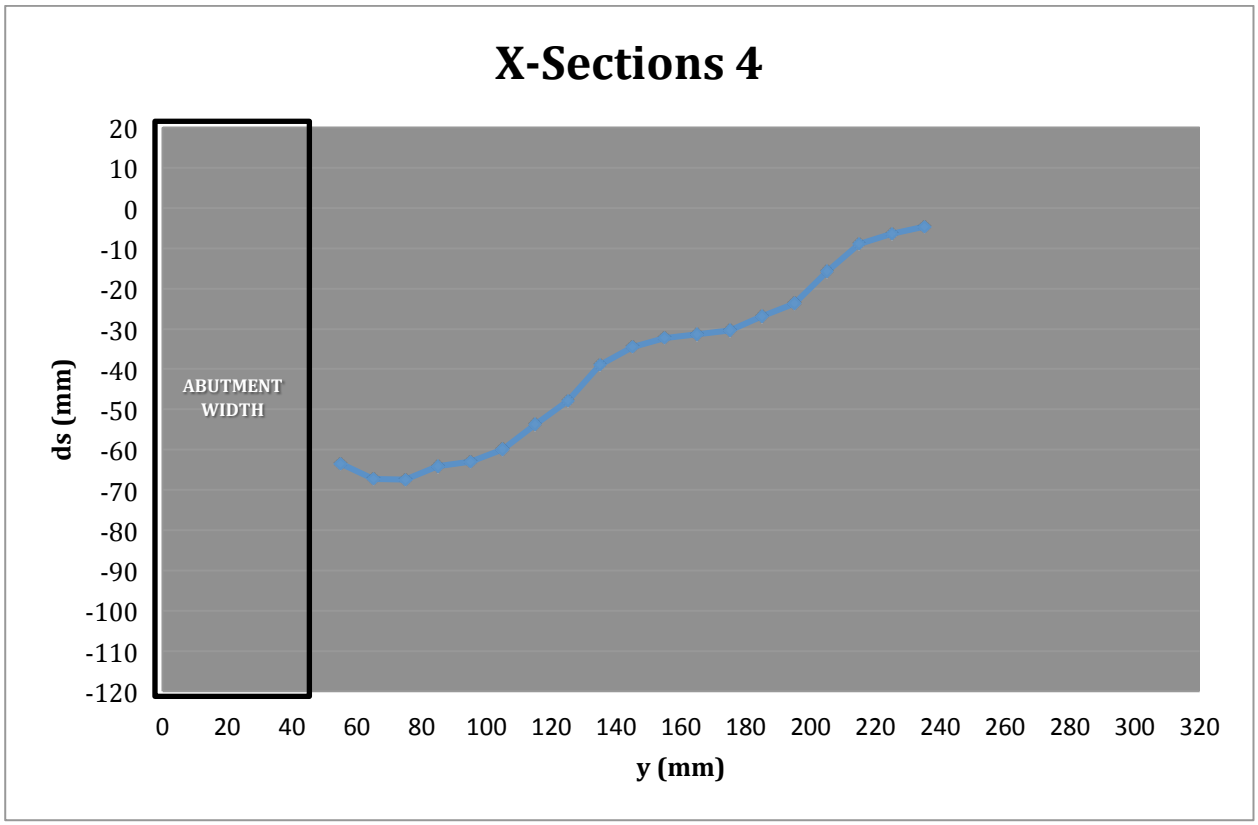
X-Sections 4
ABUTMENT WIDTH
ds (mm)
y (mm)
20
10
0
-10
-20
-30
-40
-50
-60
-70
-80
-90
-100
-110
-120
0
20
40
60
80
100
120
140
160
180
200
220
240
260
280
300
320

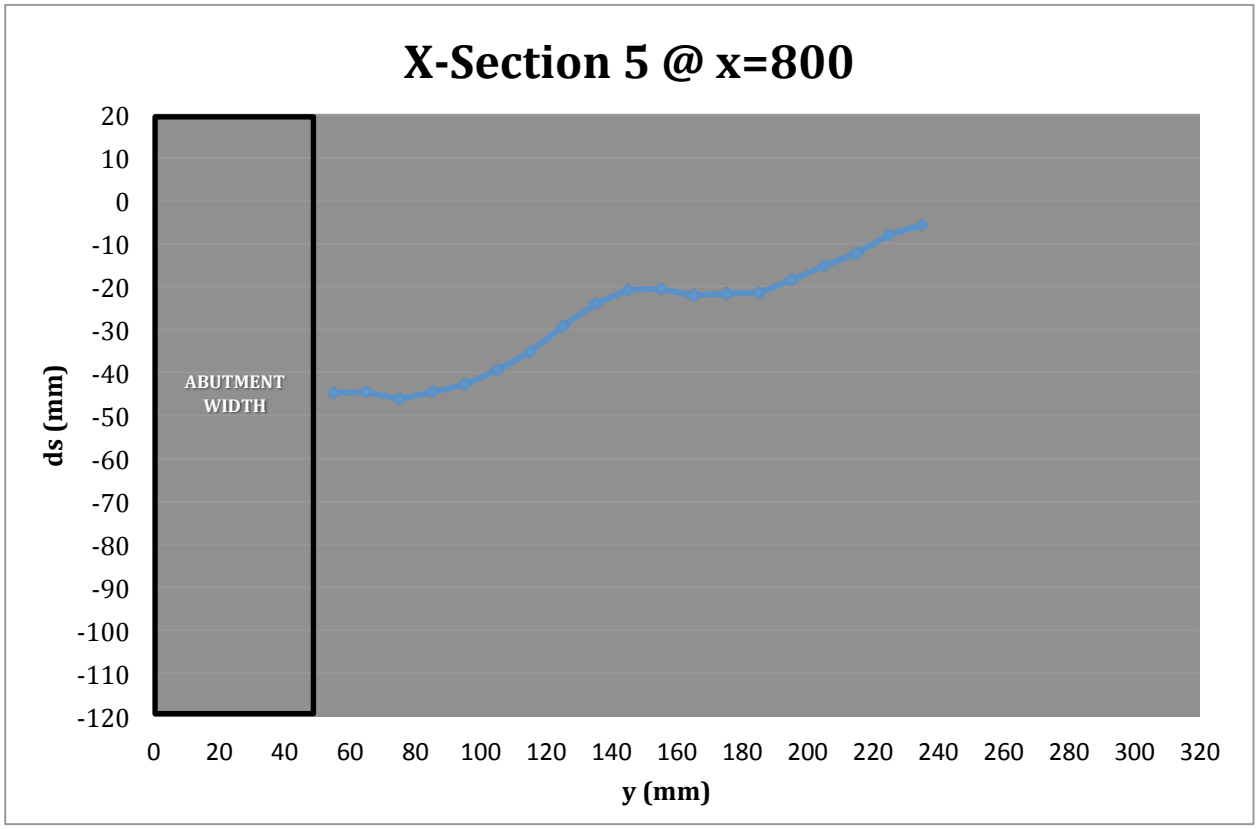
X-Section 5 @ x=800
ABUTMENT WIDTH
ds (mm)
y (mm)
20
10
0
-10
-20
-30
-40
-50
-60
-70
-80
-90
-100
-110
-120
0
20
40
60
80
100
120
140
160
180
200
220
240
260
280
300
320

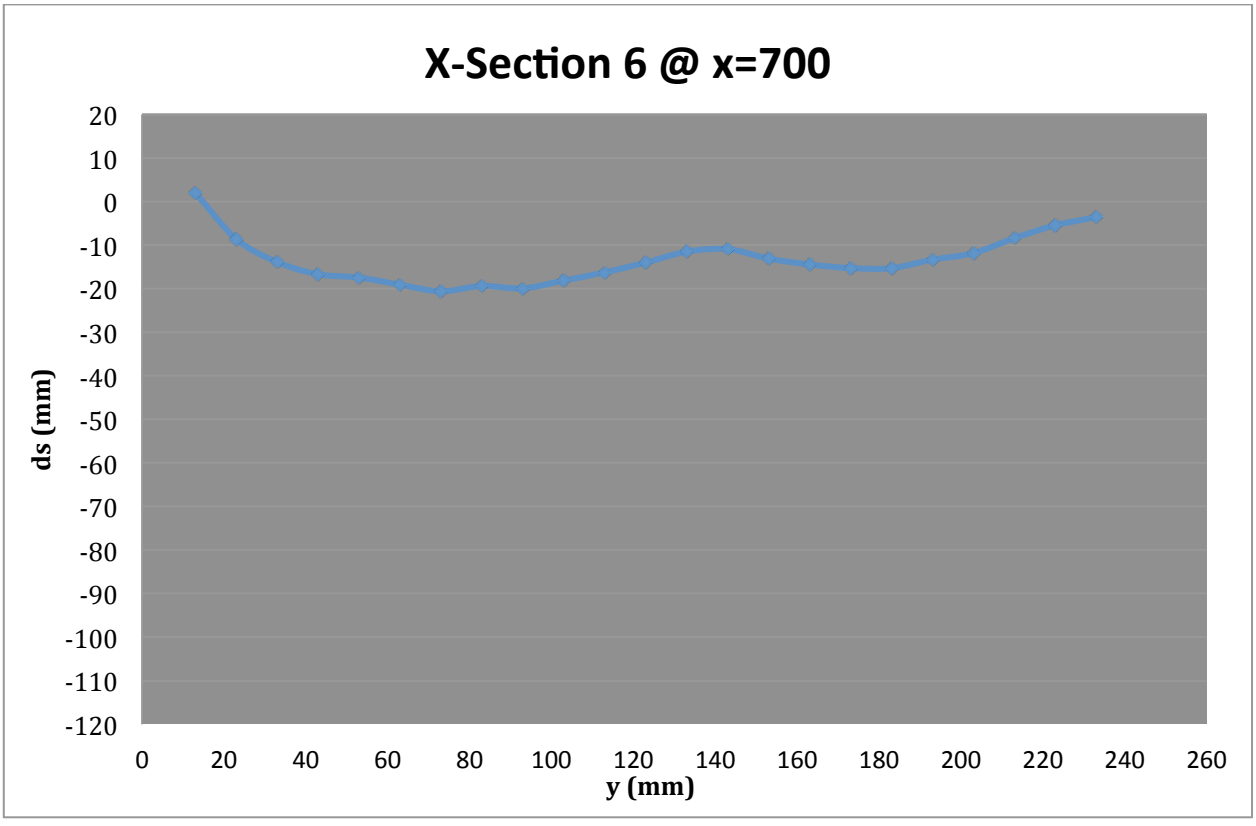
X-Section 6 @ x=700
ds (mm)
y (mm)
20
10
0
-10
-20
-30
-40
-50
-60
-70
-80
-90
-100
-110
-120
0
20
40
60
80
100
120
140
160
180
200
220
240
260

Test B-1 First Survey

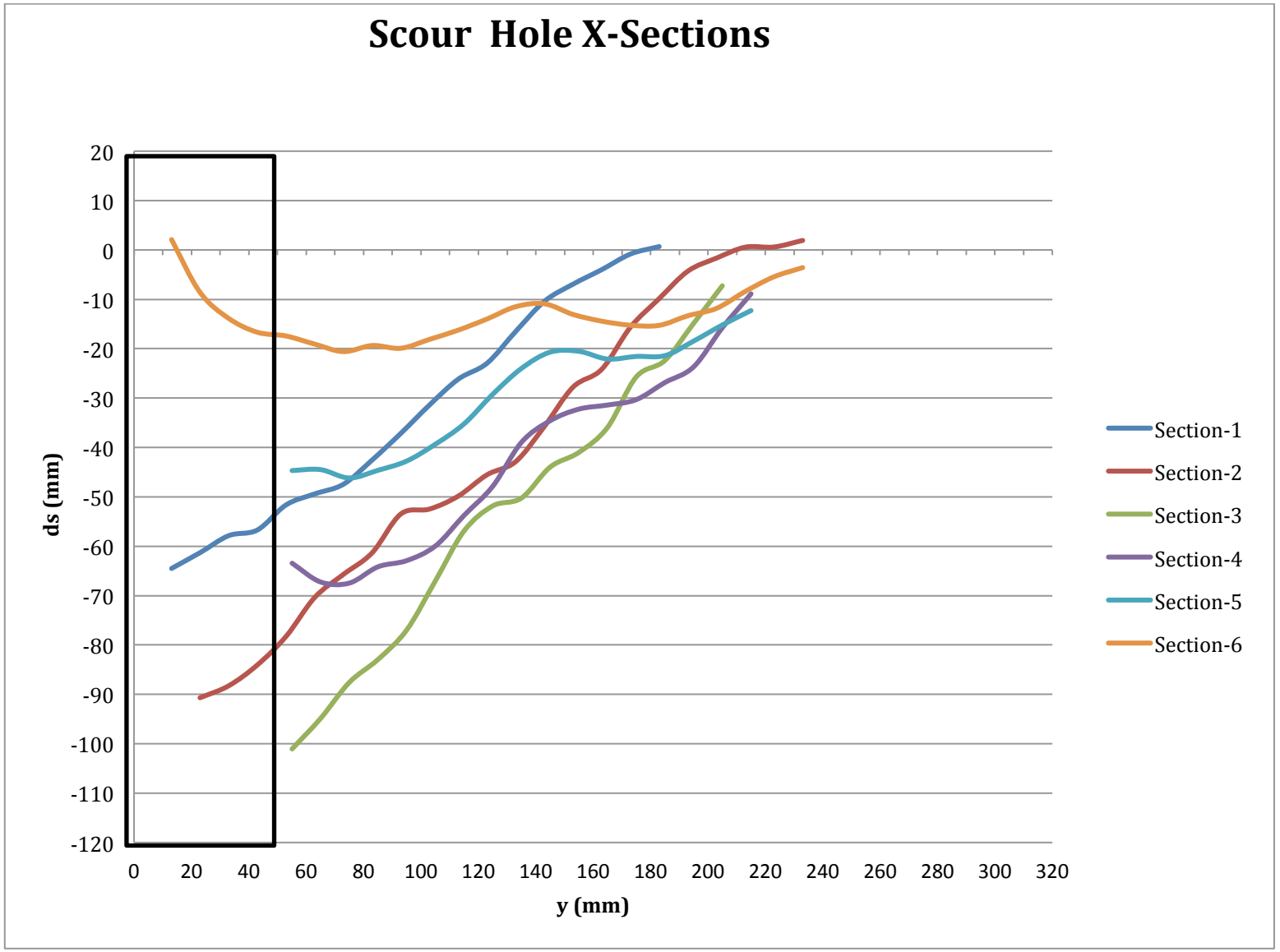

Section Comparison Series A

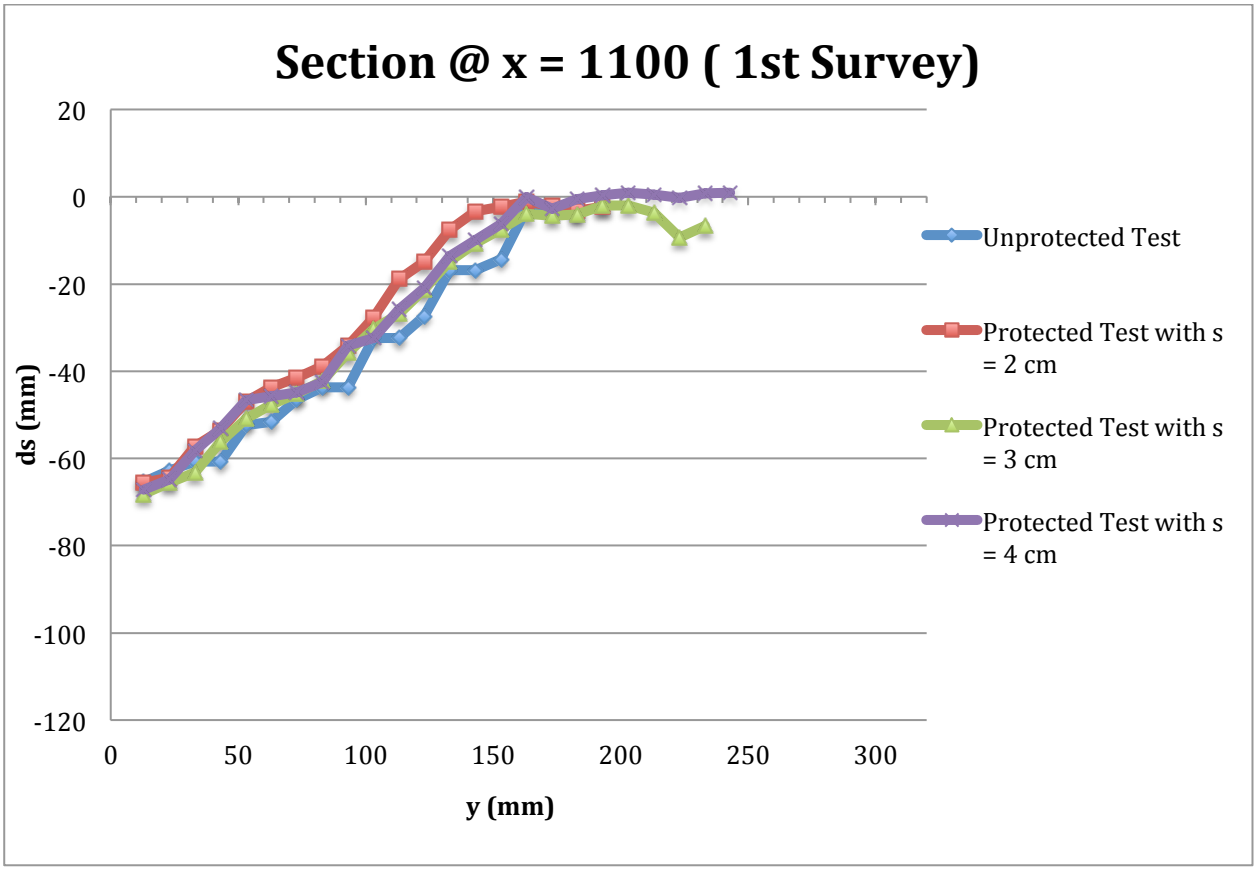
Section @ x = 1100 (1st Survey)
20
0
-20
-40
-60
-80
-100
-120
ds (mm)
0
50
100
150
200
250
300
y (mm)
Unprotected Test
Protected Test with s = 2 cm
Protected Test with s = 3 cm
Protected Test with s = 4 cm

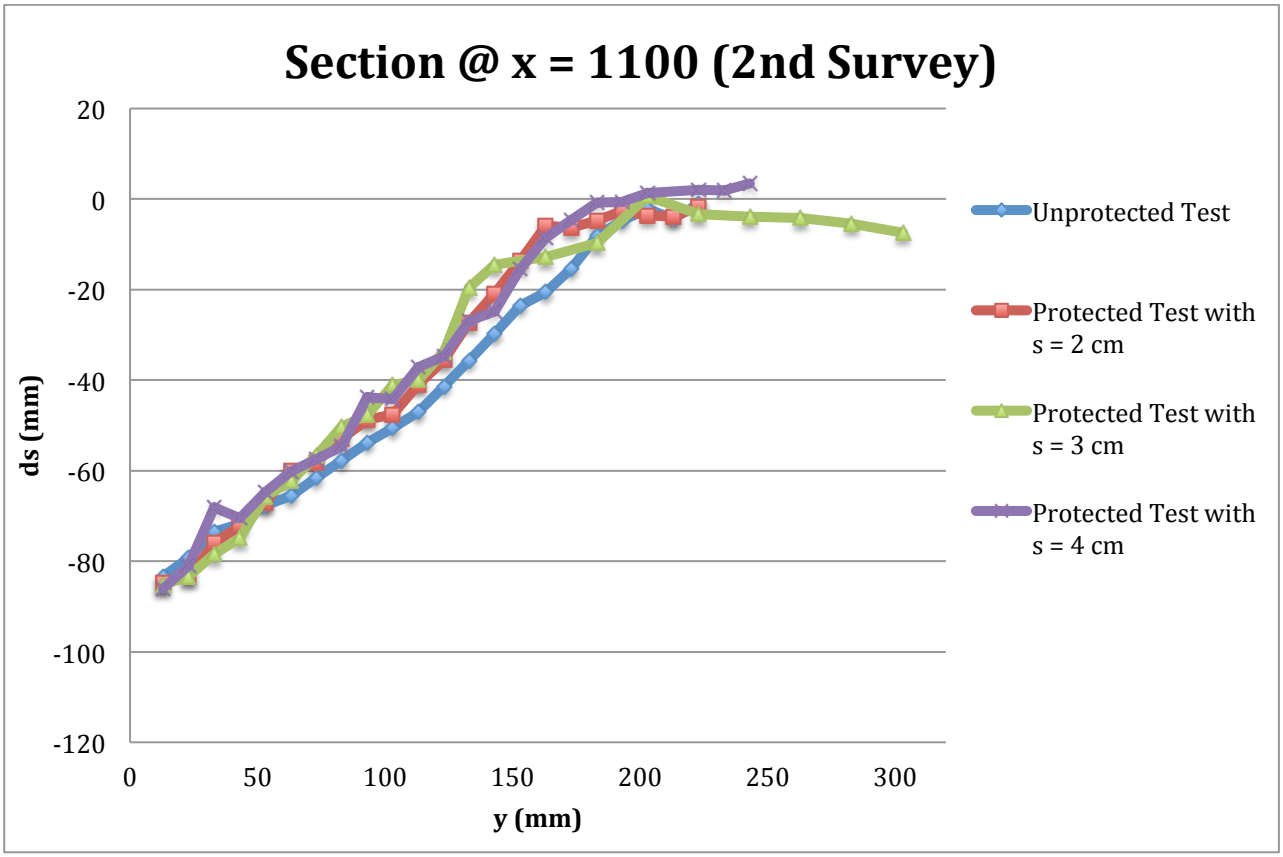
Section @ x = 1100 (2nd Survey)
20
0
-20
-40
-60
-80
-100
-120
ds (mm)
0
50
100
150
200
250
300
y (mm)
Unprotected Test
Protected Test with s = 2 cm
Protected Test with s = 3 cm
Protected Test with s = 4 cm

Section Comparison Series B

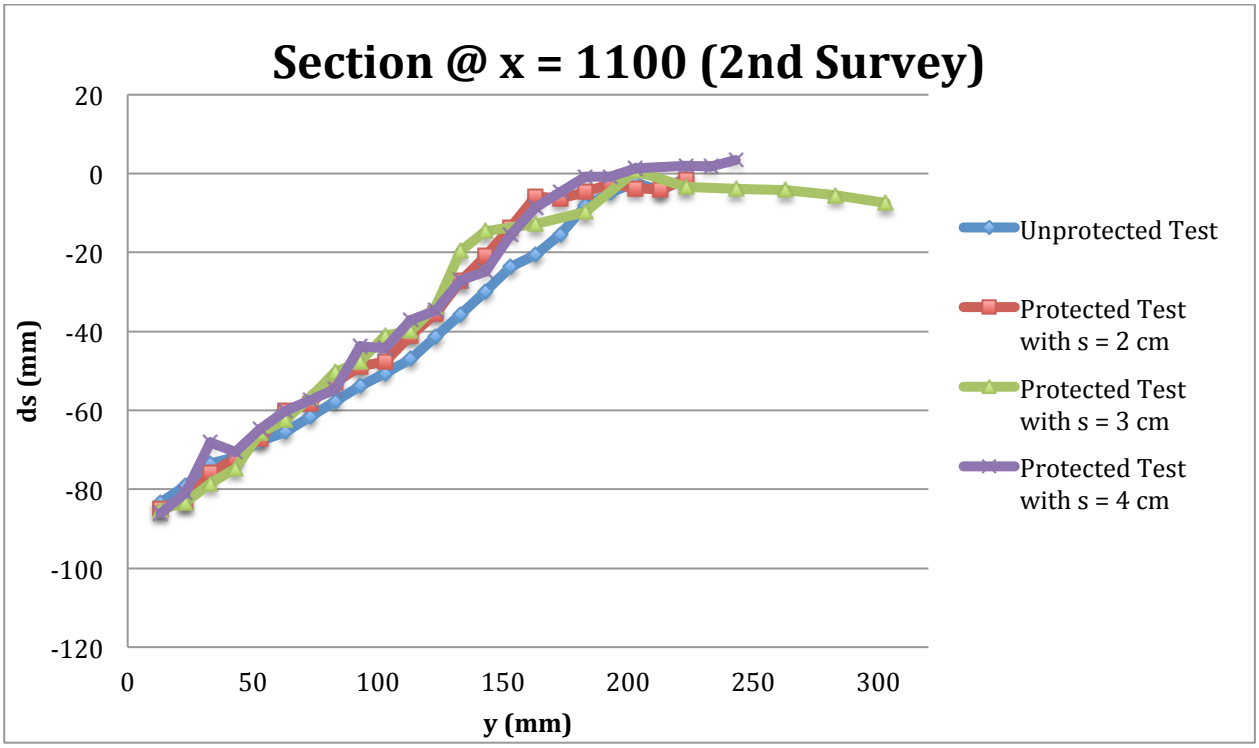
Section @ x = 1100 (2nd Survey)
20
0
-20
-40
-60
-80
-100
-120
ds (mm)
0
50
100
150
200
250
300
y (mm)
Unprotected Test
Protected Test with s = 2 cm
Protected Test with s = 3 cm
Protected Test with s = 4 cm

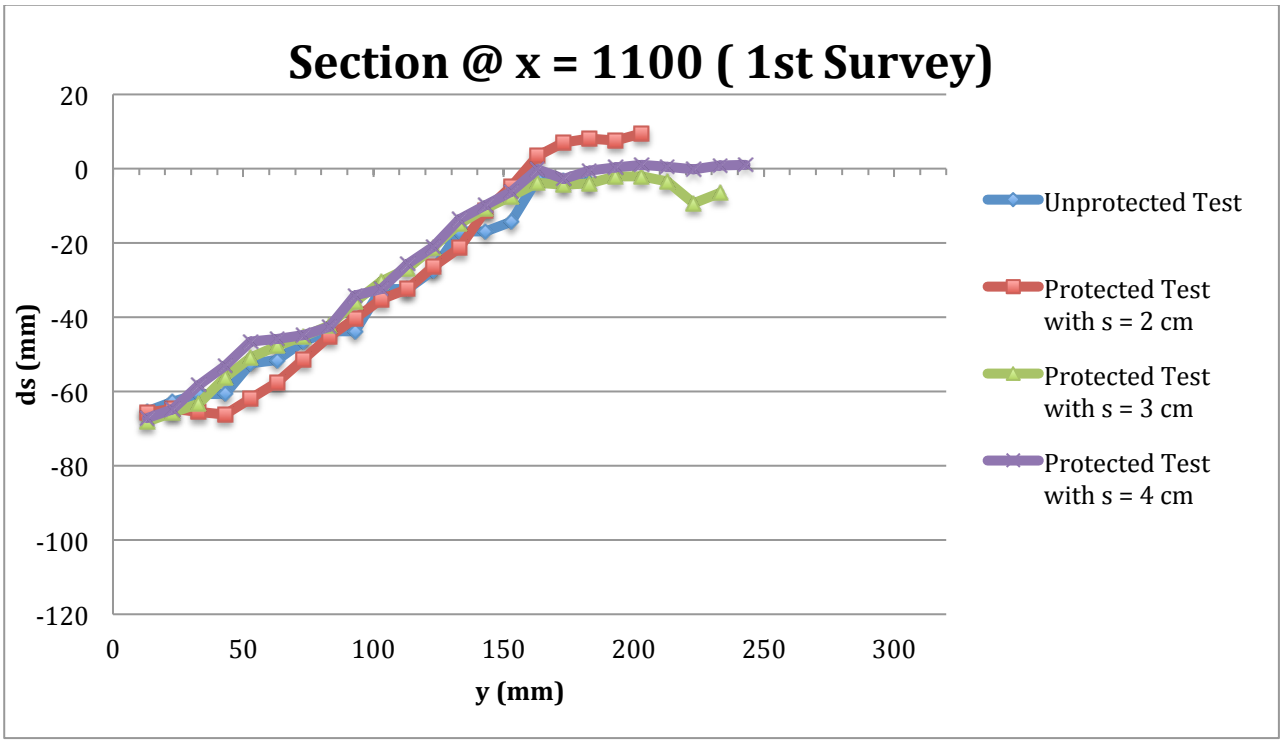
Section @ x = 1100 (1st Survey)
20
0
-20
-40
-60
-80
-100
-120
ds (mm)
0
50
100
150
200
250
300
y (mm)
Unprotected Test
Protected Test with s = 2 cm
Protected Test with s = 3 cm
Protected Test with s = 4 cm